UNIVERSITÀ DEGLI STUDI DI TORINO

Dipartimento di Chimica Generale ed Organica Applicata e
Dipartimento di Scienze Oncologiche

Dottorato di Ricerca in
SISTEMI COMPLESSI APPLICATI ALLA BIOLOGIA POST-GENOMICA

XX CICLO

TITOLO DELLA TESI:

Protein-Ligand and Protein-Protein Interaction Studies: Development of a Spectroscopy-based Approach

TESI PRESENTATA DA:
Nadia Barbero

TUTOR:
Prof. Federico Bussolino

COORDINATORE DEL DOTTORATO:
Prof. Federico Bussolino

Anni Accademici: **2004/2007**

Settore Scientifico-Disciplinare: **CHIM/06**

INDEX

CHAPTER 2 – Bioconjugation

CHAPTER 3 – BSA Interaction with Fluorescein Sodium Salt

CHAPTER 4 – GST – GST(B14) Interaction

CHAPTER 5 – GST-Tat86 – Peptide Interaction

CHAPTER 6 – MEK-ERK Interaction

Aim of the Work

In the post-genomic era, the importance of protein-protein interaction is becoming even more apparent. There is evidence that most, if not all, catalytic and regulatory pathways operate as networks, with frequent and extensive input from signalling pathways, feedback and cross-talk.

Quantitative determinations of the dissociation constants of biomolecular interactions, in particular protein-protein interactions, are essential for a detailed understanding of the molecular basis of their specificities. The essence of biological specificity resides in the energetic, dynamic and structural aspects of biomolecular interactions. Although a great deal of emphasis has been placed on elucidation of structural aspects of biomolecules, our understanding of biomolecular interactions and specificities cannot proceed in the absence of knowledge on the energetics and dynamics of the systems. Fluorescence spectroscopy is particularly well suited for such studies.

Affinity constants are numeric representations of the strength with which two molecules interact and can provide insight into the mechanism of interactions and, when coupled with biological experiments, can aid in predicting if and when specific interactions function in cell. The aim of this work is to provide an understanding of affinity constants and how to experimentally measure them for biomolecular interactions.

This work is part of a wider research project whose aim is the modeling of known converging signal pathways elicited by tyrosine receptor kinases involved in angiogenesis. This approach could provide a useful tool to understand what are the mechanisms of each signaling and to find some sensible nodes of the protein network that would allow to finely tune cell functions.

For the above mentioned long term project, a complete signaling cascade was reconstructed by mathematical description of the INTEGRIN/VEGFR-induced pathways and the attention was focused on a useful group of proteins to work on. Some proteins, which do not belong to the pathway, were chosen to be used as a test for this short term project for the development of a method for interaction studies. The selected proteins were: Bovine Serum Albumin (BSA) whose interaction with a small fluorescent ligand was studied, GST-Tat86 interaction with a small peptide and GST which interacts with his antibody α-GST (B14). All these interactions were followed by different methods:

1. *Steady-State Fluorescence Intensity* leading to K_d and K_a, i.e. the equilibrium dissociation and association binding constants, determination by nonlinear regression analysis.

2. *Steady-State Fluorescence Anisotropy* which is based on the observation of the molecular movement of a fluorescent molecule in solution (fluorescent probes can be present as intrinsic or extrinsic fluorophores) leading to the same equilibrium binding constants as mentioned above.
3. *Stopped-Flow Fluorescence Intensity and Anisotropy* providing the second- (k_{on}) and the first-order (k_{off}) rate constant as well as the equilibrium dissociation constant (from the k_{off}/k_{on} ratio) for the reaction.

Abstract

A complete signaling cascade was reconstructed by mathematical description of the INTEGRIN/VEGFR-induced pathways and the attention was focused on a useful group of proteins to work on. Some proteins, which do not belong to the pathway, were chosen to be used as a test for the development of a method for interaction studies. Four different interactions were used in order to explore four different kinds of interactions: protein-ligand, protein-antibody, protein-peptide and protein-protein interactions.

The binding of fluorescein sodium salt with different bovine serum albumins (BSA) was investigated by steady-state and stopped-flow fluorescence. This interaction was chosen for a preliminary study for protein-ligand interactions because of BSA low cost and availability. The dissociation and association rate constants (k_{on} and k_{off}) were determined from the kinetic studies while the dissociation and association binding constants (K_d and K_a) were determined both by the quenching of the fluorescence of BSA in the presence of fluorescein and from stopped-flow measurements from the k_{on}/k_{off} ratio. This work also reports the distance between tryptophan and bound fluorescein based on Förster's energy transfer theory and a thermodynamic study of the mode of interaction which is important for confirming binding modes.

The interaction between GST with his antibody α-GST (B14) was studied by fluorescence anisotropy, after GST bioconjugation with fluorescein-5-maleimide, leading to the K_d and K_a determination which have resulted in agreement with the data found in literature referring to protein-antibody interaction.

GST-Tat86 interaction with two small peptides (CT319 and V2) having similar aa sequence and the same biological activity was studied by steady-state fluorescence exploiting the intrinsic Trp residues fluorescence. The results show that the obtained binding constants differ in the same set of interactions. One set of results is in agreement with the K_d obtained from BIAcore studies and reported by Marchiò *et al.* (*Blood* **2005,** *105,* 2802-2811) for a very similar interaction. The variation of the obtained binding constants can be due to the presence of many tryptophan residues each with a different environment. The reaction was then followed by steady-state and stopped-flow fluorescence after the peptide bioconjugation.

Finally, the interaction between two proteins belonging to the above-mentioned pathway was studied. The interaction between MEK-ERK was followed by stopped-flow fluorescence after ERK bioconjugation with fluorescein-5-maleimide. The second-order rate constant k_{on} is $2.84 \cdot 10^8$ M^{-1} sec^{-1} while the k_{off} has a small negative value. This shows that the interaction is nearly completely shifted toward the complex formation. The binding constant

obtained is in agreement with the few data available in literature referring to this interaction obtained either from simulation/prediction analysis or different techniques.

Therefore, this work has provided evidences of the possibility of studying protein-ligand interactions by spectroscopic methods but has also outlined all the difficulties and the limits of the reported techniques. In particular it should be stressed the need of high quantity of high purity proteins or, more generally, biomolecules.

Chapter 1 - Spectroscopic Methods

Introduction

Fluorescence spectroscopy has been widely used to study ligand–protein interaction because of its simplicity and sensitivity. Fluorescence methods are particularly popular because they are well suited for protein-ligand interactions with dissociation constants in the range of 10^{-4} to 10^{-8} M, where some protein–nucleic acid dissociation constants fall.

Many fluorescence parameters, such as anisotropy, intensity and energy transfer efficiency, are sensitive to formation of protein–ligand complexes and can be utilized to derive binding isotherms[1]. The change in fluorescence intensity on formation of a protein-ligand complex is one of the simplest ways to measure binding of a ligand to a protein.

1.1 Fluorescence Anisotropy

Introduction

Measurement of fluorescence anisotropy[2] is a powerful tool in biochemical research and medical testing. Anisotropy measurements provide information on the size and shape of proteins or the rigidity of various molecular environments. Anisotropy measurements have been used to measure protein-protein associations, fluidity of membranes and for immunoassays of numerous substances.

Anisotropy measurements are based on the principle of photoselective excitation of fluorophores by polarized light. Fluorophores preferentially absorb photons whose electric vectors are aligned parallel to the transition moment of the fluorophore. The transition moment has a defined orientation with respect to the molecular axis. In an isotropic solution, the fluorophores are oriented randomly. Upon excitation with polarized light, one selectively excites those fluorophore molecules whose absorption transition dipole is parallel to the electric vector of the excitation (Figure 1.1).

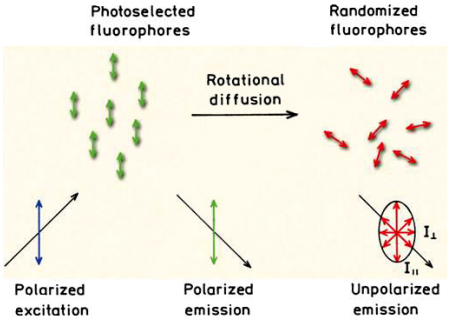

Figure 1.1 – Effects of polarized excitation and rotational diffusion on the polarization or anisotropy of the emission[2]

This selective excitation results in a partially oriented population of fluorophores (photoselection) and in partially polarized fluorescence emission. Emission also occurs with the light polarized along a fixed axis in the fluorophore.

The measurements of fluorescence anisotropy is illustrated in Figure 1.2. For most experiments the sample is excited with vertically polarized light. The electric vector of the excitation light is oriented parallel to the vertical *z*-axis.

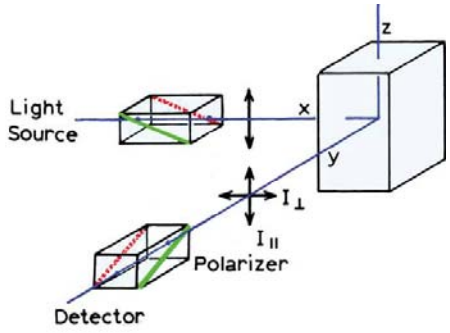

Figure 1.2 – Schematic diagram for measurement of fluorescence anisotropy[2]

The intensity of the emission is measured through a polarizer. When the emission polarizer is oriented parallel (*par*) to the direction of the polarized excitation, the observed intensity is called I_{par}. Likewise, when the polarizer is perpendicular (*per*) to the excitation, the intensity is called I_{per}. These intensity values are used to calculate the anisotropy[3]:

$$r = \frac{I_{par} - I_{per}}{I_{par} + 2I_{per}} \qquad [1.1]$$

where I_{par} and I_{per} are the fluorescence intensities of the vertically (*par*) and horizontally (*per*) polarized emission, when the sample is excited with vertically polarized light.

The anisotropy is a dimensionless quantity that is independent of the total intensity of the sample. This is because the difference ($I_{par} - I_{per}$) is normalised by the total intensity, which is $I_T = I_{par} + 2I_{per}$. The anisotropy is an intensity ratiometric measurement. In the absence of artefacts the anisotropy is independent of the fluorophore concentration.

In earlier publications and in the clinical literature, the term polarization is frequently used:

$$P = \frac{I_{par} - I_{per}}{I_{par} + I_{per}} \qquad [1.2]$$

Anisotropy and polarization are both expressions for the same phenomenon and these values can be interchanged using equation 1.3 and 1.4:

$$P = \frac{3r}{2+r} \qquad [1.3] \qquad\qquad r = \frac{2P}{3-P} \qquad [1.4]$$

The polarization and the anisotropy contain the same information, but the use of anisotropy is preferred because it is normalized by the total intensity which results in simplification of the equations.

1.1.1 Effects of Rotational Diffusion on Fluorescence Anisotropy: The Perrin Equation

Several phenomena can decrease the measured anisotropy to values lower than the maximum theoretical values. The most common cause is rotation diffusion (Figure 1.1). Such diffusion occurs during the lifetime of the excited state and displaces the emission dipole of the fluorophore. Measurements of this parameter provide information about the relative angular displacement of the fluorophore between the times of absorption and emission. In fluid solution most fluorophores rotate extensively in 50 to 100 ps. Hence, the molecules can rotate many times during the 1-10 ns excited-state lifetime, and the orientation of the polarized emission is randomized. For this reason fluorophores in non-viscous solution typically display anisotropy near zero.

The effects of rotational diffusion can be decreased if the fluorophore is bound to a macromolecule. For instance, it is known that the rotational correlation time for the protein human serum albumin (HSA) is near 50 ns. Suppose HSA is covalently labelled with a fluorophore whose lifetime is 10 ns. Assuming no other processes result in loss of anisotropy, the expected anisotropy is given by the Perrin equation[4,5,6]:

$$r = \frac{r_0}{1+(\tau/\theta)} \qquad [1.5]$$

where r_0 is the anisotropy that would be measured in the absence of rotational diffusion and θ is the rotational correlation time for the diffusion process. In this case binding of the fluorophore to the protein has slowed the probe's rate of rotational motion. Assuming $r_0 = 0.4$, the anisotropy is expected to be 0.20. Smaller proteins have shorter correlation times and are expected to yield lower anisotropies. The anisotropies of larger proteins can also be low if they are labelled with long-lifetime fluorophores. The essential point is that the rotational correlation times for most proteins are comparable to typical fluorescence lifetimes. As a result, measurements of fluorescence anisotropy will be sensitive to any factor that affects the rate of rotational diffusion. The rotational rates of fluorophores in cell membranes also occur on the nanoscale timescale and the anisotropy values are thus sensitive to membrane composition. For these reasons, measurements of fluorescence polarization are widely used to study the interactions of biological macromolecules.

1.1.2 Molecular Information from Fluorescence Anisotropy

As stated before, fluorophores absorb light along a particular direction with respect to the molecular axes. The phenomenon of fluorescence polarization can be used to measure the apparent volume (or molecular weight) of proteins. This measurement is possible because larger proteins rotate more slowly. Hence, if a protein binds to another protein, the rotational rate decreases and the anisotropy increases (Figure 1.3). The rotational rate of a molecule is often described by its rotational correlation time θ, which is related to:

$$\theta = \frac{\eta V}{RT} \qquad [1.6]$$

where η is the viscosity, V is the molecular volume, R is the gas constant and T is the temperature in K. Suppose a protein labelled with DNS-Cl (Figure 1.3). If the protein associates with another protein, the volume increases and so does the rotational correlation time. This causes the anisotropy to increase because of the relationship between the steady-state anisotropy *r* to the rotational correlation time θ (Equation 1.5).

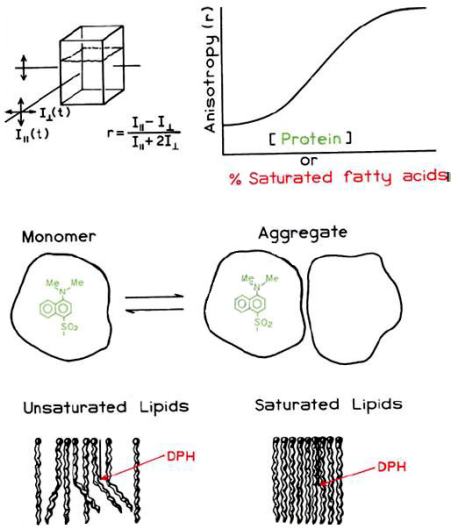

Figure 1.3 – Effect of protein association and membrane microviscosity on the fluorescence anisotropy[2]

Fluorescence polarization measurements have also been used to determine the apparent viscosity of the side chain region of membranes. Such measurements of microviscosity are typically performed using a hydrophobic probe like DPH (Figure 1.3), which partitions into the membrane. The viscosity of membranes is known to decrease in the presence of unsaturated fatty acid side chains. Hence, an increase in the amount of unsaturated fatty acid is expected to decrease the anisotropy.

Association reactions can also be followed by anisotropy measurements. Figure 1.4 shows anisotropy measurements of melittin upon addition of calmodulin[7]. Calmodulin does not contain any tryptophan, so the total tryptophan emission is only due to melittin. Upon

addition to calmodulin the melittin anisotropy increases about twofold. This effect is due to slower rotational diffusion of the melittin-calmodulin complex as compared to melittin alone. The emission spectra of melittin show that the tryptophan residue becomes shielded from the solvent upon binding to calmodulin. The tryptophan residue is probably located at the interface between the two proteins.

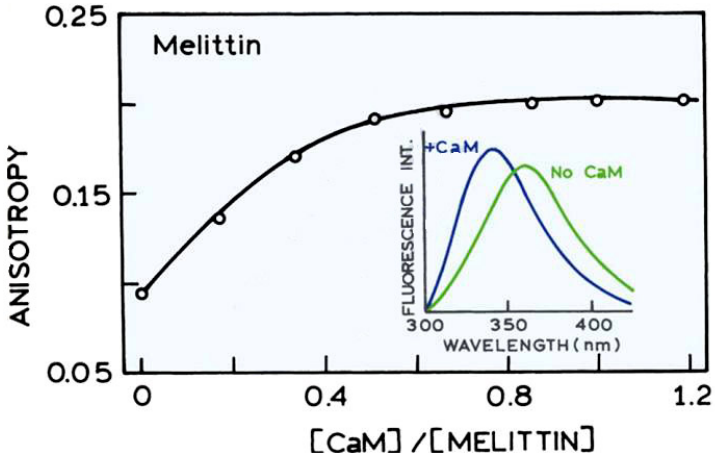

Figure 1.4 – Effect of melittin-calmodulin association on the anisotropy of melittin. Inset: Emission spectra of melittin in the presence and absence of calmodulin (CaM)[2,7]

1.1.3 Fluorescence Polarization as a Tool to Analyze Protein-ligand Interactions

Quantitative determinations of the dissociation constants of biomolecular interactions, in particular protein-protein interactions, are essential for a detailed understanding of the molecular basis of their specificities.

The essence of biological specificity resides in the energetic, dynamic, and structural aspects of biomolecular interactions. Although a great deal of emphasis has been placed on elucidation of structural aspects of biomolecules (primarily through the use of X-ray diffraction studies and, more recently, NMR methodologies) our understanding of biomolecular interactions and specificities cannot proceed in the absence of knowledge on the energetics and dynamics of the systems ability to interact, with varying degrees of affinity and specificity, with other proteins. In some cases, the interacting proteins may be identical, such as with oligomeric proteins composed of like subunits. Oligomeric proteins containing multiple and identical, distinct polypeptides chains are common and many examples of dimers, trimers, tetramers, hexamers, and even higher aggregates are well known. Oligomeric proteins containing multiple, nonidentical subunits are also known, ranging from simple heterodimers to large protein complexes such as ribosomes.

Fluorescence polarization (FP) is a powerful and sensitive technique for the study of molecular interactions in solution. FP is not a new technique in theory: its theoretical basis was first reported by Perrin in 1926[4] and first developed by Weber[8,9].

Fluorescence polarization is a powerful technique for characterizing macromolecular associations and can provide equilibrium determinations of protein-DNA and protein-protein interactions.

The determination of binding interactions by fluorescence polarization has several advantages over standard methods of assessing macromolecular interactions. First, fluorescence polarization is performed in solution and can provide a true equilibrium measurement of binding. Methods involving the separation of bound from free ligand, such as the electrophoretic mobility shift assay or precipitation methods, disturb the reaction equilibrium and therefore accurate quantification, particularly for low affinity interactions. In addition, fluorescence polarization, unlike equilibrium dialysis, is generally applicable; molecules need not to be of dissimilar size to measure equilibrium binding. Assembly of protein-nucleic acid, protein-protein, and multicomponent complexes can be measured relatively easily. Furthermore, various conditions of ionic strength, divalent cation and buffer can be tested rapidly, including conditions that may not be compatible with other methods (for example, native gel electrophoresis). Finally, in contrast to Surface Plasmon Resonance [Pharmacia BIACore (Pharmacia, Piscataway, NJ) or Fison Applied Sensor (Fisons Instruments, Danvers, MA)], all binding components are in solution, and relatively simple instrumentation is required.

FP is based on the observation of the molecular movement of the fluorescent molecules in solution and does not require physical separation of the excess ligand or acceptor. FP is now used, for example, in the DNA–protein, DNA–DNA interactions, and protein–protein interactions. Immunoassays using FP technique have been employed for the assay of vancomycin[10] and digoxin[11] in sera. Recently, some applications of FP to the analysis of environmental pollutants have also been reported[12].

Figure 1.5 illustrates how FP is employed in the measurement of a binding reaction. Molecules in solution rotate and tumble. In the case of small molecules, the movement is very rapid, but the movement of larger molecules becomes slower. When fluorescent-labelled small molecules in solution are excited with a plane polarized light (Figure 1.5, top), the emitted light is depolarized due to fast movement of the molecule. However, when the fast-moving small fluorescent-labelled molecule is bound to the receptor having a large molecular mass, the movement of the conjugate is restricted and becomes slow. When such a conjugate is irradiated with a polarized light, the emitted light is obviously less depolarized. (Figure 1.5, bottom). Difference between these states is dependent on the number of bound molecules and the binding constant also called affinity constant.

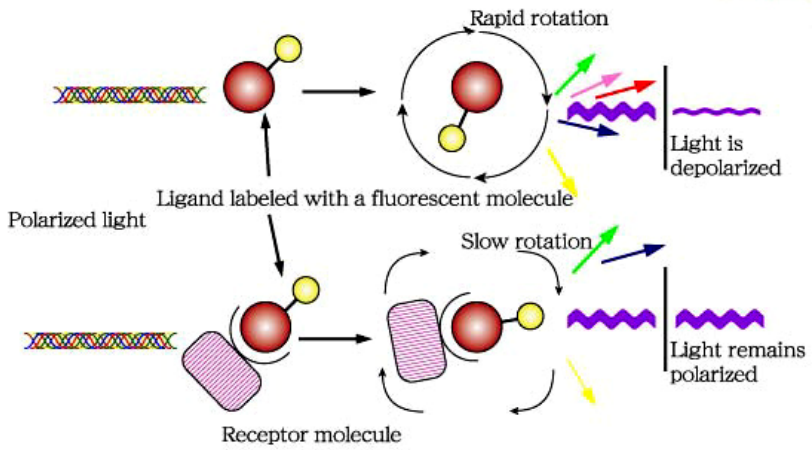

Figure 1.5 - Principle of the assay of binding reaction using fluorescence polarization[13] *(http://www.glycoforum.gr.jp/)*

A binding isotherm can be easily constructed by titrating a binding protein into a solution of fixed concentration of small fluorescent-tagged ligand molecules. From such data, K_d and K_a can be obtained by nonlinear regression analysis.

In the binding studies using FP, an appropriate fluorescent-labelled ligand to attain sensitivity has to be selected. In a typical procedure, the concentration of the fluorescent-labelled ligand is kept constant, and FPs are measured by changing the concentrations of the receptor solution. The FP value at each concentration is measured and used to generate a binding isotherm. The fluorescent labelling method is also important in FP measurement. In some cases, fluorescence intensity of the labelled ligand changes upon binding due to the change in the microenvironment of the fluorescent probe.

There are many applications using FP in DNA–protein and DNA–DNA interactions[14], protein–protein interactions[15], protease assays[16], immunoassays[17], conformational changes of proteins[18], and cell-biochemical studies[19].

The measurements of binding by fluorescence polarization requires a somewhat different analysis than traditional binding assays, mainly because binding is inferred from the anisotropy values, yielding an expression for fractional binding. This analysis can be simply related to traditional binding assays, however. Consider a simple binding interaction between two molecular species, L and R[13]:

$$\mathbf{L + R} \underset{\mathbf{k_2}}{\overset{\mathbf{k_1}}{\rightleftharpoons}} \mathbf{L{:}R}$$

L in this case could represent a DNA-binding protein associating with a fluorescein tagged DNA-binding sequence, R. This equation may also be applied to describe the association of an additional protein to a preformed protein-DNA complex.

The rate of formation or dissociation of the complex L:R can be expressed as: $d[L:R]/dt = k_1 [L][R] - k_2 [L:R]$. At equilibrium, by definition, $d[L:R]/dt = 0$ and $k_2 [L:R] = k_1 [L][R]$. Thus,

$$K_a = \frac{k_1}{k_2} = \frac{[L:R]}{[L][R]} \qquad [1.7]$$

Note that the equilibrium association constant is inversely related to the dissociation constant

$$K_a = \frac{1}{K_d} \qquad [1.8]$$

representing the affinity of L for R. Fluorescence anisotropy does not actually measure these parameters but provides an index of the fraction of L bound to R. Thus:

$$F_b = \frac{A - A_f}{A_b - A_f} = \frac{[L:R]}{[R_T]} \qquad [1.9]$$

where [R] represents the total receptor concentration and where A is the measured anisotropy in a mixture of free and bound fluorescent molecules with anisotropies of A_f and A_b respectively. Experimentally, the total ligand concentration and total receptor concentrations ($[L_T]$ and $[R_T]$) are known from the experimental protocol. $[R_T]$ is constant and $[L_T]$ is experimentally altered as A is measured. However, the free ligand and receptor concentrations, [L] and [R], and the concentration of the complex [L:R], are not directly measured. In addition, in most experiments $[R_T]$ cannot be kept $<< K_d$; therefore, a significant amount of L added becomes bound to R. Thus $[L] = [L_T]$ and $[R] + [R_T]$. However, we can solve Equation 1.9 explicitly in terms of $[L_T]$, $[R_T]$, and K_a since

$$K_a = \frac{[L:R]}{[L][R]} \qquad \text{and} \qquad [L_T] = [L] + [L:R] \qquad [R_T] = [R] + [L:R]$$

[1.10] [1.11] [1.12]

Thus,

$$K_a = \frac{[L:R]}{([L_T] - [L:R])([R_T] - [L:R])} \qquad [1.13]$$

Solving for [L:R] in terms of K_a, $[L_T]$ and $[R_T]$:

$$[L:R] = \left[\frac{1 + K_a[L_T] + K_a[R_T] - \sqrt{\left[(1 + K_a[L_T] + K_a[R_T])^2 - 4[L_T][R_T]K_a^2\right]}}{2K_a} \right] \qquad [1.14]$$

Substituting this expression for [L:R] into Equation 1.9, and solving for A (the measured anisotropy) yields:

$$A = A_f + (A_b - A_f) \times \left[\frac{1 + K_a[L_T] + K_a[R_T] - \sqrt{\left[(1 + K_a[L_T] + K_a[R_T])^2 - 4[L_T][R_T]K_a{}^2\right]}}{2K_a[R_T]} \right] \quad [1.15]$$

In this equation, $[L_T]$ and $[R_T]$ are known, and A is measured. The data (A vs. $[L_T]$) may be fitted to this model by nonlinear least squares analysis (with commercial programs such as SigmaPlot, or Kaleidagraph), giving initial parameter estimates for A_b, A_f, and K_a.

This equation is essentially that used by Heyduk and Lee[20,21]. If [L] approximates $[L_T]$, a simpler equation may be derived from Equation 1.13:

$$A = A_f + (A_b - A_f)\left[\frac{K_a[L]}{1 + K_a[L]} \right] \quad [1.16]$$

1.2 Stopped-flow

Introduction

Many methods are available for measuring the equilibrium binding constant of a protein with a ligand, where the ligand can be a small molecule or another macromolecule such as a protein or nucleic acid. However, many biological processes are controlled not by equilibrium constants but by the kinetics of the interaction between protein and ligand and for this reason it is necessary to measure the association and dissociation rate constants in order to fully understand a system. Although this can be done using surface plasmon resonance techniques, and in certain cases by NMR measurements, rapid-reaction methods are generally the method of choice if a suitable intrinsic optical probe exists in the system or an extrinsic probe can be introduced.

Rapid-reaction methods include stopped-flow techniques in which the solutions are rapidly mixed, or relaxation methods in which an equilibrium mixture is perturbed by rapid-changes in temperature (T-jump) or pressure (P-jump).

1.2.1 Principle of Operation of the Stopped-flow Instrument

The stopped-flow technique was originally developed by Chance and Gibson[22] from the continuous flow technique. Continuous flow was used by Hartridge and Roughton[23] to study the binding of oxygen to haemoglobin. Solutions of haemoglobin and oxygen were rapidly mixed together and passed down a glass tube (Figure l.6 a). The age of the reaction solution at any given point along the tube is defined by the flow rate and the volume between mixing and that point. Therefore, by making measurements along the length of the tube, the time course of the reaction could be followed. For example, if the mixed solution has a linear

flow rate of 10 metres/sec, making measurements every 1 cm gives the reaction profile at 1 msec time points. In this way, even though the measurements took several minutes to make at each point, reactions could be followed on the millisecond time scale. However, this technique is very expensive with regard to solution volumes and can only be used where large amounts of protein and ligand are readily available. The advent of photomultiplier tubes in the 1940s allowed light to be monitored on a rapid time scale and led to the development of the stopped-flow method, although use has been recently made of the continuous flow method which has allowed reactions on the sub-millisecond time scale to be measured.

In the stopped-flow technique[24], two solutions are rapidly mixed together and at any given point the age of the solution is defined by the flow rate and the volume between mixing and observation. However, by the use of a back syringe, the flow of mixed reactants is suddenly stopped and the reaction is followed in real time with a suitable detection system (Figure l.6 b). Figure 1.7 shows a typical stopped-flow trace which illustrates the processes occurring in the instrument where the recording device is storing data from 50 msec before the point when flow stops. The reaction is that of N-acetyl tryptophanamide with excess N-bromosuccinimide[25] which results in the loss of the N-acetyl tryptophanamide fluorescence. Initially we see the signal from the end of the previous run on the instrument which has negligible fluorescence.

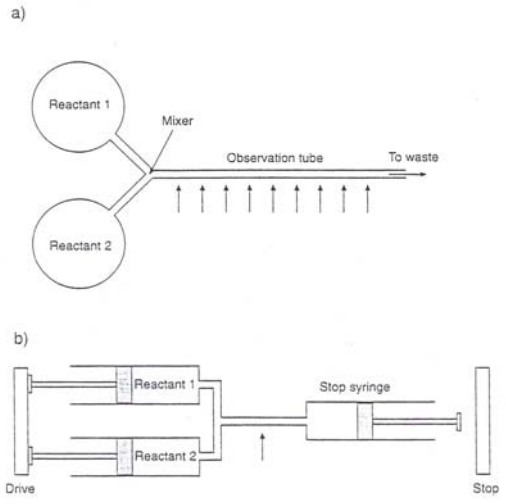

Figure 1.6 - Diagrammatic representations of (a) the continuous flow and (b) the stopped-flow methods. The arrows represent the points of observation[24]

When the reactant syringes are driven forward, the new solution displaces the old solution from the observation cell. Then a period of constant signal is seen. Over this time, the reactant solution has a constant age as described for the continuous flow method. This age is defined as the dead-time of the instrument and is the shortest time from which reactions can be monitored. When the flow stops, the reaction is followed with time.

In the above example, the reaction was followed by monitoring fluorescence. Owing to the inherent sensitivity of this method, it is widely used for stopped-flow studies although absorbance measurements are also used. Other specialized methods of detection that have been used include CD, NMR, FTIR, and calorimetry.

In a typical stopped-flow experiment, equal volumes of the two reactant solutions are mixed. The concentrations in the observation cell are therefore half of those in the syringe and it is important to define which concentration is being quoted.

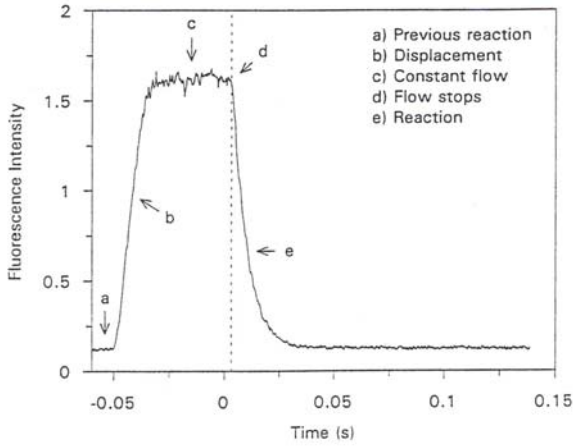

Figure 1.7 - A typical stopped-flow trace showing the different phases of the observed signal. In this example, the recording was commenced at 50 msec before flow stopped in order to illustrate all of the phases[24]

1.2.2 First- and Second-order Reactions

A short basic theory section, dealing with first- and second-order reactions[26,27,28], is necessary for a correct interpretation of data. Time courses can follow a number of mathematical forms depending on mechanism. The software that runs stopped-flow spectrophotometers provides fitting programs to extract rate constants. The operator must however decide the likely form of the curve and the time range over which the curves should be fitted.

1.2.2.1 First-order Irreversible Reactions

In a first-order reaction:

$$A \xrightarrow{k} B$$

the rate of loss of A is given by:

$$\frac{-d[A(t)]}{dt} = k[A(t)] \qquad [1.17]$$

Integrating gives:

$$\ln[A(t)] - \ln[A_0] = -kt \qquad [1.18]$$

where $[A_0]$ is the initial concentration of A, and [A(t)] is the concentration of A at time *t*. This can be rearranged to give:

$$\ln[A(t)] = \ln[A_0] - kt \qquad [1.19]$$

or

$$[A(t)] = [A_0]e^{-kt} \qquad [1.20]$$

Experimental data can be fitted to the linear equation (Equation 1.19) by plotting ln [A(t)] against *t* which gives a straight line of slope k. However, the use of nonlinear least squares fitting procedures allow the data to be fitted directly to Equation 1.20.

Two consequences of the properties of first-order reactions follow from these equations. First, since the value of kt is proportional to the natural logarithm of the ratio of $[A_0]$ to [A(t)], absolute concentration units for A(t) do not need to be measured, only some property which is proportional to the ratio of $[A_0]$ and [A(t)]. Secondly, the time taken to complete a definite fraction of the reaction is independent of the initial concentration of A. For example, for the reaction to proceed to 50% completion (i.e. when $[A_0]/[A(t)] = 2$) then substituting for $[A_0]/[A(t)]$ in Equation 1.18 gives:

$$t_{1/2} = \frac{\ln(2)}{k} = \frac{0.69}{k} \qquad [1.21]$$

where $t_{1/2}$ is the time taken for half the reaction to occur. This provides a rapid method for evaluating the value of k from the half-time of a first-order reaction.

1.2.2.2 Second-order irreversible reactions

Second-order reactions are best studied under one of two special conditions. The first of these is when the concentration of one of the reactants is in a large excess over the other and so does not effectively change over the time course of the reaction. This is called a pseudo first-order reaction. For the reaction:

$$A + B \xrightarrow{k} C$$

the rate of formation of C is given by:

$$\frac{d[C(t)]}{dt} = k[A(t)][B(t)] \qquad [1.22]$$

where [A(t)] and [B(t)] are the concentrations of A and B at time t.

If $[A_o] >> [B_o]$, [A(t)] can be regarded as a constant and equal to $[A_o]$, so the rate equation is:

$$\ln[B(t)] - \ln[B_0] = -([A_0]k)t \qquad [1.23]$$

This has the same form as Equation 1.18 where $k_{obs} = [A_o]\,k$ with units of sec^{-1}.

If the observed rate constant is determined with respect to [A_o], a plot of k_{obs} against [A_o] gives a straight line of slope k with units of M^{-1} sec^{-1} (if [A] is measured in M, i.e. mol/L).

The second condition under which a second-order reaction is often measured is when the concentrations of the two reactants are equal. Equation 1.22 then becomes:

$$\frac{d[C(t)]}{dt} = k[A(t)]^2 \qquad [1.24]$$

which on integration gives:

$$\frac{1}{[A(t)]} - \frac{1}{[A_0]} = kt \qquad [1.25]$$

and the experimental data can be fitted to this equation. It should be noted that the initial concentrations of reactants need to be known since the second-order constant involves a concentration term. In this case, at half completion of the reaction:

$$[A(t)] = [A_0]/2 \qquad [1.26]$$

so

$$\frac{2}{[A_0]} - \frac{1}{[A_0]} = kt_{1/2} \qquad [1.27]$$

or

$$t_{1/2} = \frac{1}{k[A_0]} \qquad [1.28]$$

Unlike first-order reactions, the half-time of the reaction is dependent on the concentration of A_0 and so the half-time progressively increases as the reaction proceeds.

If neither of the two special conditions can be used, the general equation for a second-order reaction is:

$$kt = \frac{1}{[A_0] - [B_0]} \ln \frac{[B_0][A(t)]}{[A_0][B(t)]} \qquad [1.29]$$

1.2.2.3 First-order reversible reaction

The above discussions have assumed that the reactions under study are irreversible. This is usually not true in practice. If a first-order reaction is reversible:

$$A \underset{k_{-1}}{\overset{k_1}{\rightleftharpoons}} B$$

At equilibrium:

$$K = \frac{[B_{eq}]}{[A_{eq}]} = \frac{k_1}{k_{-1}} \qquad [1.30]$$

where K is the equilibrium constant for the reaction and $[A_{eq}]$ and $[B_{eq}]$ are the concentrations of A and B at equilibrium. At equilibrium:

$$k_1[A_{eq}] = k_{-1}[B_{eq}] \qquad [1.31]$$

The rate of approach to equilibrium is given by:

$$k_1([A_0] - [B_{eq}]) - k_{-1}[B_{eq}] = 0 \qquad [1.32]$$

$$[A_0] = \frac{k_{-1}}{k_1}[B_{eq}] + [B_{eq}] \qquad [1.33]$$

$$\frac{d[B(t)]}{dt} = k_1([A_0] - [B(t)]) - k_{-1}[B(t)] \qquad [1.34]$$

$$\frac{d[B(t)]}{dt} = k_{-1}[B_{eq}] + k_1[B_{eq}] - k_1[B(t)] - k_{-1}[B(t)] \qquad [1.35]$$

$$= (k_{-1} + k_1)([B_{eq}] - [B(t)]) \qquad [1.36]$$

This has the same form as an irreversible first-order reaction (Equation 1.17) except that the observed rate constant is the sum of k_1 and k_{-1}. When k_{-1} is reduced to zero, this equation becomes equivalent to Equation 1.17.

Knowledge of the equilibrium constant allows individual values of k_1 and k_{-1} to be determined from Equation 1.30.

1.2.2.4 Second-order Reversible Reactions

As with irreversible second-order reactions, these are best done under pseudo first-order conditions for ease of analysis of the data.

In the scheme:

$$A + B \underset{k_{-1}}{\overset{k_1}{\rightleftharpoons}} AB$$

k_1 is the second-order association rate constant and k_{-1} is the first-order dissociation rate constant. If [A] is much larger than [B], its concentration is effectively constant during the time course of the reaction.

If [B(t)] is the concentration of B at time t and $[B_{eq}]$ is the concentration of B at equilibrium, $[B_o]$ is the concentration of B at time zero, and similar notations are used for the concentrations of A and AB.

At equilibrium:

$$k_1[A][B_{eq}] = k_{-1}[AB_{eq}] \quad [1.37]$$

Therefore

$$k_1[A][B_{eq}] - k_{-1}[AB_{eq}] = 0 \quad [1.38]$$

Since [A] remains constant throughout the reaction, $k_1[A]$ is a constant and is defined here as k'. Therefore:

$$k'[B_{eq}] - k_{-1}[AB_{eq}] = 0 \quad [1.39]$$

since:

$$[B_{eq}] = [B_0] - [AB_{eq}]$$

$$k'([B_0] - [AB_{eq}]) - k_{-1}[AB_{eq}] = 0$$

$$k'[B_0] - k'[AB_{eq}] - k_{-1}[AB_{eq}] = 0$$

$$[B_0] = \frac{k'[AB_{eq}] + k_{-1}[AB_{eq}]}{k'} \quad [1.40]$$

$$= \frac{k_{-1}}{k'}[AB_{eq}] + [AB_{eq}] \quad [1.41]$$

The rate of formation of AB is given by the equation:

$$\frac{d[AB(t)]}{dt} = k'[B(t)] - k_{-1}[AB(t)] \quad [1.42]$$

Since:

$$[B(t)] = [B_0] - [AB(t)]$$

$$\frac{d[AB(t)]}{dt} = k'([B_0] - [AB(t)]) - k_{-1}[AB(t)] \quad [1.43]$$

By using equation 25 for substituting $[B_0]$:

$$= k'((k_{-1}/k')[AB_{eq}] + [AB_{eq}] - [AB(t)]) - k_{-1}[AB(t)]$$

$$= k_{-1}[AB_{eq}] + k'[AB_{eq}] - k'[AB(t)] - k_{-1}[AB(t)]$$

$$= (k_{-1} + k')([AB_{eq}] - [AB(t)]) \quad [1.44]$$

This has the same form as a first-order reaction shown in Equation 1.17. A plot of $\ln([AB_{eq}] - [AB(t)])$ against time will therefore yield an observed first-order rate constant, k_{obs}, which is equal to $k' + k_{-1}$. Since $[AB_{eq}] = [B_o] - [B_{eq}]$ and $[AB(t)] = [B_o] - [B(t)]$, a plot of $\ln([B(t)] - [B_{eq}])$ will yield the same information. Again, concentrations need not to be in any specific units and any parameter proportional to concentration of the species can be used.

If the reaction is performed over a range of concentrations of A, the dependence of k_{obs} on $[A_0]$ can be measured. Since:

$$k_{obs} = k_1[A_0] + k_{-1} \qquad [1.45]$$

a plot of k_{obs} against $[A_0]$ will give a straight line of slope k_1 (second-order rate constant; units, M^{-1} sec^{-1}) and intercept on the ordinate of k_{-1} (first-order rate constant; units, sec^{-1}). Hence k_1 and k_{-1} can be determined together with the value of the equilibrium dissociation constant (k_{-1}/k_1) for the reaction.

1.2.3 Measurement of association and dissociation rate constants

As described in Section 1.2.2.2, second-order reactions are best studied under conditions where the concentrations of the reactants are such that one is in a large excess over the other or that the concentrations of both reactants are equal. This makes the analysis easier although the advent of global analysis methods reduces these restrictions. However, in the following discussion, use is made of pseudo first-order conditions in which there is excess ligand over protein. The question arises of what exactly a large excess means. Gutfreund[26] simulated a ligand binding reaction at different ratios of reactant concentrations and then fitted the simulated data to single exponentials. He showed that analysing the data over 97% of the theoretical time course, a three-fold excess of one reagent gave a 11% error in the fitted rate constant whereas a ten-fold excess gave only a *3%* error. However, it should be noted that in practice when the concentration of the excess reactant approaches that of the other, the reaction becomes more second-order, with a long 'tail' and so the end-point may not be well defined, thus increasing the error. It is important that the end-point of the reaction is well defined. If it is chosen before the real end of a first-order reaction, the rate constant derived will be faster than the actual rate constant, and if chosen before the end of a second-order reaction may show a perfectly good fit to a first-order reaction.

For excess reactant conditions (pseudo first-order), it is best to have the fluorophore attached to the low reactant concentration species, since in the opposite case, the background signal will be increased as the concentration of excess reactant increases. However, in certain cases this may be overcome by making use of fluorescence energy transfer which enables the bound form of the fluorophore to be excited selectively. For example, Woodward *et al.*[29] studied the interaction of myosin subfragment 1 with 2'-0-(3'-0)-N-methyl-anthraniloyl ATP by exciting the tryptophans of the subfragment 1 and monitoring the fluorescence of the N-methylanthraniloyl moiety. In this way they were able to observe the interaction at 1 μM subfragment 1 with up to 100 μM ATP analogue and still have an observable signal.

Before making kinetic measurements it is preferable to perform a steady-state spectral titration of the protein and ligand.

1.2.4 Fluorescence Anisotropy

This, along with other fluorescence based methods, has already been covered in the previous subchapters. Here the attention is focused on its particular relevance to stopped-flow measurements. In fluorescence anisotropy measurements a fluorophore is excited with vertically polarized light and the intensity I of the emitted light polarized parallel (*par*) and perpendicular (*per*) to the plane of the exciting light is measured.

As stated before, there are two advantages of making fluorescence anisotropy measurements over intensity measurements. First, since the anisotropy of a fluorophore is related to its rotational correlation time, changes in anisotropy give structural information. Secondly, fluorescence anisotropy changes may occur during a binding process which are not accompanied by an intensity change.

For stopped-flow fluorescence anisotropy measurements, the instrument first needs to be equipped with a polarizer filter on the excitation path which can be rotated through 90° to give light polarized either vertical or horizontal to the laboratory axis. It is best to make measurements in the 'T' format with two photomultipliers at right angles to the incident light, one with a polarizer filter monitoring light polarized parallel and one polarized perpendicular to the exciting light.

Since the two photomultipliers will respond differently to the intensity of the parallel and perpendicular light, it is first necessary to normalize them. This is done by exciting the fluorophore with horizontally polarized light. The amount of light depolarized to either the parallel or perpendicular planes to the photomultipliers will then be equal and so the high voltage on each photomultiplier is adjusted to give the same output signal.

The sample is then irradiated with vertically polarized light and the stopped-flow measurements made, recording the output from each photomultiplier simultaneously where I_{par} is the signal at the parallel photomultiplier and I_{per} is the signal at the perpendicular photomultiplier. Anisotropy is then calculated from the relationship given above and the total intensity can be determined from the relationship:

$$I = I_{par} + 2I_{per}$$

Therefore, at any given time the observed anisotropy in a reaction of A converting to B will be:

$$r_{obs}(t) = f_a(t)r_a + f_b(t)r_b \qquad [1.46]$$

where $f_a(t)$ and $f_b(t)$ are the fractional intensities of A and B respectively at time t, and r_a is the anisotropy of A and r_b is the anisotropy of B.

$$f_a(t) = \frac{[A(t)]}{[A(t)] + D[B(t)]} \qquad \text{and} \qquad f_b(t) = 1 - \frac{[A(t)]}{[A(t)] + D[B(t)]}$$

[1.47] [1.48]

Where D is the factor by which B is more fluorescent than A on a molar basis. Substituting the values of f_a and f_b into equation 1.46 shows that the anisotropy at any given time is given by:

$$r_{obs}(t) = \frac{[A(t)](r_a - r_b)}{[A(t)] + D[B(t)]} + r_b \qquad [1.49]$$

If A is decaying to B exponentially, then the concentrations of A and B at any given time are:

$$[A(t)] = [A_0]e^{-kt}$$

$$[B(t)] = [A_0] - [A(t)] \qquad [1.50]$$

where $[A_0]$ is the initial concentration of [A].

Substituting these equations into Equation 1.49 gives the observed anisotropy for the process at any given time as:

$$r_{obs}(t) = \frac{(r_a - r_b)}{(1 - D) + De^{kt}} + r_b \qquad [1.51]$$

By fitting the anisotropy data to this equation where D is determined from the relative values of the intensity at the start and end of the reaction, values of the observed rate constant from the anisotropy data agree with the intensity data. It should be noted that from inspection of Equation 1.51, the closer D is to unity, the closer the anisotropy data will be to a single exponential.

A fuller description of stopped-flow fluorescence anisotropy measurements is given by Otto et al.[30], and methods are presented where both the intensity and anisotropy data can be combined in a single analysis.

1.3 Probes to Monitor Stopped-flow Reactions

Introduction

In order to follow the reaction course, a signal is required whose changes on ligand binding can be monitored with time. This may be intrinsic to the system, or one of the components of the system is modified either covalently or non-covalently with an extrinsic probe[31]. Anyway, the ideal probe should have a high molar extinction coefficient and a high

quantum yield (so that it is easily detected by the system) and should allow faithful monitoring the reaction. Intrinsic fluorophores are those that occur naturally and include the aromatic amino acids, NADH, flavins, derivatives of pyridoxyl and chlorophyll. Extrinsic fluorophores are added to the sample to provide fluorescence when none exists or to change the spectral properties of the sample. Extrinsic fluorophores include dansyl, fluorescein, rhodamine and numerous other substances.

1.3.1 Intrinsic Probes

Intrinsic probes may be located within the protein, a prosthetic group or cofactor, such as flavins[32], NADH[33], pyridoxal-5'-phosphate[34] or a substrate or other ligand.

Intrinsic protein fluorescence originates with the aromatic amino acids[35,36,37] tryptophan (trp), tyrosine (tyr) and phenylalanine (phe) (Figure 1.8). The indole groups of tryptophan residues are the dominant source of UV absorbance and emission in proteins. Tyrosine has a quantum yield similar to tryptophan (Table 1.1) but its emission spectrum is more narrowly distributed on the wavelength scale (Figure 1.9). This gives the impression of a higher quantum yield for tyrosine. In native proteins the emission of tyrosine is often quenched, which may be due to its interaction with the peptide chain or energy transfer to tryptophan. Denaturation of proteins frequently results in increased tyrosine emission.

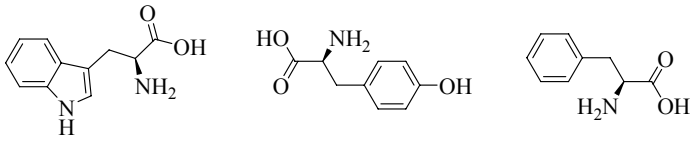

Tryptophan Tyrosine Phenylalanine

Figure 1.8 – Intrinsic biochemical fluorophores

Species	λ_{ex} (nm)	λ_{em} (nm)	Bandwidth (nm)	Quantum Yield	Lifetime (ns)
Phenylalanine	260	282	-	0.02	6.8
Tyrosine	275	304	34	0.14	3.6
Tryptophan	295	353	60	0.13	3.1 (mean)

Table 1.1 – Fluorescence Parameters of Aromatic Amino Acids in Water at Neutral pH[35]

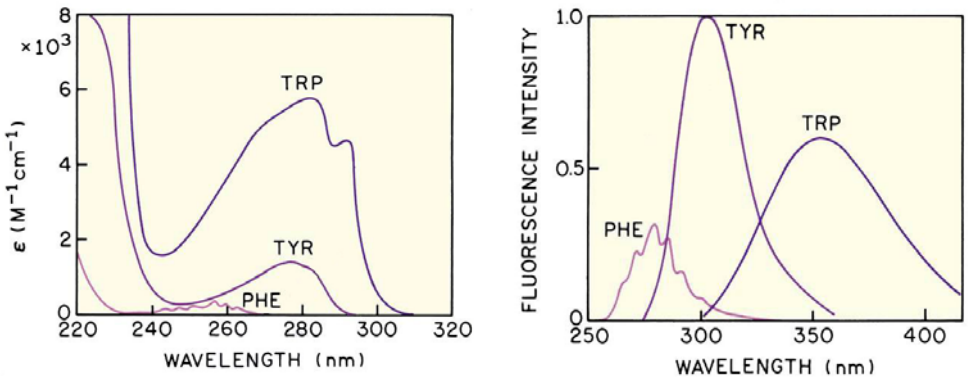

Figure 1.9 – Absorption and emission spectra of the fluorescent amino acids in water, pH 7.0[2]

The emission of tryptophan is highly sensitive to its local environment and is thus often used as a reporter group for protein conformational changes. Spectral shifts of protein emission have been observed as a result of several phenomena, including binding of ligands, protein-protein association and protein unfolding. Fluorescence lifetimes of tryptophan residues range from 1 to 6 ns. Tryptophan fluorescence is subject to quenching by iodide, acrylamide and nearby disulfide groups.

1.3.2 Extrinsic Probes

Extrinsic probes[31] must be used when the system under study has no useful intrinsic probes or a reaction produces no fluorescence change from intrinsic probes.

Extrinsic probes come in many forms such as non-covalently and covalently attached to the protein of interest at a specific site. Useful fluorescence is obtained by labelling the molecule with an extrinsic probe. For proteins it is frequently desirable to label them with chromophores with longer excitation and emission wavelengths than the aromatic amino acids.

1.3.2.1 Non-covalent Modification of Proteins

The most widely used compounds for non-covalent attachment to proteins are 1-anilinonaphtalene-8-sulphonate (1-8 ANS) and bis-ANS. These compounds are virtually non-fluorescent in aqueous solution but fluoresce intensely in apolar solvents or when partitioned into hydrophobic clefts or the core of a protein[38]. The emission wavelength maxima (around 480 nm and 500 nm in methanol for ANS and bis-ANS, respectively) are also highly dependent upon the polarity of the environment. They have found use in protein folding/unfolding studies[39]. ANS and bis-ANS have also been used to study protein conformational changes[40] and ligand binding[41].

1.3.2.2 Covalent Modification of Proteins and Ligands

Numerous fluorophores are available for covalent and non-covalent labelling of proteins. The covalent probes can have a variety of reactive groups for coupling with amines or sulfhydryl or histidine side chains in proteins. Some of the more widely used are shown in Figure 1.10. Dansyl chloride (DNS-Cl) was originally described by Weber[42] and he described the advantages of extrinsic probes in biochemical research.

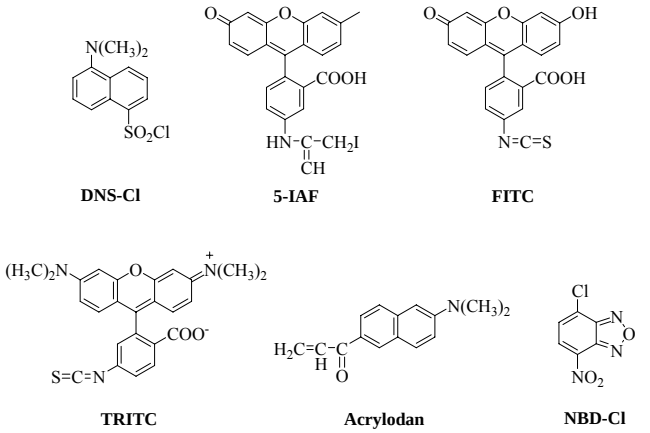

Figure 1.10 – Reactive probes for conjugation with macromolecules

Fluoresceins and rhodamines are also widely used as extrinsic labels (Figure 1.11). These dyes have long absorption maxima near 480 and 600 nm and emission wavelengths from 510 to 615 nm, respectively. Fluoresceins and rhodamines are not sensitive to solvent polarity and an additional reason for their widespread use is the high molar extinction coefficient near 80000 $M^{-1}cm^{-1}$. A wide variety of reactive derivative are available including iodoacetamides, isothiocyanates amd maleimides. Iodoacetamides and maleimides are typically used for labelling sulfhydryl groups, whereas isothiocyanates, N-hydroxysuccinimide and sulfonyl chlorides are used for labelling amines[43].

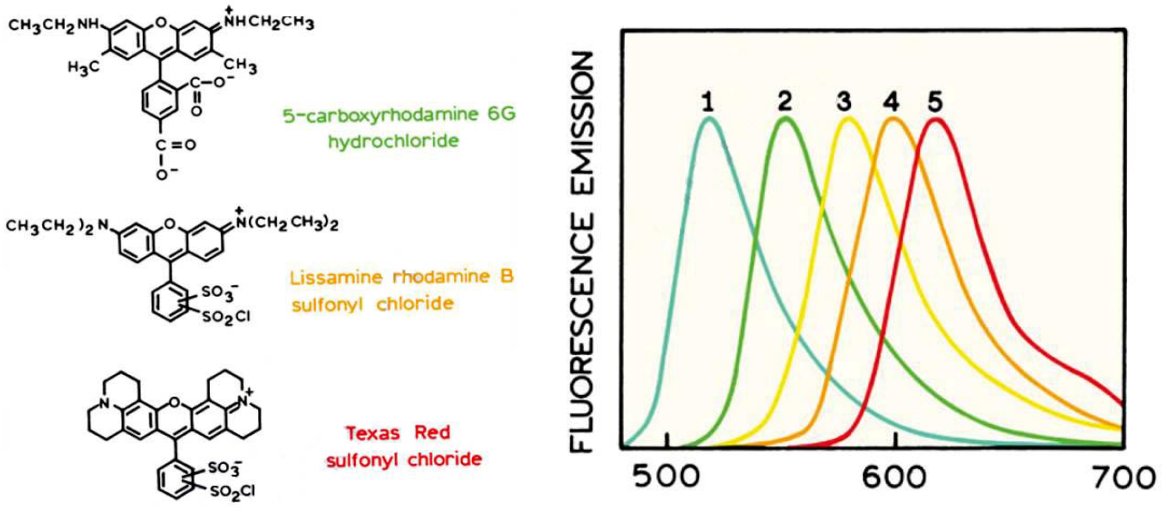

Figure 1.11 – Structures and normalized fluorescence emission spectra of goat anti-mouse IgG conjugates of (1) fluorescein, (2) rhodamine 6G, (3) tetramethylrhodamine, (4) Lissamine rhodamine B and (5) Texas Red dyes[2]

The reasons for selecting these probes include high quantum yields and the long wavelengths of absorption and emission, which minimized the problems of background fluorescence from biological samples and eliminate the need for quartz optics. The lifetimes of these dyes are near 4 ns and their emission spectra are suitable for quantifying the associations of small labelled molecules with proteins via changes in fluorescence polarization.

1.3.2.3 Near-Infrared (NIR) Dyes

The cyanine dyes were initially used as membrane potential probes and evolved into some of the more commonly used long-wavelength dyes. Long-wavelength probes are of current interest for several reasons. The sensitivity of fluorescence detection is often limited by the autofluorescence of biological samples. As the excitation wavelength becomes longer, the autofluorescence decreases and hence detectability over background increases[44]. Long-wavelength dyes can be excited with laser diodes. The most familiar long-wavelength dyes are the cyanine dyes such as the Cy-3, Cy-5 and Cy-7 in Figure 1.12. Such dyes have absorption and emission wavelengths above 550 nm[45]. The cyanine dyes typically display small Stokes shift with the absorption maxima about 30 nm blue shifted from the emission maxima, as shown for Cy-3. A wide variety of conjugatable cyanine dyes are available. Charged side chains are used for improved water solubility or to prevent self-association, which is a common cause of self-quenching in these dyes.

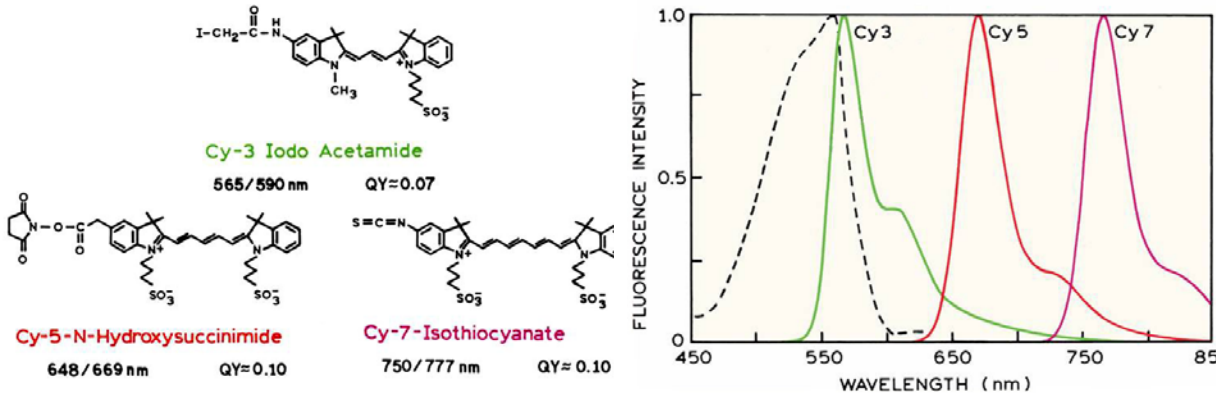

Figure 1.12 – Chemically reactive cyanine dyes. The dashed line shows the absorption spectrum of Cy3[2]

A diversity of molecules display fluorescence and numerous interactions and processes can alter the spectral properties. Fluorophores can be covalently attached to macromolecules or designed to interact with specific ions. Emission can occur from the UV to the NIR (Near-Infrared) and probes are available with short (ns) and long (μs to ms) lifetimes.

The technology of probe chemistry is rapidly changing and new probes are allowing previously impossible experiments to be performed.

1.4 Quenching

Introduction

Fluorescence quenching[2] refers to any process that decreases the fluorescence intensity of a sample. A variety of molecular interactions can result in quenching and it can occur by different mechanism. These include excited-state reactions, molecular rearrangements, energy transfer, ground-state complex formation and collisional quenching. Collisional quenching occurs when the excited-state fluorophore is deactivated upon contact with some other molecule in solution, which is called the quencher. Fluorescence quenching can occur by a variety of other processes. Fluorophores can form nonfluorescent complexes with quenchers. This process is referred to as static quenching since it occurs in the ground state and does not rely on diffusion or molecular collisions.

1.4.1 Theory of static quenching

Quenching can occur as a result of the formation of a nonfluorescent ground-state complex between the fluorophore and quencher. When this complex absorbs light it immediately returns to the ground state without emission of a photon (Figure 1.13).

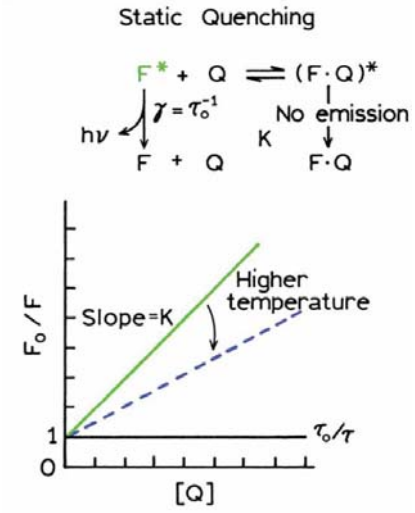

Figure 1.13 – Schematic representation of static quenching[2]

For static quenching the dependence of the fluorescence intensity upon quencher concentration is easily derived by consideration of the association constant for complex formation. This constant is given by

$$K_S = \frac{[F-Q]}{[F]\cdot[Q]} \qquad [1.52]$$

where [F-Q] is the concentration of the complex, [F] is the concentration of uncomplexed fluorophore and [Q] is the quencher concentration. If the complexed species is non-fluorescent then the fraction of the fluorescence that remains (F/F_0) is given by the fraction of the total fluorophores that are not complexed: $f = F/F_0$. Recalling that the total concentration of fluorophore [F_0] is given by:

$$[F_0] = [F] + [F-Q] \qquad [1.53]$$

substitution into equation 1.52 yields:

$$K_S = \frac{[F_0]-[F]}{[F]\cdot[Q]} = \frac{[F_0]}{[F]\cdot[Q]} - \frac{1}{[Q]} \qquad [1.54]$$

We can substitute the fluorophore concentration for fluorescence intensities and rearrangements of Equation 1.54 yields the so called Stern-Volmer equation for static quenching:

$$\frac{F_0}{F} = 1 + K_S[Q] \qquad [1.55]$$

Like for dynamic quenching, the dependence of F_0/F on [Q] is linear but the quenching constant is now the association constant. Unless additional information is provided, fluorescence quenching data obtained by intensity measurements alone can be explained by either dynamic or static processes. The magnitude of K_S can sometimes be used to demonstrate that dynamic quenching cannot account for the decrease in intensity. The measurement of fluorescence lifetimes is the most definitive method to distinguish static and dynamic quenching.

1.4.2 Combined Dynamic and Static Quenching

In many instances the fluorophore can be quenched both by collisions and by complex formation with the same quencher. The characteristic feature of the Stern-Volmer plots in such circumstances is an upward curvature, concave towards the *y*-axis (Figure 1.14).

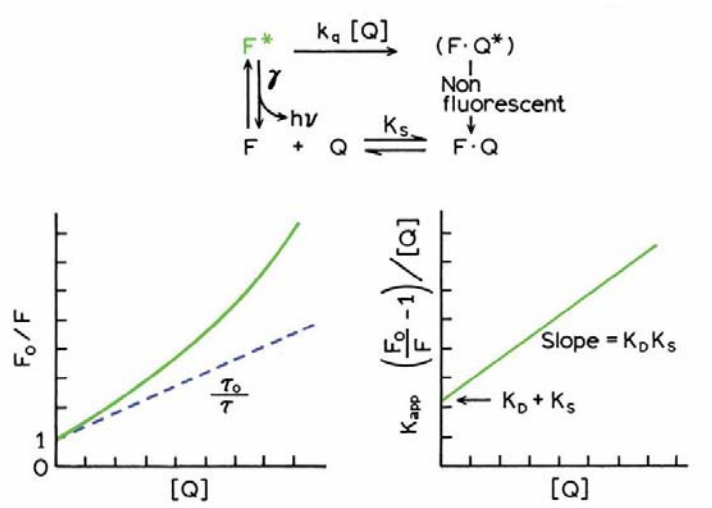

Figure 1.14 – Combined dynamic and static quenching of the same population of fluorophores[2]

Then the fractional fluorescence remaining (F/F_0) is given by the product of the fraction not complexed (f) and the fraction not quenched by collisional encounters. Hence

$$\frac{F}{F_0} = f\,\frac{\gamma}{\gamma + k_q[Q]} \qquad [1.56]$$

Knowing that $f^{-1} = 1+K_S[Q]$, inversion of Equation 1.56 and rearrangements of the last term on the right yields

$$\frac{F_0}{F} = (1 + K_D[Q])(1 + K_S[Q]) \qquad [1.57]$$

This modified form of the Stern-Volmer equation is second order in [Q], which accounts for the upward curvature observed when both static and dynamic quenching occur for the same fluorophore.

The dynamic portion of the observed quenching can be determined by lifetime measurements. That is, $\tau_0/\tau = 1+K_D[Q]$ the dashed line in figure 1.14. If lifetime measurements are not available, then equation 1.57 can be modified to allow a graphical separation of K_S and K_D. Multiplication of the terms in parentheses yields:

$$\frac{F_0}{F} = 1 + (K_D + K_S)[Q] + K_D K_S[Q]^2 \qquad [1.58]$$

$$\frac{F_0}{F} = 1 + K_{app}[Q] \qquad [1.59]$$

where

$$K_{app} = \left[\frac{F_0}{F} - 1\right]\frac{1}{[Q]} = (K_D + K_S) + K_D K_S[Q] \qquad [1.60]$$

The apparent quenching constant is calculated at each quencher concentration. A plot of K_{app} versus [Q] yields a straight line with an intercept of K_D+K_S and a slope of $K_S K_D$

(Figure 1.14). The individual values can be obtained from the two solutions of the quadratic equation.

1.4.3 Fluorescence Quenching for Binding Studies

Fluorescence quenching measurements have been widely used to study the interactions of organic compounds with proteins[46,47,48]. This method can reveal accessibility of quenchers to protein's fluorophores, help understanding proteins' binding mechanisms to compounds and provide clues to the nature of the binding phenomenon.

A great number of papers appeared dealing with protein-ligand interactions quenching studies. One of the most studied protein is certainly Bovine Serum Albumin (BSA) for its availability, low cost, stability and unusual ligand-binding properties.

One of the latest paper[49] concerning protein-ligand interaction studies provided an approach for studying the binding of a protein (BSA) to rose bengal (RB) by employing absorption, fluorescence, circular dichroism (CD) and lifetime measurements. The analysis of fluorescence data showed that the BSA fluorescence was quenched by RB through both dynamic and static quenching.

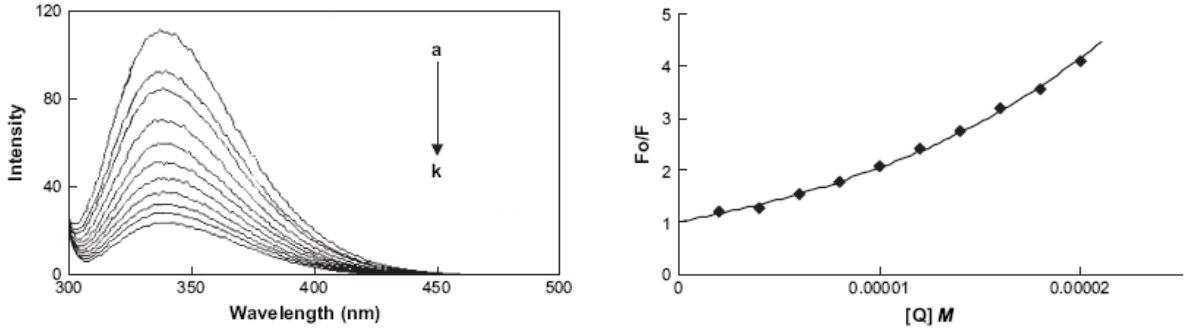

Figure 1.15 – Left: Fluorescence spectra of BSA in the presence of RB. BSA concentration was fixed at 12 mM (a). RB concentrations were 2 (b), 4 (c), 6 (d), 8 (e), 10 (f), 12 (g), 14 (h), 16 (i), 18 (j), and 20 mM (k). Right: Stern-Volmer plot for the binding of RB to BSA

The spectral data have revealed the conformational changes in BSA upon interaction with RB and various binding parameters have been evaluated. The thermodynamic parameters, ΔH^0 and ΔS^0 were observed to be -79.61 kJ mol^{-1} and -143.37 J mol^{-1} K^{-1}, respectively. The negative value of ΔG^0 reveals that the interaction process is spontaneous. An important source of negative contribution to ΔH^0 and ΔS^0 will arise if a hydrogen bond is formed[50]. The negative ΔH^0 and ΔS^0 values for the interaction of RB and BSA indicate that the binding is mainly enthalpy driven and entropy is unfavourable for it, and that the hydrogen bonding and van der Waals forces played major role in the interaction. The quantitative analysis of CD results revealed that the α-helicity of BSA decreased from 66.4%

(in free BSA) to 48.64% (in bound BSA). The binding average distance, r between the BSA tryptophans (2) (donor) and RB (acceptor) was determined based on Förster's theory and it was found to be 2.75 nm. The effects of common ions on the binding constant of RB-BSA were also examined.

Another work by the same authors[48] appeared providing an approach for studying the binding of BSA with bromopyrogallol red (BPR) using absorption, fluorescence, CD and lifetime measurements. The results showed that BSA fluorescence was quenched by BPR through both dynamic and static quenching. The value of n was determined approximately equal to 1 indicating that there is one class of binding site to BPR in BSA. In BSA, the tryptophan residues involved in binding could be either Trp 135 or Trp 214. Of both tryptophans in BSA, Trp 135 is more exposed to a hydrophilic environment, whereas Trp 214 is deeply buried in the hydrophobic loop[51]. So, from the value of n it is proposed that BPR most likely binds to the hydrophobic pocket located in subdomain II A; that is to say Trp 214 is near or within the binding site[52].

The binding of wogonin with BSA[53] was also investigated at different temperatures by fluorescence, CD and Fourier transform infrared spectroscopy (FT-IR) at pH 7.40. The association constants K_a were determined by Stern-Volmer equation based on the quenching of the fluorescence of BSA in the presence of wogonin, which were in agreement with the constants calculated by Scatchard plots. The thermodynamic parameters were calculated according to the Van't Hoff equation and the result indicated that ΔH^0 and ΔS^0 had a negative value (-12.02 kJ/mol) and a positive value (58.72 J/mol K), respectively. On the basis of the displacement experimental and the thermodynamic results, it is considered that wogonin binds to site I (subdomain IIA) of BSA mainly by hydrophobic interaction. Sudlow *et al.*[54] have suggested two distinct binding sites on BSA, site I and site II, site I of BSA showed affinity for warfarin, phenylbutazone, etc. and site II for ibuprofen, flufenamic acid etc. Digitoxin binding is independent of sites I and II[53]. To determine the specificity of the drug binding, competition experiments were performed with phenylbutazone, flufenamic acid, and digitoxin in connection with Sudlow's classification of the binding sites. Table 1.2 shows the changes in fluorescence of wogonin bound to BSA on the addition of other drugs.

K (without the site probe (10^5 M^{-1})	K (with PB) (10^5 M^{-1})	K (with FA) (10^5 M^{-1})	K (with Dig) (10^5 M^{-1})
1.53	1.26	1.62	1.42

Table 1.2 - The comparison of binding constant of wogonin to BSA before and after the addition of the site probe, 296 K

Wogonin was not significantly displaced by flufenamic acid or by digitoxin (site III). However, phenylbutazone (site I) gave a significant displacement of wogonin suggesting that wogonin binding site on BSA is site I, so the site I is the main binding site for wogonin binding to BSA through hydrophobic force. The studied results by FT-IR and CD experiment indicated that the secondary structures of protein have been perturbed by the interaction of wogonin with BSA.

Reference List

1. Ward, L. D. Measurement of ligand binding to proteins by fluorescence spectroscopy. *Methods Enzymol.* **1985,** *117*, 400-414.

2. Lakowicz, J. R. *Principles of Fluorescence Spectroscopy;* Third ed.; Springer-Verlag: New York, 2006.

3. Jablonski, A. On the notion of the emission anisotropy. *Bull. Acad. Pol. Sci. Ser. A* **1960,** *8*, 259-264.

4. Perrin, F. Polarisation de la lumière de fluorescence: vie moyenne des molécules dans l'état excité. *J. Phys. Radium* **1926,** *7*, 390-401.

5. Perrin, F. La Fluorescence des solutions: induction moleculaire. Polarisation et durée d'emission. Photochimie. *Ann. Phys.* **1929,** *12*, 169-275.

6. Perrin, F. Fluorescence: durée élémentaire d'émission lumineuse. *Conférences D'Actualités Scientifiques et Industrielles* **1931,** *22*, 2-41.

7. Lakowicz, J. R.; Gryczynski, I.; Laczko, G.; Wiczk, W.; Johnson, M. L. Distribution of distances between the tryptophan and the N-terminal residue of melittin in its complex with calmodulin, troponin C, and phospholipids. *Protein Sci.* **1994,** *3*, 628-637.

8. Jameson, D. M. Gregorio Weber, 1916-1997: A Fluorescent Lifetime. *Biophys. J.* **1998,** *75*, 419-421.

9. Weber, G.; Bablouzian, B. Construction and Performance of a Fluorescence Polarization Spectrophotometer. *J. Biol. Chem.* **1966,** *241* (11), 2558-2561.

10. Kingery, J. R.; Sowinski, K. M.; Kraus, M. A.; Klaunig, J. E.; Mueller, B. A. Vancomycin assay performance in patients with end-stage renal disease receiving hemodialysis. *Pharmacotherapy* **2000,** *20* (6), 653-656.

11. Westphal, K.; Weinbrenner, A.; Giessmann, T.; Stuhr, M.; Franke, G.; Zschiesche, M.; Oertel, R.; Terhaag, B.; Kroemer, H. K.; Siegmund, W. Oral bioavailability of digoxin is enhanced by talinolol: Evidence for involvement of intestinal P-glycoprotein. *Clin. Pharmacol. Ther.* **2000,** *68* (1), 6-12.

12. Bolger, R.; Wiese, T. E.; Ervin, K.; Nestich, S.; Checovich, W. Rapid Screening of Environmental Chemicals for Estrogen Receptor Binding Capacity. *Environ. Health Perspect.* **1998,** *106* (9), 551-557.

13. Lundblad, J. R.; Laurance, M.; Goodman, R. H. Fluorescence Polarization Analysis of Protein-DNA and Protein-Protein Interactions. *Mol. Endocrinol.* **1996,** *10*, 607-612.

14. Murakami, A.; Nakaura, M.; Nakatsuji, Y.; Nagahara, S.; Trancong, Q.; Makino, K. Fluorescent-Labeled Oligonucleotide Probes - Detection of Hybrid Formation in Solution by Fluorescence Polarization Spectroscopy. *Nucleic Acid Res.* **1991,** *19* (15), 4097-4102.

15. Jiskoot, W.; Hoogerhout, P.; Beuvery, E. C.; Herron, J. N.; Crommelin, D. J. A. Preparation and Application of Fluorescein-Labeled Peptide for Determining the Affinity Constant of a Monoclonal-Antibody Hapten Complex by Fluorescence Polarization. *Anal. Biochem.* **1991,** *196* (2), 421-426.

16. Okamoto, T.; Ueda, K.; Maeda, H.; Kambara, T. Determination of lysozyme activity by fluorescence polarization in rheumatoid synovial fluids and release of lysozyme from polymorphonuclear leukocytes by chemotactic factors. *J. Immunol. Methods* **1987,** *103* (2), 221-227.

17. Coxon, R. E.; Hodginson, A. J.; Sidki, A. M.; Landon, J.; Gallacher, G. *Ther. Drug Monitor.* **1987,** *9*, 478-483.

18. Busby, T. F.; Ingham, K. C. Thermal stability and ligand-binding properties of human plasma alpha 1-acid glycoprotein (orosomucoid) as determined with fluorescent probes. *Biochim. Biophys. Acta* **1986,** *871* (1), 61-71.

19. Shiotsuki, K.; Hirata, T.; Ota, M.; Kimura, K.; Hiyoshi, Y.; Yamashita, F.; Yokoyama, M. M. Characterization of lymphocytes in a patient with Wiskott-Aldrich syndrome: studies by fluorescence polarization. *J. clin. lab. immunol.* **1989,** *28* (4), 201-205.

20. Heyduk, T.; Lee, J. C.; Ebright, Y. W.; Blatter, E. E.; Zhou, Y. H.; Ebright, R. H. CAP Interacts with RNA-Polymerase in Solution in the Absence of promoter DNA. *Nature* **1993,** *364* (6437), 548-549.

21. Heyduk, T.; Lee, J. C. Application of fluorescence energy transfer and polarization to monitor Escherichia coli cAMP receptor protein and lac promoter interaction. *Proc. Natl. Acad. Sci. USA* **1990,** *87*, 1744-1748.

22. Gibson, Q. H. Rapid mixing: Stopped flow. *Methods Enzymol.* **1969,** *16*, 187-228.

23. Roughton, F. J. W. *Rates and mechanisms of reactions;* Wiley: New York, 1963.

24. Eccleston, J. F.; Hutchinson, J. P.; White, H. D. Stopped-flow Techniques. In *Protein-ligand Interactions, Structure and Spectroscopy: A Practical Approach*, Harding, S. E., Chowdhry, B. Z., Eds.; Oxford University Press: 2001; pp 201-237.

25. Peterman, B. F. Measurement of the Dead Time of a Fluorescence Stopped-flow Instrument. *Anal. Biochem.* **1979,** *93*, 442-444.

26. Gutfreund, H. *Kinetics for the life sciences;* Cambridge University Press: Cambridge, 1995.

27. Fersht, A. *Enzyme structure and mechanism;* 2nd ed.; W. H. Freeman & Co.: New York, 1984.

28. Johnson, K. A. *The enzymes;* 1992; Vol. 20.

29. Woodward, S. K. A.; Eccleston, J. F.; Geeves, M. A. Kinetics of the Interaction of 2'(3')-O-(N-Methylanthraniloyl)-ATwPi th Myosin Subfragment 1 and Actomyosin Subfragment 1 : Characterization of Two Acto4 1-ADP Complexes. *Biochemistry* **1991,** *30* (2), 422-430.

30. Otto, M. R.; Lillo, M. P.; Beechem, J. M. Resolution of Multiphasic Reactions by the Combination of Fluorescence Total-intensity and Anisotropy Stopped-Flow Kinetic Experiments. *Biophys. J.* **1994,** *67*, 2511-2521.

31. Gore, M. G.; Bottomley, S. P. Stopped-flow Fluorescence Spectroscopy. In *Spectrophotometry & Spectrofluorimetry*, Gore, M. G., Ed.; Oxford University Press: 2000; pp 241-264.

32. Chaiyen, P.; Brissette, P.; Ballou, D. P.; Massey, V. Thermodynamics and Reduction Kinetics Properties of 2-Methyl-3-hydroxypyridine-5-carboxylic Acid Oxygenase. *Biochemistry* **1997,** *36*, 2612-2621.

33. Holbrook, J. J.; Yates, D. W.; Reynolds, S. J.; Evans, R. W.; Greenwood, C.; Gore, M. G. Protein Fluorescence of Nicotinamide Nucleotide-Dependent Dehydrogenases. *Biochem. J.* **1972,** *128*, 933-940.

34. Ikushiro, H.; Hayashi, H.; Kawata, Y.; Kagamiyama, H. Analysis of the pH- and Ligand-Induced Spectral Transitions of Tryptophanase: Activation of the Coenzyme at the Early Steps of the Catalytic Cycle. *Biochemistry* **1998,** *37*, 3043-3052.

35. Demchenko, A. P. *Ultraviolet Spectroscopy of Proteins;* Springer-Verlag: New York, 1981.

36. Longworth, J. W. Luminescence of Polypeptides and proteins. In *Excited State of Proteins and Nucleic Acids*, Steiner, R. F., Welnryb, I., Eds.; Plenum: New York, 1971; pp 319-484.

37. Permyakov, E. A. *Luminescent Spectroscopy of Proteins;* CRC Press: London, 1993.

38. Slavik, J. Anilinonaphthalene sulfonate as a probe of membrane composition and function. *Biochim. Biophys. Acta* **1982,** *694* (1), 1-25.

39. Jones, B. E.; Beechem, J. M.; Matthewsu, C. R. Anilinonaphthalene sulfonate as a probe of membrane composition and function. *Biochemistry* **1995,** *34*, 1867-1877.

40. Gibbons, D. L.; Horowitz, P. M. Exposure of Hydrophobic Surfaces on the Chaperonin Groel Oligomer by Protonation or Modification of HIS-401. *J. Biol. Chem.* **1995,** *270* (13), 7335-7340.

41. Lin, Z.; Schwarz, F. P.; Eisenstein, E. The Hydrophobic Nature of Groel-Substrate Binding. *J. Biol. Chem.* **1995,** *270* (3), 1011-1014.

42. Weber, G. Polarization of the Fluorescence of Macromolecules. *Biochem. J.* **1952,** *51*, 155-167.

43. Waggoner, A. Covalent labeling of proteins and nucleic acids with fluorophores. *Methods Enzymol.* **1995,** *246*, 362-373.

44. Thompson, R. B. Red and near-infrared fluorometry. In *Topics in Fluorescence Spectroscopy*, Lakowicz, J. R., Ed.; Plenum Press: New York, 1994; pp 151-152.

45. Buschmann, V.; Weston, K. D.; Sauer, M. Spectroscopic Study and Evaluation of Red-Absorbing Fluorescent Dyes. *Bioconjugate Chem.* **2003,** *14*, 195-204.

46. Bi, S.; Song, D.; Tian, Y.; Zhou, X.; Liu, Z.; Zhang, H. Molecular spectroscopic study on the interaction of tetracyclines with serum albumins. *Spectrochim. Acta A* **2005,** *61*, 629-636.

47. Feng, X. Z.; Lin, Z.; Yang, L. J.; Wang, C.; Bai, C. Investigation of the interaction between acridine orange and bovine serum albumin. *Talanta* **1998,** *47*, 1223-1229.

48. Shaikh, S. M. T.; Seetharamappa, J.; Ashoka, S.; Kandagal, P. B. A study of the interaction between bromopyrogallol red and bovine serum albumin by spectroscopic methods. *Dyes and Pigments* **2007,** *73*, 211-216.

49. Shaikh, S. M. T.; Seetharamappa, J.; Kandagal, P. B.; Manjunatha, D. H.; Ashoka, S. Spectroscopic investigations on the mechanism of interaction of bioactive dye with bovine serum albumin. *Dyes and Pigments* **2007,** *74*, 665-671.

50. Ross, P. D.; Subramanian, S. Thermodynamics of Protein Association Reactions: Forces Contributing to Stability. *Biochemistry* **1981,** *20*, 3096-3102.

51. Deepa, S.; Mishra, A. K. Fluorescence spectroscopic study of serum albumin–bromadiolone interaction: fluorimetric determination of bromadiolone. *J. Pharm. Biomed. Anal.* **2005,** *38*, 556-563.

52. Sulkowska, A. Interaction of drugs with bovine and human serum albumin. *J Mol Struct* **2002,** *614*, 227-232.

53. Tian, J.; Liu, J.; Hub, Z.; Chen, X. Interaction of wogonin with bovine serum albumin. *Bioorg. Med. Chem.* **2005,** *13*, 4124-4129.

54. Sudlow, G.; Birkett, D. J.; Wade, D. N. The Characterization of Two Specific Drug Binding Sites on Human Serum Albumin. *Mol. Pharm.* **1975,** *11*, 824-832.

Chapter 2 – Bioconjugation

2.1 Introduction

Bioconjugation[1] involves the linking of two or more molecules (one of them being a biological molecule at least) to form a novel complex having the combined properties of its individual components. Natural or synthetic compounds with their individual activities can be chemically combined to create unique substances possessing carefully engineered characteristics. Thus, a protein able to bind discretely to a target molecule within a complex mixture may be cross-linked with another molecule capable of being detected to form a traceable conjugate. The detection component provides visibility for the targeting component, producing a complex that can be localized, followed through various processes, or used for measurements.

Through careful modification or conjugation strategies, the structure and function of proteins can be investigated, active site conformation discovered, or receptor-ligand interactions revealed. Without the development of bioconjugate chemistry to produce the associated labelled, modified, or conjugated molecules, much of life science research as we know it today would be impossible.

Modification and conjugation techniques are dependent on two interrelated chemical reactions: the reactive functional groups present on the various cross-linking or derivatizing reagents and the functional groups present on the target macromolecules to be modified. Without both types of functional groups being available and chemically compatible, the process of derivatization would be impossible.

Protein molecules are perhaps the most common targets for modification or conjugation techniques. As the mediators of specific activities and functions within living organisms, proteins can be used *in vitro* and *in vivo* to effect certain tasks. Having enough quantity of a protein that can bind a particular target molecule can result in a way to detect or assay the target, providing the protein behaviour which can be followed or measured by some experimental technique. If such a protein does not possess an easily detectable component, it often can be modified to contain a chemical or biological tracer to allow detectability. This type of protein complex can be designed to retain its ability to bind its natural target, while the tracer portion can provide the means to find and measure the location and amount of target molecules.

Detection, assay, tracking or targeting of biological molecules by using the appropriately modified proteins are the main areas of application for modification and

conjugation systems. The ability to produce a labelled protein having a specificity for another molecule provides the key component for much of biological research, clinical diagnostics and human therapeutics.

2.2 Tags and Probes

Tags and probes are relatively small modifying agents that can be used to label proteins, nucleic acids and other molecules. These compounds often contain groups that provide sensitive detectability by virtue of some intrinsic chemical or atomic property such as fluorescence, visible chromogenic character, radioactivity or bioaffinity toward another protein. Most probes can be designed to contain a reactive portion capable of coupling to the functional groups of biomolecules. After modification of a protein via this reactive part, the probe becomes covalently attached, thus permanently tagging it with a unique detectable property.

Fluorescent labels can provide tremendous sensitivity due to their large quantum emission yield upon excitation. Proteins, nucleic acids and other molecules can be labelled with fluorescent probes to provide highly receptive reagents for numerous *in vitro* assay procedures. For instance, fluorescently tagged antibodies can be used to probe cells and tissues for the presence of particular antigens and then detected through the use of fluorescence microscopy techniques.

There are many fluorophores available for a wide range of applications and each with a different reactive group (amine-reactive and thiol-reactive) able to couple to specific functional groups or target molecules.

2.3 Thiol-Reactive Dyes

Thiol-reactive dyes are principally used to prepare fluorescent peptides, proteins and oligonucleotides for probing biological structure, function and interactions. Because the thiol functional group is not very common in most proteins and can be labelled with high selectivity, thiol-reactive reagents often provide a means of modifying a protein at a defined site. Thiol-reactive probes can be used to:

- analyze the topography of proteins in biological membranes using polar thiol-reactive fluorescent reagents;
- determine distances within the protein or between the protein and a ligand using excited-state energy transfer;

- follow changes in protein conformation using environment-sensitive probes;
- site-selectively label proteins in order to study protein–protein and protein–nucleic acid interactions using fluorescence anisotropy[2].

In proteins, thiol groups (also called mercaptans or sulfhydryls) are present in cysteine residues. Thiols can also be generated by selectively reducing cystine disulfides with reagents such as dithiothreitol (DTT)[3] or 2-mercaptoethanol, each of which must then be removed by dialysis or gel filtration before reaction with the thiol-reactive probe[4]. Unfortunately, removal of DTT or 2-mercaptoethanol is sometimes accompanied by air oxidation of the thiols back to the disulfides. Reformation of the disulfide bond can be avoided by using the reducing agent tris-(2-carboxyethyl)phosphine[5,6] which usually does not need to be removed prior to thiol modification because it does not contain thiols.

The common thiol-reactive functional groups are primarily alkylating reagents, including iodoacetamides, maleimides, benzylic halides and bromomethylketones. Arylating reagents such as NBD halides react with thiols or amines by a similar substitution of the aromatic halide by the nucleophile. Reaction of any of these functional groups with thiols usually proceeds rapidly at or below room temperature in the physiological pH range (pH 6.5–8.0) to yield chemically stable thioethers.

2.3.1 Maleimides

Maleimides are excellent reagents for thiol-selective modification, quantitation and analysis. In this reaction, the thiol is added across the double bond of the maleimide to yield a thioether (Figure 2.1).

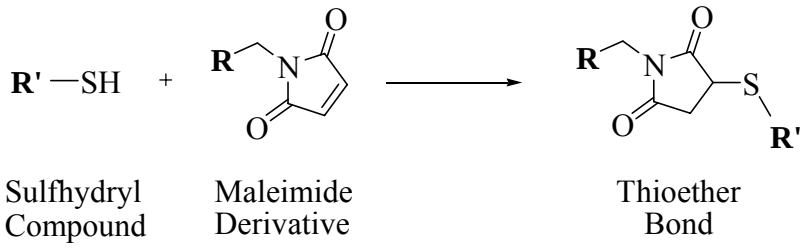

Figure 2.1 – Scheme of thioether bond formation

Reaction of maleimides with amines usually requires a higher pH than reaction of maleimides with thiols. Hydrolysis of the maleimide to an unreactive product can compete significantly with thiol modification, particularly above pH 8. Furthermore, once formed, maleimide adducts can hydrolyze to an isomeric mixture of maleamic acid adducts, which may cause a significant change in the fluorescence properties of the conjugate[7], or they can

ring-open by nucleophilic reaction with an adjacent amine to yield crosslinked products[8]. This latter reaction can potentially be enhanced by raising the pH above 9 after conjugation. Several maleimides including 7-diethylamino-3-(4'-maleimidylphenyl)-4-methylcoumarin and *N*-(7-dimethylamino-4-methylcoumarin-3-yl)maleimide, as well as the pyrene and stilbene derivatives are not appreciably fluorescent until after conjugation with thiols, and may therefore be useful for thiol quantitation.

2.3.2 Fluorescein Derivatives

Fluorescein is perhaps the most popular of all fluorescent labelling agents. Its fluorescent character is created by the presence of a multiring aromatic structure due to the planar nature of its upper, fused three-ring system (Figure 2.2).

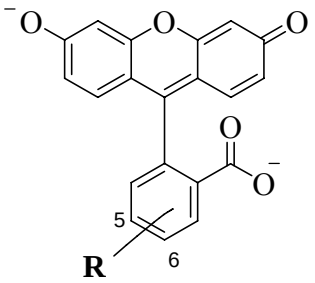

Figure 2.2 – Reactive Fluorescein Derivatives, Fluorescein derivatives are produced through modification at the C-5 or C-6 position on the lower ring

2.3.3 Fluorescein-5-maleimide

Fluorescein-5-maleimide is a fluorescent probe containing a sulfhydryl-reactive maleimide group on its lower ring structure. Modification of sulfhydryl-containing molecules under physiological pH conditions results in stable thioether bonds (Figure 2.1). The double bond of maleimides may undergo an alkylation reaction with sulfhydryl groups to form stable thioether bond.

Maleimide reactions are specific for sulfhydryl groups in the pH range 6.5-7.5[9,10,11,12]. At pH 7.5, the reaction of the maleimide with sulfhydryls proceeds at a rate 1000 times greater than its reaction with amines.

The derivative thus possesses fluorescent properties closely characteristic of fluorescein molecules: excitation wavelength = 490 nm; emission wavelength = 515 nm, in the green spectral region.

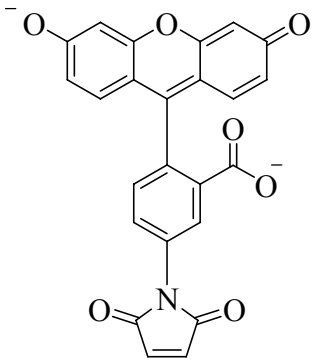

Figure 2.3 –Fluorescein-5-maleimide

Conjugates prepared by fluorescein-5-maleimide are among the most intensely fluorescent probes available. Fluorescein-5-maleimide has been used in numerous applications, including labelling the transmembrane glycoprotein H-2K^k on both the N- and the C-terminal regions to investigate the structure of the molecule[13], for the determination of two different conformations of the protein actin[14], in the study of a bacterial sensory receptors[15], in the structural mapping of chloroplast coupling factor[16] for localization of the stilbenedisulfonate receptor on human erythrocytes[17], in investigating the calcium-dependent ATPase protein structure of sarcoplasmic reticulum[18], and to study the movement of tRNA during peptide bond formation on ribosomes[19].

- **Bioconjugation Protocol**

1) The sulfhydryl-containing protein was dissolved at a concentration of 1-10 mg/ml in 20 mM sodium phosphate, 0.15 M NaCl, pH 7.2.
2) Fluorescein-5-maleimide was dissolved in DMF at a concentration of 10 mM protecting it from light.
3) A 25-fold molar excess of fluorescein-5-maleimide solution was added to the protein solution.
4) The solution was allowed to react for 2-4 h at room temperature in the dark.
5) The derivative was immediately purified using gel filtration on PD10 columns Sephadex® G-25 (Amersham Bioscience) using a phosphate buffer saline solution (pH=7.4) as eluent. It is important to protect the solutions from light during the chromatography.

The dye/protein ratios (**D/P**) of the conjugates were determined by the absorption spectra of the labelled proteins, registered in PBS (pH=7.4) according to the relationship:

$$D/P = \frac{A_{\max} \cdot \varepsilon_{prot}}{(A_{280} - cA_{\max}) \cdot \varepsilon_{dye}}$$

where A_{280} is the absorption of the conjugate at 280 nm; A_{max} is the absorption of the conjugate at the absorption maximum of the corresponding fluorescein-5-maleimide; *c* is the correction factor (*c*=0.29 for fluorescein dyes); $\varepsilon_{protein}$ and ε_{dye} (63096 cm^{-1} M^{-1}) are the molar extinction coefficients for the protein used and fluorescein-5-maleimide, respectively.

Extinction coefficient of the free dye (ε_{dye}) was calculated from the slope of a Lambert-Beer plot while extinction coefficient of the protein was calculated.

The molar extinction coefficient of a protein can be estimated from knowledge of its amino acid composition[20]. From the molar extinction coefficient of tyrosine, tryptophan and cystine (cysteine does not absorb appreciably at wavelengths >260 nm, while cystine does) at a given wavelength, the extinction coefficient of the native protein in water can be computed using the following equation[21]:

$$\varepsilon = (nW \times 5500) + (nY \times 1490) + (nC \times 125)$$

where *n* is the number of each tryptophan (W), tyrosine (Y) and cysteine (C) residue respectively and the stated values are the amino acid molar absorptivities at 280 nm.

2.3.4 Synthesis of Fluorescein-5-maleimide[22]

- **Synthesis of N-(5-Fluoresceinyl)maleamic Acid**

To a stirred solution of amine **I** (2.88 mmol) in AcOH (300 ml) maleic anhydride (2.88 mmol) was added and the resulting solution was stirred at r.t. for 4 hours. Precipitated amic acid **II** was filtered, washed with EtOAc (600 ml), dried and used as such without further purification.

Yield: 74%

Yellow solid

Mp: >300°C

- **Synthesis of N-(5-Fluoresceinyl)maleimide**

HMDS (Hexamethyldisilazane) (1.37 g, 8.48 mmol) was added to a stirred suspension of amic acid **II** (0.95 g, 2.12 mmol) and $ZnCl_2$ (0.58 g, 4.24 mmol) in a mixture of benzene (115 ml) and DMF (13 ml) and the resulting mixture was refluxed for 2.5 h. After cooling to r.t., the mixture was filtered and filtrate was concentrated under vacuum. The residual DMF portion was poured into ice-water (50 ml) and the aqueous phase was acidified tp pH 4.0 by adding 0.1 N HCl. On cooling, fluorescein-5-maleimide **III** (0.84 g) was obtained in 92.3% yield as an orange-yellow solid, mp>300°C.

^{1}H NMR (DMSO-d^6): δ = 10.20 (s, 2H), 8.00 (d, J = 1.1 Hz, 1H), 7.80 (dd, J = 1.6, 8.2 Hz, 1H), 7.42 (d, J = 8.1 Hz, 1H), 7.28 (s, 2H), 6.55-6.71 (m, 6H).

MS (ESI): m/z (%) = 428 (M-1), 458 (M -1, 33)

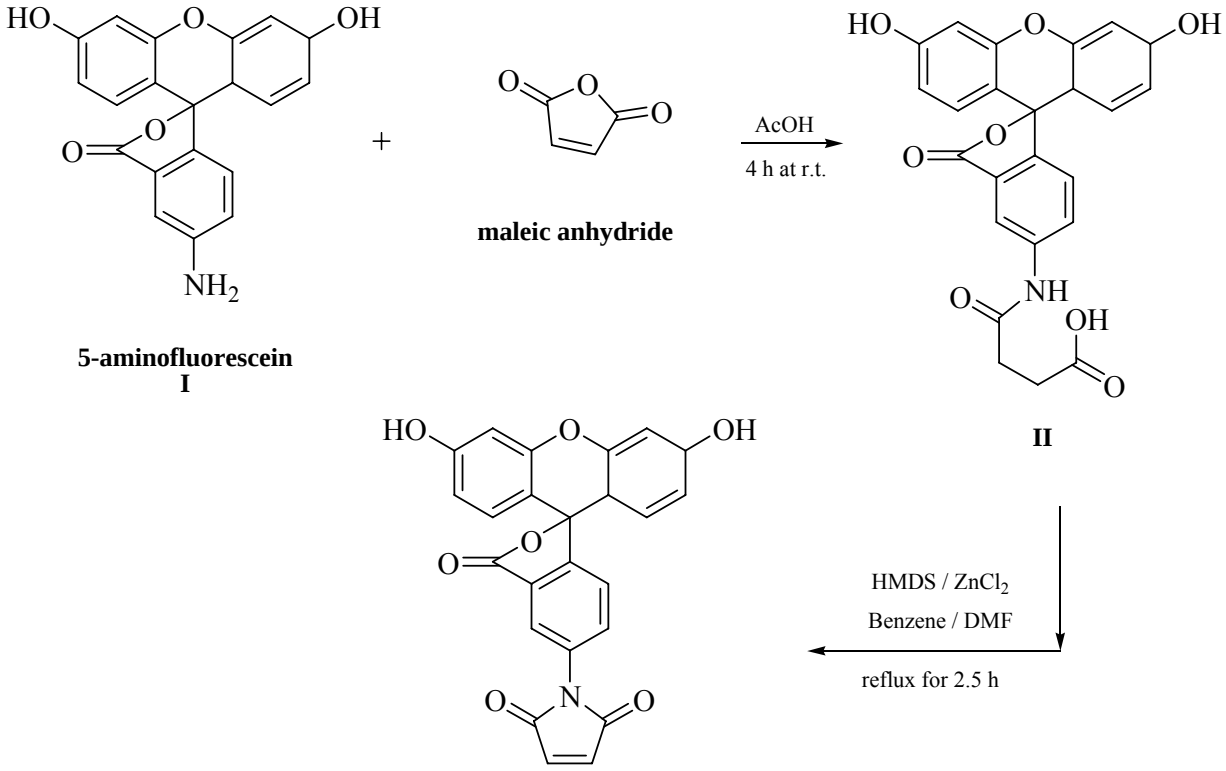

Figure 3.4 – Synthesis of fluorescein-5-maleimide

Reference List

1. Hermanson, G. T. *Bioconjugate Techniques;* Academic Press: 1996.

2. Rusinova, E.; Tretyachenko-Ladokhina, V.; Vele, O. E.; Senear, D. F.; Ross, J. B. A. Alexa and Oregon Green dyes as fluorescence anisotropy probes for measuring protein–protein and protein–nucleic acid interactions. *Anal. Biochem.* **2002,** *308*, 18-25.

3. Gorman, J. J.; Corino, G. L.; Mitchell, S. J. Fluorescent labeling of cysteinyl residues Application to extensive primary structure analysis of proteins on a microscale. *Eur. J. Biochem.* **1987,** *168*, 169-179.

4. Jocelyn, P. C. Chemical reduction of disulfides. *Methods Enzymol.* **1987,** *143*, 246-256.

5. Getz, E. B.; Xiao, M.; Chakrabarty, T.; Cooke, R.; Selvin, P. R. A Comparison between the Sulfhydryl Reductants Tris(2-carboxyethyl)phosphine and Dithiothreitol for Use in Protein Biochemistry. *Anal. Biochem.* **1999,** *273*, 73-80.

6. Burns, J. A.; Butler, J. C.; Moran, J.; Whitesides, G. M. Selective Reduction of Disulfides by Tris(2-carboxyethy1)phosphine. *J. Org. Chem.* **1991,** *56*, 2648-2650.

7. Ishii, Y.; Lehrer, S. S. Effects of the state of the succinimido-ring on the fluorescence and structural properties of pyrene maleimide-labeled $_{\alpha\alpha}$-tropomyosin. *Biophys. J.* **1986,** *50*, 75-80.

8. Wu, C.-W.; Yarbrough, L. R.; Wu, F. Y.-H. N-(1-Pyrene)maleimide: A Fluorescent Cross-Linking Reagent. *Biochemistry* **1976,** *15* (13), 2863-2868.

9. Smyth, D. G.; Blumenfeld, O. O.; Konigsberg, W. Reactions of N-Ethylmaleimide with Peptides and Amino Acids. *Biochem. J.* **1964,** *91*, 589-595.

10. Heitz, J. R.; Anderson, C. D.; Anderson, B. M. Inactivation of yeast alcohol dehydrogenase by N-alkylmaleimides. *Arch. Biochem. Biophys.* **1968,** *127*, 627.

11. Gorin, G.; Martin, P. A.; Doughty, G. Kinetics of the reaction of N-ethylmaleimide with cysteine and some congeners. *Arch. Biochem. Biophys.* **1966,** *115*, 593.

12. Partis, M. D.; Griffiths, D. G.; Roberts, G. C.; Beechey, R. B. Cross-linking of protein by ω-maleimido alkanoyl N-hydroxysuccinimido esters. *J. Biol. Chem.* **1983,** *257*, 9640-9647.

13. Cardoza, J. D.; Kleinfeld, A. M.; Stallcup, K. C.; Mescher, M. F. Hairpin Configuration of H-2K^k in Liposomes Formed by Detergent Dialysis. *Biochemistry* **1984,** *23*, 4401-4409.

14. Konno, K.; Morales, M. F. Exposure of actin thiols by the removal of tightly held calcium ions. *Proc. Natl. Acad. Sci. USA* **1985,** *82*, 7904-7908.

15. Falke, J. J.; Dernburg, A. F.; Sternberg, D. A.; Zalkin, N.; Milligan, D. L.; Koshland, D. E. **Structure of a Bacterial Sensory Receptor**. *J. Biol. Chem.* **1988,** *263* (29), 14850-14858.

16. Snyder, B.; Hammes, G. G. Structural Mapping of Chloroplast Coupling Factor. *Biochemistry* **1984,** *23*, 5787-5795.

17. Rao, A.; Martin, P.; Reithmeier, R. A. F.; Cantley, L. C. Location of the Stilbenedisulfonate Binding Site of the Human Erythrocyte Anion-Exchange System by Resonance Energy Transfer. *Biochemistry* **1979,** *18* (21), 4505-4516.

18. Bigelow, D. J.; Inesi, G. Frequency-Domain Fluorescence Spectroscopy Resolves the Location of Maleimide-Directed Spectroscopic Probes within the Tertiary Structure of the Ca- ATPase of Sarcoplasmic Reticulum. *Biochemistry* **1991,** *30*, 2113-2125.

19. Odom, O. W.; Picking, W. D.; Hardesty, B. Movement of tRNA but Not the Nascent Peptide during Peptide Bond Formation on Ribosomes. *Biochemistry* **1990,** *29*, 10734-10744.

20. Gill, S. C.; von Hippel, P. H. Calculation of protein extinction coefficients from amino acid sequence data. *Anal. Biochem.* **1989,** *182*, 319-326.

21. Pace, C. N.; Vajdos, F.; Fee, L.; Grimsley, G.; Gray, T. How to measure and predict the molar absorption coefficient of a protein. *Protein Sci.* **1995,** *4*, 2411-2423.

22. Reddy, P. Y.; Kondo, S.; Fujita, S.; Toru, T. Efficient synthesis of fluorophore-linked maleimide derivatives. *Synthesis* **1998,** *7*, 999-1002.

Chapter 3 – BSA interaction with Fluorescein sodium salt

3.1 BSA in binding studies

Serum albumins are the most extensively studied and applied proteins because of its availability, low cost, stability and unusual ligand-binding properties. For this reason, a huge number of papers and reviews dealing with albumins have been published so far[1,2]. Albumin is the most abundant protein in blood plasma and serves as a depot protein and transport protein for numerous endogenous and exogenous compounds. Albumin is also the principal factor in contributing to the colloid osmotic pressure of the blood and has been suggested as a possible source of amino acids for various tissues. Without question, albumin is the most multifunctional transport protein and plays an important role in the transport and deposition of a variety of endogenous and exogenous substances in blood[3] due to the existence of a limited number of binding regions of very different specificity[2,4].

Perhaps, the most outstanding property of albumin is its capacity to bind reversibly a numerous variety of ligands[2,4]. The physiological importance of albumin and the relative ease with which it can be isolated and purified on a large scale have resulted in a great number of binding studies. Reviews have previously appeared dealing, in relatively general terms, with binding of small molecules to albumin and other proteins[2,4]. These proteins have the interesting properties of binding a variety of hydrophobic ligands such as fatty acids, lysolecithin, bilirubin, warfarin, tryptophan, steroids, anaesthetics and several dyes[2,3].

Most ligands are bound reversibly and typical association constants (K_a) range from 10^4 to 10^6 M^{-1}. Because of the incredible diversity of ligands bound by albumin, early researchers saw ligand binding to serum albumin as non-specific in nature and did not recognize that there were discrete sites per se. Instead they envisaged the ligands as randomly attached to the surface, somewhat like a sponge. This view of albumin has changed over the past years, and now it is generally recognized that there are a small number of distinct binding locations[2].

Bovine Serum Albumin (BSA) is constituted by 582 amino acid residues and on the basis of the distribution of the disulfide bridges and of the amino acid sequence it seems possible to regard BSA as composed of three homologous domains linked together. The domains can all be subdivided into two subdomains. As proposed by Kragh-Hansen[4], there are at least six binding regions and another characteristic feature of albumin-ligand interactions seems to be the presence of one or two high affinity binding sites (primary sites) and a number of sites with lower affinity.

Albumin is clearly an extraordinary molecule of manifold functions and applications. Quenching measurements of albumin fluorescence is an important method to study the interactions of compounds with protein[5,6,7]. It can reveal accessibility of quenchers to albumin's fluorophores, help understanding albumin's binding mechanisms to compounds and provide clues to the nature of the binding phenomenon.

Dyes are being increasingly used in clinical and medicinal applications[8,9,10]. The discovery that some dyes would stain certain tissues and not others led to the idea that dyes might be found that would selectively stain, combine with and destroy pathogenic organisms without causing appreciable harm to the host. Actually, some azo, thiazine, triphenyl methane and acridine dyes came into use as antiseptic trypanocides and for other medicinal purposes[11]. It is also known that certain dyes like fluorescein and rose bengal are preferentially adsorbed by cancerous cells[10].

Many drugs and other bioactive small molecules bind reversibly to albumin and other serum components, which then function as carriers. Serum albumin often increases the apparent solubility of hydrophobic drugs in plasma and modulates their delivery to cell in vivo and in vitro. Consequently, it is important to understand the mechanism of interaction of a bioactive compound with protein.

Drug-protein interactions are important since most of the drugs and other bioactive small molecules are extensively and reversibly bound to serum albumin and they are transported mainly as a complex with protein. The nature and magnitude of drug-protein interaction influences the biological activity (efficacy and rate of delivery) of the drug[12]. Many drugs, including anti-coagulants, tranquillizers, and general anaesthetics, are transported in the blood while bound to albumin[13]. It is then important to study the binding parameters in order to know and try to control the pharmacological response of drugs and design of dosage forms. This kind of studies may provide salient information on the structural features that determine the therapeutic effectiveness of drugs/dyes, and hence become an important research field in chemistry, life science and clinical medicine[12,14,15]. Serum albumin is considered as a model for studying drug-protein interaction in vitro since it is the major binding protein for drugs and other physiological substances.

The use of dyes for protein determination is well established[16,17]. However, other parameters such as mode of interaction, association constant and number of binding sites are important, when dyes are used as drugs. Several spectrophotometric methods such as fluorescence, UV-Vis, CD, Light Scattering, FT-IR, nuclear magnetic resonance (NMR) have been used to study the interaction of small molecules and proteins and clarify the conformational change of protein[7,18,19]. Some techniques such as electrochemical technique[20]

and capillary electrophoresis[21] have also been utilized for the evaluation of binding mode and binding constants. Among them, fluorescence spectroscopy has been widely used due to its exceptional sensitivity, selectivity, convenience and abundant theoretical foundation. Critical literature survey reveals that attempts have not been made so far to investigate the mechanism of interaction of fluorescein sodium salt (Figure 3.1) with BSA. The present work deals with the mechanism of binding of fluorescein sodium salt with different BSA by fluorescence steady-state and stopped-flow measurements. A complete study dealing with fluorescein sodium salt and BSA coming from different purification processes is also reported for the first time.

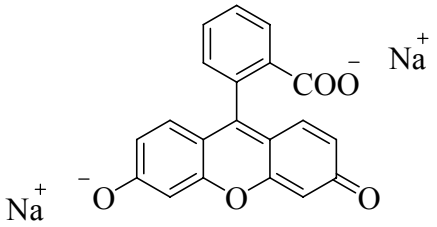

Figure 3.1 - Structure of Fluorescein Sodium Salt

3.2 Quantitative Determination of Equilibrium Binding Isotherms for Ligand-Macromolecule Interactions

The binding of fluorescein sodium salt with different kinds of BSA was investigated at different temperatures by fluorescence and absorption measurements at pH 7.50.

Various binding parameters have been evaluated. The thermodynamic parameters have also been investigated by performing the interaction at different temperature (15, 25 and 40°C).

The association and dissociation constants K_a and K_d were determined by the quenching of the fluorescence of BSA in the presence of fluorescein (see Chapter 1). Agreement was found for the constants calculated by different methods, i.e. Lineweaver-Burk, the Stern-Volmer equation and a non linear regression method using a one site binding model. The number of binding sites (n) was also determined by using a modified Stern-Volmer equation.

Thermodynamic studies provide information that is necessary in order to understand the forces that drive the formation of ligand-macromolecule complexes. Knowledge of the energetics of these interactions is also indispensable for characterization of functionally important structural changes that occur within the studied complexes. Quantitative examination of the equilibrium interactions are designed to provide the stoichiometry of the

formed complexes, how strong or how specific are the interactions, how the equilibrium binding and kinetics parameters depend on solution variables (temperature, pressure, pH, salt concentration, etc.) and what are the molecular forces involved in the formation of the studied complexes.

Equilibrium isotherms for the binding of a ligand to a macromolecule represent the relationship between the degree of ligand binding and the free ligand concentration. A true thermodynamic binding isotherm is model-dependent and reflects only this relationship.

Any method used to quantitatively study ligand binding to a macromolecule must relate the extent of the complex formation to the free ligand concentration in solution. Numerous techniques have been developed to study equilibrium properties of specific and non-specific ligand-macromolecule interactions in which binding is directly monitored, including equilibrium dialysis, ultrafiltration, column chromatography, filter binding assay and gel electrophoresis[22,23]. These direct methods are very straightforward; however they are usually time consuming and some, like filter binding or gel shift assays, are non-equilibrium techniques which require careful control before the reliable equilibrium binding data can be obtained. Therefore, these direct methods are usually applied to system where the indirect spectroscopic approaches cannot be used, due to the lack of suitable signal changes accompanying the formation of the complex.

Using indirect methods, the binding of the ligand is determined by measuring the physico-chemical parameter of the macromolecule-ligand mixture, most often a spectroscopic one, e.g. absorbance, circular dichroism or fluorescence. The change in the physico-chemical parameter is than correlated with the concentration of the free and bound species. The advantages of using spectroscopic measurements are that these can be performed without perturbing the equilibrium and are relatively easy to apply.

Two types of titrations can be performed in order to examine a binding isotherm in studies of ligand-macromolecule interactions. In one case, the macromolecule is titrated with a ligand and is usually referred to as a *normal* titration, since the total average degree of binding increases as the titration progresses.

In the second case, the ligand is titrated with the macromolecule. This type of titration is usually called a *reverse* titration, since the binding density decreases throughout the titration[24]. Generally, the type of titration that is performed depends on whether or not the signal that is monitored is from the macromolecule (normal) or the ligand (reverse).

3.2.1 Experimental

- *Reagents*

Different kinds of Bovine Serum Albumin (BSA) were obtained from Sigma-Aldrich and were used as received:

BSA	Manufacturer code	Purity	Further Purification
A	Fluka - 05488	>96%	1) heat shock 2) charcoal 3) extensive dialysis
B	Fluka - 05479	>92%	1) heat shock
C	Aldrich - A 7030	>98%	1) heat shock 2) charcoal

*Table 3.1 – Different BSA used. NB: Heat shock purification removes **globulins** and Charcoal or organic solvent (i.e. iso-octane) precipitation removes **fatty acids***

Fluorescein Sodium Salt for fluorescence was purchased from Fluka and used without any further purification. The solutions of Fluorescein Sodium Salt and BSA were prepared in 0.1 M HEPES (from Sigma-Aldrich) buffer of pH 7.5.

All reagents were of analytical reagent grade and double distilled water was used throughout. BSA solution was prepared based on its molecular weight of 66,000.

- *Apparatus*

Fluorescence measurements were recorded using a LS55 Perkin Elmer spectrofluorimeter equipped with a xenon lamp source, a 5 mm path length quartz cell and a thermostat bath.

UV-Vis measurements were recorded using a Shimadzu UV-1700 Pharma Spec Spectrophotometer equipped with 1.0 cm path length quartz cells.

- *Experimental procedures*

Experiments were performed in a time drive mode in order to check whether the solution had reached the stability. Samples were excited at 295 nm and monitored at 350 nm in order to selectively excite the BSA Trp residues. Slits widths were 2.5/5 nm.

After pre-equilibration, the appropriate amount of protein stock solution was added and the fluorescence signal monitored until stable. The sample was then titrated with aliquots (10 or 20 μl) of fluorescein sodium salt solution. Fluorescence spectra were recorded at 15, 25 and 40°C.

Titrations carried out by an addition of ligand causes dilution of the protein and hence reduction of the fluorescence intensity. For this reason, the volume dilution was kept

minimum (total added volume was 320 μl) and a simple correction factor based on the added volume was used for obtaining a correct measure of fluorescence intensity.

- *Effect of protein concentration on measurement of dissociation constant*

Based on preliminary experiments, BSA concentration was kept fixed at 1 μM and drug concentration was varied from 0.1 to 2 μM. Actually, to obtain accurate binding constants from fluorescence measurements, the protein concentrations titrated should be near or less than the dissociation constant and the concentration of ligand should be varied from two orders of magnitude below to two orders of magnitude above the K_d[25]. In all ligand-binding experiments, protein concentration is held constant and increasing concentrations of ligand are added. Monitoring quenching of tryptophan fluorescence yielded much better signal to noise ratio than monitoring increases in ligand fluorescence.

If the total protein concentration is much less than the dissociation constant of the protein–ligand complex, then the free ligand concentration $[L_f] >> \sum_i [P{\cdot}L_i]$, where $[P{\cdot}L_i]$ values are the concentrations of different protein–ligand complexes. In such a case the quenching profile is devoid of any significant stoichiometric information and the dissociation constant can be extracted directly.

When the protein concentration is much higher than the dissociation constant of the protein–ligand complex, virtually all added ligand will form complex until saturation. In this case, only stoichiometric information is present at the break point, which is devoid of any information about the binding constant. These situations are shown in Figure 3.2. Clearly it is difficult to extract any information about the dissociation constant with protein concentrations about one order of magnitude higher than the dissociation constant. If the protein concentration is in between, information about both stoichiometry and the binding constant is present and can be extracted.

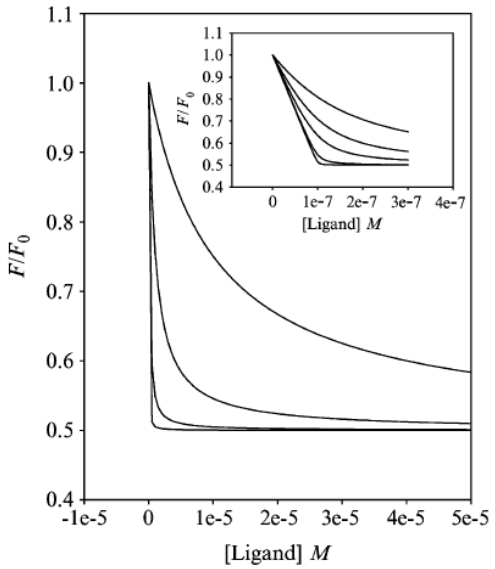

Figure 3.2 - Simulation of the effect of relative values of protein concentration and the dissociation constant. The protein concentration was fixed at 10^{-7}M and the curves from right to left are for K_d values of 10^{-5}, 10^{-6}, 10^{-7}, and 10^{-8}M, respectively. Inset: The stoichiometric points in detail. The curves are for K_d values of 10^{-7}, $3 \cdot 10^{-8}$, 10^{-8}, 10^{-9}, and 10^{-10}M from right to left. The simulation was carried out with SigmaPlot, using a single-site binding equation

Thus, the choice of protein concentration is critical for estimating the dissociation constant. It is preferable to have the protein concentration below the dissociation constant of the protein–ligand complex. In systems where ligand–protein dissociation constants are so low that one is compelled to work at submicromolar concentrations, the stability of the protein, from both biological and spectroscopic point of view, becomes important. In several cases in which the protein concentration was kept low, we have seen red shifting of emission maxima on incubation at temperatures above 30°C. This may be a consequence of lower stability of some proteins at low concentrations and may be catalyzed by solid surface. The stability of the protein must be ascertained before proceeding with the titration, particularly if the titration is carried out at low protein concentrations and relatively high temperatures. The sensitivity of currently available spectrofluorometers allows use of protein concentration up to about 10^{-8} M, depending on its tryptophan content. Hence ligand-protein dissociation constants in the subnanomolar range are at present inaccessible by this method.

- *Total Intensity Correction*

This correction is necessary because of the intrinsic bias introduced by the right angle observation geometry. When carrying out intensity measurements on systems that show changes in polarisation (such as fluorescein binding to BSA) one must be careful to obtain the true total intensity which means exciting with parallel polarized light and determining the

parallel and perpendicular intensities of the emission. Then total intensity equals the parallel intensity plus two times the perpendicular intensity.

- *Inner Filter Effect*

The biggest problem in the measurement of internal aromatic fluorescence quenching comes from the inner filter effect (IFE). Many ligands have strong absorbance in the range of excitation and emission wavelengths normally used for tryptophan fluorescence measurements (280–295 and 330–350 nm, respectively). The inner filter effect arises from the fact that although a typical cuvette has a cross-section of 10 · 10 mm, the actual volume from which the fluorescence is observed is in the middle of the cross-section and is small. Before the exciting light reaches that volume or the emitted light reaches the photomultiplier tube, the light must travel through the absorbing solution. If the absorbance is high, the light intensity reaching the active volume or the photomultiplier tube is reduced. Thus the absorbing solution acts as a filter and the effect is known as the inner filter effect. If the ligand has absorbance at the emission or excitation wavelength, it is mandatory that a correction for the inner filter effect be employed. The simplest correction for inner filter effect is given by the following formula and is widely used.

$$F_{corr} = F_{obs} \cdot 10^{(A_{ex}+A_{em})\cdot L/2} \qquad [3.1]$$

Where L is the pathlength of the cuvette used, the A terms are the absorbances at the excitation and emission wavelengths, and the F values are the corrected and observed fluorescence intensities.

UV-Vis measurements were performed in order to check if inner filter effect was to be considered. IFE was negligible since BSA absorbance value was very low (Abs=0.020).

3.2.2 Data Analysis and Results

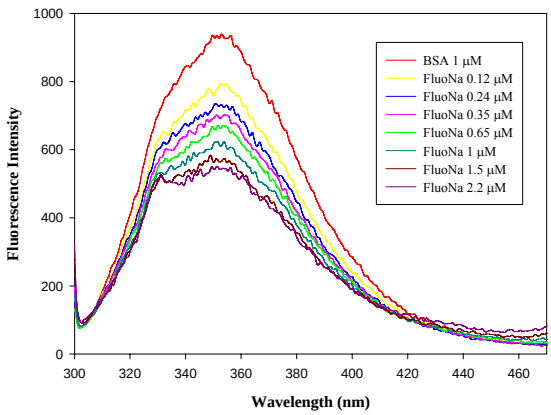

Figure 3.3 - Fluorescence spectra of the interaction between BSA and fluorescein sodium salt

Fluorescence intensity spectra were collected over a range of 300 and 460 nm as reported in Figure 3.3. As it can be seen from the cited figure, by increasing the ligand concentration, there is a decrease of the BSA fluorescence intensity but the emission maximum does not move to shorter or longer wavelength. As a preliminary study, some BSA/fluorescein ratio concentrations were investigated and a binding curve was constructed in order to check which range of concentration has to be taken for the interaction study. The chosen concentrations have been reported in the experimental section.

The obtained maximum fluorescence intensity was recorded and data were treated by several methods for analyzing quenching titration data:

- **Non Linear Least Squares**

The most straightforward way of analyzing data is to use a nonlinear least-squares fit procedure. Three basic assumptions must be fulfilled in order to use the nonlinear least-squares fit procedure: (1) the source of major experimental errors of the data is confined to the vertical axis, that is, the determination of fluorescence intensity; (2) the errors follow normal distribution; and (3) there is no systematic error in the data. If conducted properly all three assumptions are fulfilled in fluorescence quenching experiments and hence nonlinear least-squares fit can be used to extract binding constants. The nonlinear least-squares fit procedure for analyzing binding data has been discussed in detail[26]. Many of the commercially available fitting programs (Sigma-Plot, TableCurve and GraphPad Prism) have a nonlinear least-squares fit program as part of the package. The equation is the following:

$$y = \frac{B_{max} \cdot x}{K_D + x} \qquad [3.2]$$

where:

X is the concentration of free ligand

Y is the specific binding

B_{max} is the maximum amount of the complex that can form at saturating the ligand

K_d is the equilibrium dissociation constant.

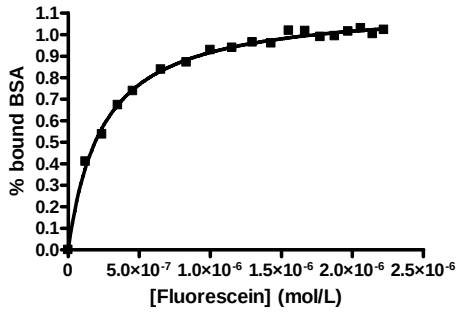

Figure 3.4 – Non linear least square analysis of the A5 experiment

- **Stern-Volmer**

The fluorescence quenching data were analyzed by the Stern-Volmer equation:

$$\frac{F}{F_0} = 1 + K_{SV}[Q] \qquad [3.3]$$

Where F_0 and F are the steady-state fluorescence intensities in the absence and presence of quencher, respectively, K_{SV} is the Stern-Volmer quenching constant and [Q] is quencher concentration (fluorescein). In the following figure a plot of F/F_0 vs. fluorescein concentration is reported, from the slope of the straight line the K_{SV} can be easily calculated. Sometimes, there is a deviation from linearity due to the possible presence of both dynamic and static quenching as reported in chapter 1.

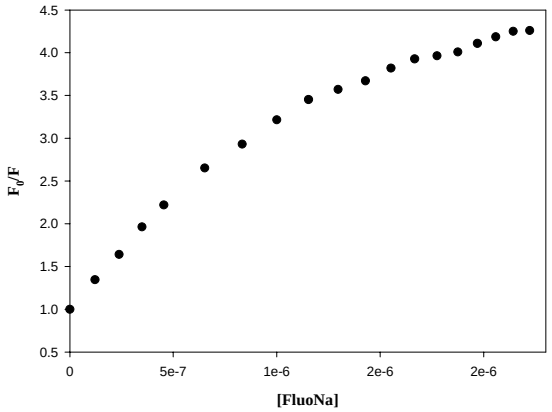

Figure 3.5 – Stern-Volmer plot of the C13 experiment

- **Modified Stern-Volmer**

The following equation is the so-called Modified Stern-Volmer[6] from which it is possible to get the K_a from the antilog of the intercept and the *n* (i.e. the number of binding sites) value from the slope of the straight regression line:

$$\log\frac{F_0 - F}{F} = \log K + n\log[Q] \qquad [3.4]$$

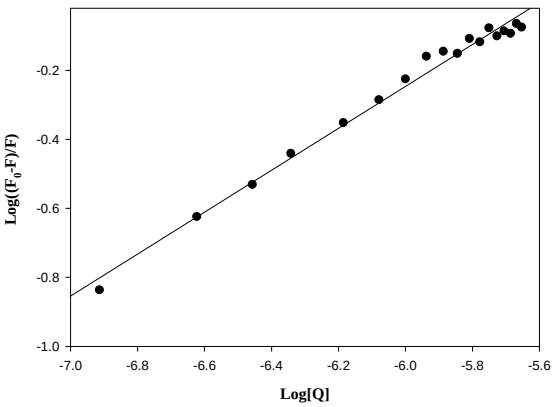

Figure 3.6 – Modified Stern-Volmer plot of the A4 experiment

- **Lineweaver-Burk**

  The third method is the Lineweaver-Burk[27] whose equation is:

$$\frac{1}{F_0 - F} = \frac{1}{F_0} + \frac{K_D}{F_0[Q]} \qquad [3.5]$$

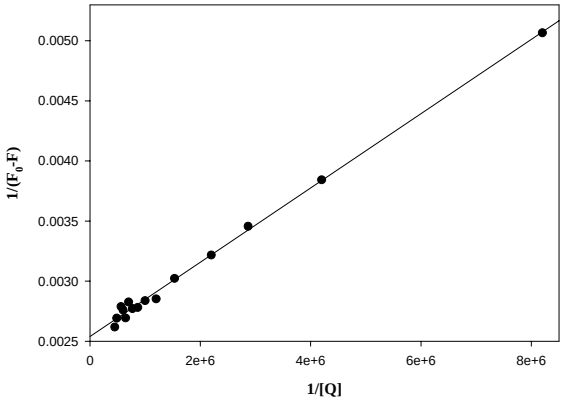

Figure 3.7 – Lineweaver-Burk graph of B4 experiment

The slope of the line is the K_D/F_0 ratio while the intercept is the reverse of F_0.

- **Scatchard's plot**

Scatchard's method[28] has been the traditional method for analysis of binding data until the introduction of non-linear fitting software. The equation of a Scatchard's plot is:

$$\frac{[L_b]}{[L_f]} = \frac{-[L_b]}{K_d} + \frac{n[R_t]}{K_d} \qquad [3.6]$$

Which fits the equation of a line where $\frac{n[R_t]}{K_d}$ is the y-intercept, $n[R_t]$ is the x-intercept and $-\frac{1}{K_d}$ is the slope.

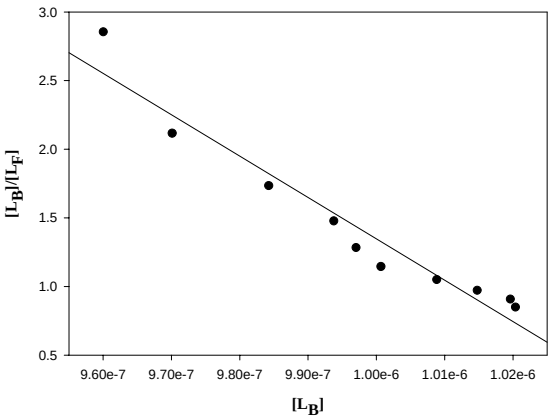

Figure 3.8 – Scatchard plot of the experiment C13

While Scatchard plots are very useful for visualizing data, they are not the most accurate way to analyze data. The problem is that the linear transformation distorts the experimental error. Linear regression assumes that the scatter of points around the line follows a Gaussian distribution and that the standard deviation is the same at every value of X. These assumptions are not true with the transformed data. A second problem is that the Scatchard transformation alters the relationship between X and Y. The value of X (bound) is used to calculate Y (bound/free), and this violates the assumptions of linear regression.

Since the assumptions of linear regression are violated, the B_{max} and K_d you determine by linear regression of Scatchard transformed data are likely to be further from their true values than the B_{max} and K_d determined by nonlinear regression. Nonlinear regression produces the most accurate results while Scatchard plots produce approximate results.

The figure below shows the problem of transforming data. The left panel shows data that follows a rectangular hyperbola (binding isotherm). The right panel is a Scatchard plot of the same data. The solid curve on the left was determined by nonlinear regression. The solid line on the right shows how that same curve would look after a Scatchard transformation. The dotted line shows the linear regression fit of the transformed data. The transformation amplified and distorted the scatter, and thus the linear regression fit does not yield the most accurate values for B_{max} and K_d. In this example, the B_{max} determined by the Scatchard plot is about 25% too large and the K_d determined by the Scatchard plot is too high. The errors could just as easily have gone in the other direction.

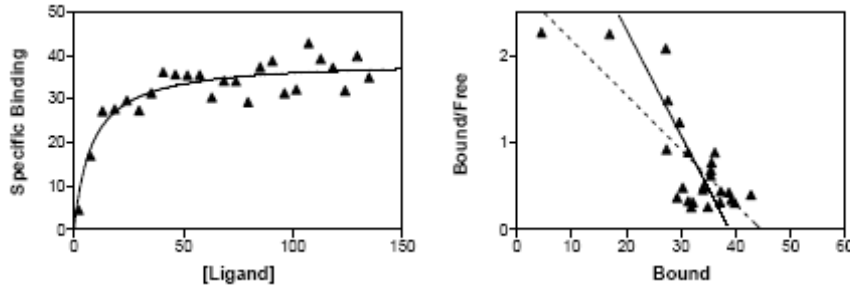

Figure 3.9 – Comparison between non-linear regression method (left) and Scatchard's method for data analysis

In the following tables a complete view of all results is reported.

- **A**

		Non-linear			Lineweaver-Burk		Modified Stern-Volmer	
		$K_d \cdot 10^{-7}$ (M)	B_{max}	$K_a \cdot 10^{6}$ (M^{-1})	$K_d \cdot 10^{-7}$ (M)	$K_a \cdot 10^{6}$ (M^{-1})	$K_d \cdot 10^{-4}$ (M)	$K_a \cdot 10^{+3}$ (M^{-1})
A1	**T=25°C**	1.00	1.071	9.97	0.995	1.01e+7		
A2		1.11	1.080	9.01	1.04	9.58		
A3		2.67	1.148	3.74	3.26	3.07		
A4	**T=25°C**	4.97	1.220	2.01	3.98	2.51	5.55	1.80
A5		2.41	1.138	4.14	2.13	4.70	10.8	0.92
A6		0.806	1.061	12.4	0.761	13.1		
A7	**T=40°C**	0.784	1.057	12.7	0.951	10.5		
A8		1.60	1.103	6.25	1.64	6.11		
A9	**T=40°C**	-	-	-				
A10		1.80	1.115	5.54	1.41	7.08		
A11	**T=15°C**	4.68	1.231	2.14	6.38	1.57		
A12		3.97	1.209	2.52	3.61	2.77		

Table 3.2 – K_d and K_a obtained for BSA A

- **B (T=25°C)**

	Non-linear			Lineweaver-Burk		Modified Stern-Volmer	
	$K_d \cdot 10^{-7}$ (M)	B_{max}	$K_a \cdot 10^{6}$ (M^{-1})	$K_d \cdot 10^{-7}$ (M)	$K_a \cdot 10^{6}$ (M^{-1})	$K_d \cdot 10^{-5}$ (M)	$K_a \cdot 10^{+4}$ (M^{-1})
B1	0.967	1.071	10.4	0.999	10.0		
B2	6.78	1.293	1.45	7.48	1.34	5.30	1.89
B3	3.12	1.159	3.21	2.52	3.97		
B4	1.11	1.078	9.01	1.27	8.03		
B5	1.96	1.115	5.10	2.19	4.57		
B6	1.48	1.095	5.05	1.34	7.44		

Table 3.3 - K_d and K_a obtained for BSA B

- **C (T=25°C)**

	$K_d \cdot 10^{-7}$ (M)	B_{max}	$K_a \cdot 10^{6}$ (M^{-1})	[BSA] (M)
C1	3.20	1.17	3.13	$1 \cdot 10^{-6}$
C2	1.91	1.12	5.24	$1 \cdot 10^{-6}$
C3	1.07	1.07	9.35	$1 \cdot 10^{-6}$
C4	2.22	1.13	4.50	$1 \cdot 10^{-6}$
C5	1.00	1.07	10.00	$1 \cdot 10^{-6}$
C6	0.66	1.05	15.15	$1 \cdot 10^{-6}$
C7	0.16	1.01	62.50	$1 \cdot 10^{-6}$
C8	0.26	1.02	38.46	$1 \cdot 10^{-6}$
C9	0.35	1.03	28.57	$1 \cdot 10^{-6}$
C10	0.26	1.04	38.46	$1 \cdot 10^{-6}$
C11	0.26	1.02	38.46	$1 \cdot 10^{-6}$
C12	0.37	1.03	27.03	$1 \cdot 10^{-6}$
C13	2.71	1.15	3.69	$1 \cdot 10^{-6}$
C14	2.30	1.21	4.35	$5 \cdot 10^{-7}$
C15	0.20	1.03	50.00	$5 \cdot 10^{-7}$

Table 3.4 - K_d and K_a obtained for BSA C

The results obtained from the fitting by Scatchard's method are not reported since the goodness of the data was really poor (this is already discussed previously). On the contrary, the agreement of the results from the other two methods (i.e. Non-linear regression and Lineweaver-Burk) is good and provides comparable values. The Modified Stern-Volmer gave less reliable data since the fitting was much more difficult due to the non perfect linear behaviour of the $\log\frac{F_0 - F}{F}$ vs. log[Q] data. As it can be seen from the reported tables, the agreement of the constants is good for the two sets of measurements of BSA A and B. The K_d and K_a obtained for the A7030 BSA (C) differ in the same set of experiments. Actually, the K_d can vary for example from $2.0 \cdot 10^{-8}$ M up to $3.20 \cdot 10^{-7}$ M, which means an order of magnitude. Surprisingly, this variation was recorded for the most purified BSA. The A7030 (C) has a 98% purity after heat shock and charcoal treatments which remove globulins and fatty acids.

One consideration about the presence of more than one tryptophan residue is needed. For single-tryptophan proteins, the quenching data can be plotted as F_0/F versus [quencher]. The slope of the line gives the Stern-Volmer constant, K_{SV} (see Chapter 1):

$$\frac{F_0}{F} = 1 + K_{SV}[Q] \qquad [3.7]$$

In multitryptophan proteins like BSA (two Trp are present), the situation is more complex. The quenching relationship is described by Equation (3.3)[29]:

$$\frac{F_0}{F} = \left\{ f_1 / \left(1 + K^1{}_{SV}[Q]\right) + f_2 \left(1 + K^2{}_{SV}[Q]\right) \right\}^{-1} \qquad [3.8]$$

Where f_1 is the fraction of fluorescence intensity contributed by the first tryptophan, f_2 is the fraction of fluorescence intensity contributed by the second tryptophan, and the superscript indices on the Stern-Volmer constants reflect the Stern-Volmer constants of the respective tryptophans.

There are a number of ways by which information about quenchabilities of different tryptophans can be obtained. A useful modification of the Stern-Volmer equation in the case of multitryptophan proteins, where one tryptophan is quenchable and the others are not, is the Lehrer equation:

$$\frac{F_0}{\Delta F} = 1/\, f_1 K^1{}_{SV}[Q] + 1/\, f_1 \qquad [3.9]$$

where f_1 is the fraction of the total fluorescence that is quenchable, ΔF is F_0 - F, and $K^1{}_{SV}$ is the Stern-Volmer constant of the quenchable tryptophan. A plot of $F_0/\Delta F$ versus 1/[Q] yields an intercept of $1/f_1$ and a slope of $1/f_1 K^1{}_{SV}$ from which the Stern-Volmer constant can be calculated[30].

- *Thermodynamic parameters*

Small molecules are bound to macromolecules by four binding modes: H-bonding, Van der Waals, electrostatic, and hydrophobic interactions. The thermodynamic parameters, enthalpy ($\Delta H°$) and entropy ($\Delta S°$) of reaction, are important for confirming binding modes. For this purpose, the temperature-dependence of the binding constant was studied. The temperatures chosen were 15, 25 and 40°C (288, 298, and 313 K) so that BSA does not undergo any structural degradation. A plot of lnK vs. $1/T$ gives a straight line according to the Van't Hoff equation:

$$\ln K = -\frac{\Delta H^0}{RT} + \frac{\Delta S^0}{R} \qquad [3.10]$$

obtained by substituting Equation 3.11 into Equation 3.12:

$$\Delta G^0 = \Delta H^0 - T\Delta S^0 \qquad [3.11]$$

$$\ln K = -\frac{\Delta G^0}{RT} \qquad [3.12]$$

The analysis of the temperature effect was carried out for the 05488 BSA (A) in order to elucidate the interaction of fluorescein with BSA.

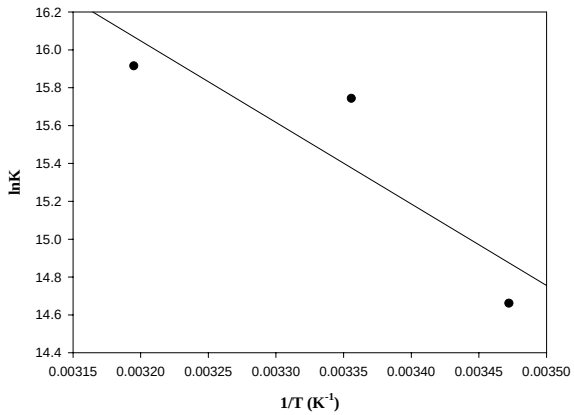

Figure 3.10 – The Van't Hoff plot, pH 7.50, [BSA] = 1 μM

Figure 3.10 is the Van't Hoff plot of the fluorescein-BSA system. Table 3.5 shows the values of ΔH^0 and ΔS^0 obtained for the binding site of the slopes and the ordinates of the origin of the fitted lines. From Table 3.5 it can be seen that both ΔH^0 and ΔS^0 have a positive value: 35.8 kJ/mol and 247.94 J/molK respectively. The negative sign for ΔG^0 means that the binding process is spontaneous. For drug-protein interaction, positive entropy is frequently taken as evidence for hydrophobic interaction, but it has been pointed out that positive entropy may also be a manifestation of electrostatic interaction[31].

ΔH^0 (kJ/mol)	ΔS^0 (J/mol K)
35.8	247.94

Temperature (K)	ΔG^0 (kJ/mol)
288	-35.624
298	-38.104
313	-41.824

Table 3.5 – Thermodynamic parameters of fluorescein-BSA interaction

- *Energy transfer between fluorescein sodium salt and BSA*

The overlap of the UV absorption spectra of fluorescein sodium salt with the fluorescence emission spectra of BSA is shown in Figure 3.11. The importance of the energy transfer in biochemistry is that the efficiency of transfer can be used to evaluate the distance between the ligand and the tryptophan residues in the protein. According to Förster's non-radiative energy transfer theory[32], the rate of energy transfer depends on: (i) the relative orientation of the donor and acceptor dipoles, (ii) the extent of overlap of fluorescence emission spectrum of the donor with the absorption spectrum of the acceptor, and (iii) the distance between the donor and the acceptor. The energy transfer effect is related not only to the distance between the acceptor and donor, but also to the critical energy transfer distance, R_0, that is:

$$E = 1 - \frac{F}{F_0} = \frac{R_0^{\,6}}{R_0^{\,6} + r^6} \qquad [3.11]$$

where F and F_0 are the fluorescence intensities of BSA in the presence and absence of fluorescein, r is the distance between acceptor and donor and R_0 is the critical distance when the transfer efficiency is 50%. $R_0^{\,6}$ is calculated using the equation:

$$R_0^{\,6} = 8.8 \times 10^{-25} k^2 N^{-4} \Phi J \qquad [3.12]$$

where k^2 is the spatial orientation factor of the dipole, N is the refractive index of the medium, Φ is the fluorescence quantum yield of the donor and J is the overlap integral of the fluorescence emission spectrum of the donor (BSA) and the absorption spectrum of the acceptor (fluorescein). J is given by:

$$J = \frac{\sum F(\lambda)\varepsilon(\lambda)\lambda^4 \Delta\lambda}{\sum F(\lambda)\Delta\lambda} \qquad [3.13]$$

where $F(\lambda)$ is the fluorescence intensity of the fluorescent donor of wavelength, λ, $\varepsilon(\lambda)$ is the molar absorption coefficient of the acceptor at wavelength, λ. In the present case, $K^2=2/3$, N=1.334 and $\Phi=0.15$[33,34]. From Eqs. 3.11 to 3.13, we would be able to calculate that $J=2.38 \cdot 10^{+13}$ $mol^{-1}cm^{-1}nm^4$, R_0=23 Å (2.3 nm), E=0.51 and r=22.1 Å (2.2 nm). The donor-to-acceptor distance, r<7 nm[19,35] indicated that the energy transfer from BSA to fluorescein

occurs with high possibility. Further the value of r obtained this way agrees very well with literature value of substrate binding to serum albumin at site II A[27,36]. The only aspect that should be noticed is that the BSA has two Trp residues, so that the donor-to-acceptor distance found is in fact an average distance of the fluorescein from the two Trp residues.

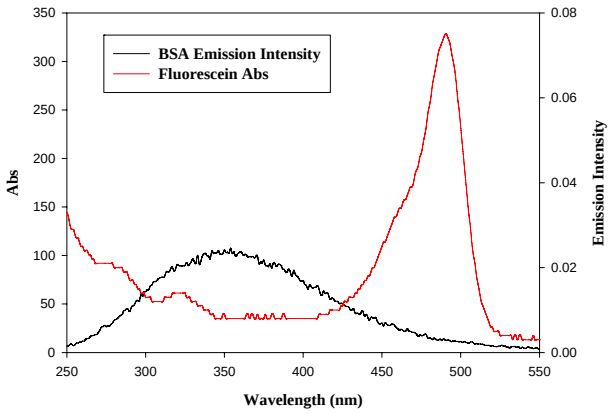

Figure 3.11 - The overlap of the fluorescence spectrum of BSA (black trace) and the absorbance spectrum of fluorescein (red trace). λ_{ex}=295 nm, λ_{em}=350 nm, [BSA]:[FluoNa]=1:1

3.3 Quantitative Determination of Kinetics Binding Constant by Fluorescence Stopped-flow

3.3.1 Experimental

- *Reagents*

Bovine Serum Albumin (BSA) A7030 (see 3.2.1) was obtained from Sigma-Aldrich and used as received.

Fluorescein Sodium Salt for fluorescence was purchased from Fluka and used without any further purification. The solutions of Fluorescein Sodium Salt and BSA were prepared in 0.1 M HEPES (from Sigma-Aldrich) buffer of pH 7.5.

All reagents were of analytical reagent grade and double distilled water was used throughout. BSA solution was prepared based on its molecular weight of 66,000.

- *Apparatus*

Fluorescence measurements were recorded using a SX20 stopped-flow spectrometer fitted with a 515 nm cut-off filter between the cell and fluorescence detector and equipped with a thermostatic bath. Data acquisition, visualisation and analysis is provided by Pro-Data software running under Windows™ XP.

- *Experimental procedures*

The excitation wavelength was 485 nm. Slits widths of the excitation monochromator were 0.2 mm. Fluorescein concentration (2 μM) was kept constant and several shots of different BSA concentration were performed:

[Fluorescein] = 2 μM in HEPES buffer;

[BSA] = 20, 40, 60, 80, 100, 120, 140 and 180 μM in HEPES buffer.

All the concentrations are syringe concentrations and will be halved into the cell. For each condition at least ten scans of about 500 data points each were acquired and averaged.

3.3.2 Data Analysis

Raw data were analyzed and plotted to a single exponential function by using Pro-Data Viewer 4.0.17 from Applied Photophysics Ltd. From this data treatment the observed rate constants (K_{obs}) were easily obtained and plotted against the BSA concentration. The association and dissociation rate constants were obtained from linear regression analysis as already reported in Chapter 1.

3.3.3 Results

Fluorescence spectroscopy is often utilized as a method to follow stopped-flow reactions because of its inherent sensitivity and timing resolution. The two basic types of fluorescence data that are usually examined are total-intensity and steady-state anisotropy (SSA). Both types of data contain information concerning changes in the relative populations of species during a reaction. However, steady-state anisotropy data contain additional information describing the average molecular motion that occurs during the lifetime of the excited-state.

Fluorescence total intensity and anisotropy are highly interrelated and contain two very complementary forms of information. Total intensity changes are useful in determining changes in populations with differing quantum yields, whereas anisotropy changes contain additional contributions caused by the rotational dynamics of the species. For cases in which the fluorescence quantum yield increases, the observed rate of anisotropy change will be more rapid than the total intensity change, whereas in cases in which the total intensity decreases, the observed change in anisotropy will lag behind. In all cases, with quantum yield changes the stopped-flow anisotropy signals cannot be fitted with models consisting of exponentials.
Total-intensity and SSA data have been used in conjunction in the past to obtain more information about ligand-receptor interactions than was present in the two types of data

alone[37,38,39]. In these studies, the combined anisotropy and intensity information was used to determine the reaction order and association/dissociation rate constants.

Although stopped-flow SSA and total-intensity studies have been performed for many years, no studies rigorously combining both data types have been described. The prevailing sentiment among kineticists has been to utilize total-intensity measurements whenever possible because the signal magnitude is always larger without polarizers.

- **Intensity**

The binding of fluorescein sodium salt to BSA was investigated under pseudo-first-order conditions by monitoring the dye fluorescence. Figure 3.12 shows that on mixing 2 μM fluorescein with 60 μM BSA there is a decrease in fluorescence intensity which can be well fitted to a single exponential with a rate constant of 264 s^{-1}.

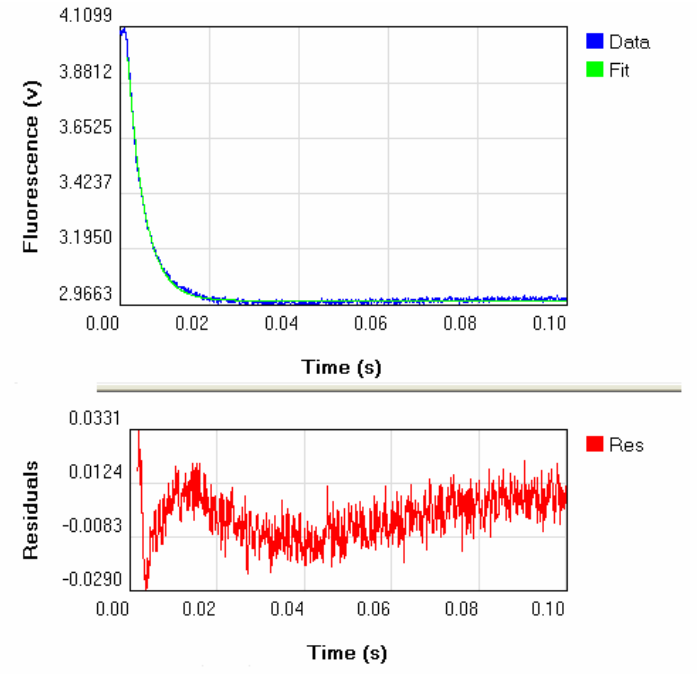

Figure 3.12 - Stopped-flow fluorescence intensity record of the binding of fluorescein sodium salt to BSA (experiment CI3). One syringe contained 2 μM fluorescein and the other syringe contained 60 μM BSA. The solid green line is the best fit to the data to a single exponential giving rate constants of 264 s^{-1}. The data are the averages of fifteen reactions. Residuals are also reported (red trace in the bottom)

The dependence of the observed rate constant of binding of fluorescein to BSA was investigated over the range of 20-180 μM BSA. As the concentration of BSA increased, the background fluorescence signal also increased with a reduction in the signal from the binding reaction. Therefore, measurements could not be made above this concentration. The dependence of the observed rate constant of binding of fluorescein to BSA concentration is shown in Figure 3.13. Although this is linear at lower concentrations, there is evidence of hyperbolic behaviour at higher concentrations.

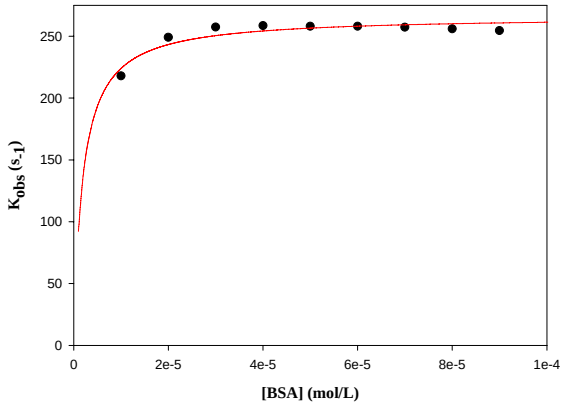

Figure 3.13 – Dependence of the observed rate constant determined by fluorescence intensity of the binding of fluorescein sodium salt to BSA concentration (experiment CI4)

There are several possible mechanisms of binding of fluorescein to BSA that could give rise to this type of behaviour. These are described by Bagshaw et al.[40,41] in interpreting their results of the binding of ATP to myosin subfragment 1. The one possibility considered here is that the hyperbolic behaviour arises from the binding of fluorescein to BSA being a two-step process in which there is a rapid equilibrium to form a collision complex, followed by an isomerization of this complex in a process which reports the change of fluorescence intensity:

$$\text{fluorescein} + \text{BSA} \underset{}{\overset{K_{1a}}{\rightleftharpoons}} \text{fluorescein}\bullet\text{BSA} \underset{k_{-1b}}{\overset{\Delta F \; k_{1b}}{\rightleftharpoons}} \text{fluorescein}\bullet\text{BSA}^*$$

Scheme 1

Then, the observed rate constant of the process will be given by:

$$k_{obs} = \frac{k_{1b}}{1 + 1/K_{1a}[BSA]} + k_{-1b} \qquad [3.14]$$

where K_{1a} is the association equilibrium constant of step 1 and k_{1b} and k_{-1b} are the rate constants for the forward and backward processes of step 2. (This treatment assumes that any subsequent processes are very slow compared to the binding and dissociation processes.) The solid line in Figure 3.12 is a fit of the data to this equation giving values of $K_{1a} = 5.3 \cdot 10^5$ M^{-1} (which is equivalent to a K_d of $1.9 \cdot 10^{-6}$ M) and $k_{1b} = 266$ s^{-1}. The intercept, as seen in the above equation, gives the value of k_{-1b} but is too close to the origin to define exactly. When $k_{obs} << k_{1b}$, then Equation 3.14 reduces to

$$k_{obs} = K_{1a}k_{1b}[BSA] \qquad [3.15]$$

Therefore, the slope of the line at low concentration of BSA is $K_{1a}k_{1b}$, giving an apparent second-order binding constant of $9.8 \cdot 10^3$ M^{-1} s^{-1}.

- **Anisotropy**

Figure 3.14 shows that on mixing 2 μM fluorescein with 20 μM BSA, there is an increase in fluorescence anisotropy which can be well fitted to a single exponential with a rate constant of 83 s^{-1}.

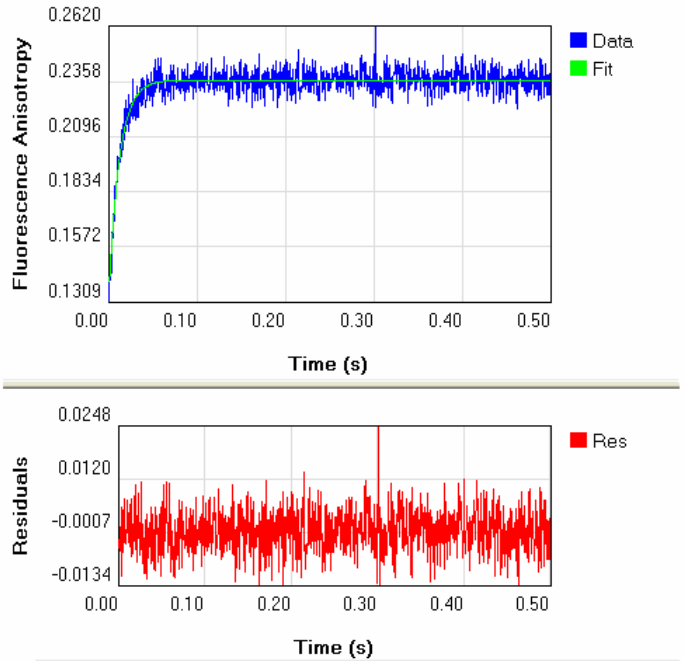

Figure 3.14 - Stopped-flow fluorescence anisotropy record of the binding of fluorescein sodium salt to BSA (experiment CA4). One syringe contained 2 μM fluorescein and the other syringe contained 20 μM BSA. The green solid line is the best fit to the data to a single exponential giving rate constants of 83 s^{-1}. The data are the averages of fifteen reactions. Residuals are also reported (red trace in the bottom)

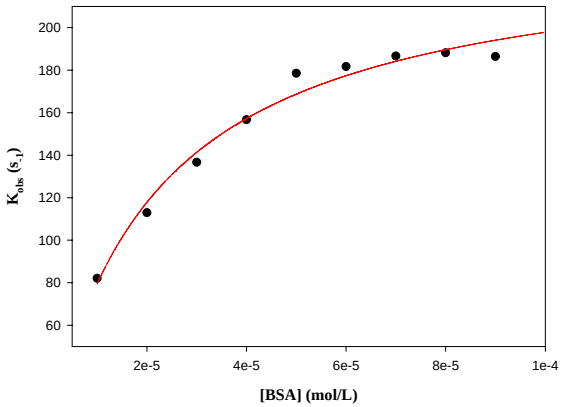

Figure 3.15 – Dependence of the observed rate constant of the binding of fluorescein sodium salt to BSA concentration (experiment CA4 using anisotropy)

The solid line in Figure 3.15 is a fit of the data to this equation giving values of K_{1a}=4.9·10^4 M^{-1} (which is equivalent to a K_d of 20.4 μM) and k_{1b}=236 s^{-1}. The intercept, as seen in the above equation, gives the value of k_{-1b} but is too close to the origin to define exactly. When k_{obs} << k_{1b}, then Equation 3.14 reduces to 3.15. Therefore, the slope of the line

at low concentration of BSA is $K_{1a}k_{1b}$, giving an apparent second-order binding constant of $2.37 \cdot 10^6\ M^{-1}\ s^{-1}$.

In the following table a summary of the results is reported. The agreement is good for data coming from each set of intensity and anisotropy measurements.

		K_{1a}	K_d	k_{1b}	k_{-1b}	$K_{1a}k_{1b}$
		M^{-1}	M	s^{-1}	$M^{-1}s^{-1}$	$M^{-1}s^{-1}$
Anisotropy	**CA1**	4.9e+4	2.04e-5	241	11.6	2.55e+6
	CA2	-	-	-	-	2.16e+6
	CA3	6.9e+4	1.45e-5	218	-	2.62e+6
	CA4	4.9e+4	2.04e-5	236	1.7	2.37e+6
Intensity	**CI1**	2.4e+5	4.2e-6	185	-	1.35e+4
	CI2	6.7e+5	1.5e-6	266	-	6.49e+3
	CI3	6.7e+5	1.5e-6	266	-	9.64e+3
	CI4	5.3e+5	1.9e-6	266	-	9.77e+3

Table 3.6 – Summary of the results for the stopped-flow anisotropy and intensity measurements

The fact that there is no agreement between the two sets of data coming from intensity and anisotropy measurements can be understood by the work of Otto et al.[42] who explained this incongruence showing that the SSA can be heavily influenced by differences in the effective quantum yields of the various species present during a reaction. In this way, the change in anisotropy will not accurately represent the change in populations over the time[43]. In reactions where both a change in anisotropy and total intensity occurs, the SSA time course and rate must differ from those observed for the total intensity. Otto et al. emphasize that subtle polarization bias effects can affect the observed intensity in reactions where a change in anisotropy accompanies the intensity change. Non-zero values of the steady-state anisotropy can affect the observed emission intensity. In reactions where a large change in SSA occurs rapidly, this polarization bias would manifest itself as an additional phase in the total-intensity reaction.

Since these results were not as good as expected and a kind of fluctuations between the obtained results was detected, a gel electrophoresis has been made in order to check all the BSA used. BSA A, B and C have been studied both in the presence and in the absence of fluorescence sodium salt and compared to other standard BSA. As it can be seen from figure 3.16, all the BSA are present as monomers and can also form dimers, trimers and tetramers. The test, even if not quantitative, can show the presence of more trimers for BSA A.

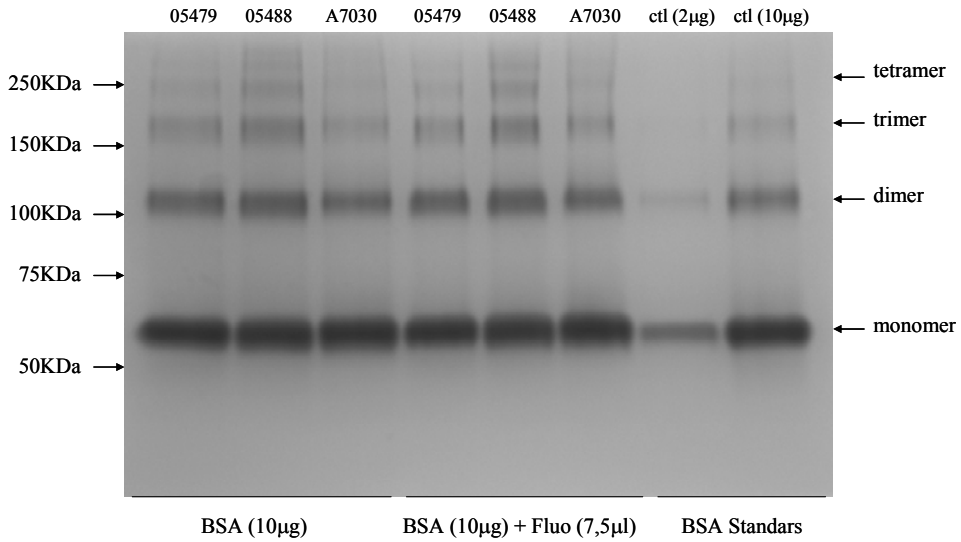

Figure 3.16 – Gel electrophoresis to test all the different BSA in the presence and in the absence of fluorescein sodium salt

3.4 Conclusions

This work provided an approach for studying the binding of BSA with fluorescein sodium salt. The interaction between different BSA and fluorescein sodium salt has been studied by following it both in the steady-state and in the stopped-flow mode. The dissociation and association rate constants (k_{on} and k_{off}) were determined from the kinetic studies while the dissociation and association binding constants (K_d and K_a) were determined both from equilibrium binding isotherms and stopped-flow measurements from the k_{on}/k_{off} ratio.

The best results were obtained by fitting raw data by non-linear regression and Lineweaver-Burk equations. The Modified Stern-Volmer and Scatchard's plots gave less reliable data since the fitting was much more difficult. The agreement of the constants is good for the two sets of measurements of BSA A and B. The K_d and K_a obtained for the A7030 BSA (C) differ in the same set of experiments.

The fact that there is no agreement between the two sets of data coming from intensity and anisotropy measurements is explained from the fact that fluorescence intensity and fluorescence anisotropy sense different aspects of the interaction. The true binding constants can be evaluated by using a global analysis which unfortunately was not available to us.
This work also reports the distance between tryptophan and bound fluorescein for the first time based on Förster's energy transfer theory.

Other further studies should be needed: the number of fluoresceins that bind to one BSA molecule, for example using equilibrium dialysis, should be evaluated and one could also take into account the fact that different fluorescein binding sites are likely to have

different quantum yields. All these results are not available due to the difficulties with instrumental availability and in performing the experiments.

Some more considerations and observations are needed. One must independently verify the oligomerization state of the BSA as a function of BSA concentration. Also one would have to verify the effect of fluorescein binding on the oligomerization state of the BSA. It was not detected in this case but many cases are known in which binding of a ligand influences the aggregation state of the protein[44]. Moreover, this shed light on a topic having the outmost importance. The purity of the biological molecule is a must to have data, since both the presence of different proteins and/or the proneness of the protein to give self assembly in dimers, trimers and so on, can heavily influence the results. For all these reasons, further studies and investigations are needed.

Reference List

1. Peters, T. Serum Albumin. *Adv. Prot. Chem.* **1985,** *37*, 161-245.
2. Carter, D. C.; Ho, J. X. Structure of Serum Albumin. *Adv. Prot. Chem.* **1994,** *45*, 153-203.
3. Kosa, T.; Maruyama, T.; Otagiri, M. Species Differences of Serum Albumins: I. Drug Binding Sites. *Pharm. Res.* **1997,** *14* (11), 1607-1612.
4. Kragh-Hansen, U. Molecular Aspects of Ligand Binding to Serum Albumin. *Pharm. Rev.* **1981,** *33* (1), 17-53.
5. Bi, S.; Song, D.; Tian, Y.; Zhou, X.; Liu, Z.; Zhang, H. Molecular spectroscopic study on the interaction of tetracyclines with serum albumins. *Spectrochim. Acta A* **2005,** *61*, 629-636.
6. Feng, X. Z.; Lin, Z.; Yang, L. J.; Wang, C.; Bai, C. Investigation of the interaction between acridine orange and bovine serum albumin. *Talanta* **1998,** *47*, 1223-1229.
7. Shaikh, S. M. T.; Seetharamappa, J.; Ashoka, S.; Kandagal, P. B. A study of the interaction between bromopyrogallol red and bovine serum albumin by spectroscopic methods. *Dyes and Pigments* **2007,** *73*, 211-216.
8. Cajlakovic, M.; Bizzarri, A.; Ribitsch, V. Luminescence lifetime-based carbon dioxide optical sensor for clinical applications. *Anal. Chim. Acta* **2006,** *573-574*, 57-64.
9. Cheng, Z.; Levi, J.; Xiong, Z.; Gheysens, O.; Keren, S.; Chen, X.; Gambhir, S. S. Near-Infrared Fluorescent Deoxyglucose Analogue for Tumor Optical Imaging in Cell Culture and Living Mice. *Bioconjugate Chem.* **2006,** *17*, 662-669.
10. Kamat, B. P.; Seetharamappa, J. Fluorescence and Circular Dichroism Studies on the Interaction of Bromocresol Purple with Bovine Serum Albumin. *Polish J. Chem.* **2004,** *78*, 723-732.
11. Seedher, N.; Saini, A. Spectrophotometric studies on the interaction of bovine serum albumin with triphenylmethane dyes. *Indian J Pharm Sci* **1998,** *60* (5), 297-301.
12. Kamat, B. P.; Seetharamappa, J. In vitro study on the interaction of mechanism of tricyclic compounds with bovine serum albumin. *J. Pharm. Biomed. Anal.* **2004,** *35*, 655-664.
13. Rang, H. P.; Dale, M. M.; Ritter, J. *Molecular Pharmacology;* 3rd ed.; Academic Press: New York, 1995.

14. Tian, J.; Liu, J.; Hub, Z.; Chen, X. Interaction of wogonin with bovine serum albumin. *Bioorg. Med. Chem.* **2005,** *13*, 4124-4129.

15. Hong, G.; Lei, L.; Liu, J.; Kong, Q.; Chen, X.; Hu, Z. The study on the interaction between human serum albumin and a new reagent with antitumour activity by spectrophotometric methods. *J. Photochem. Photobiol. A: Chemistry* **2004,** *167*, 213-221.

16. Shrivastava, H. Y.; Nair, B. U. A fluorescence-based assay for nanogramquantification of proteins using a protein binding ligand. *Anal Bioanal Chem* **2003,** *375*, 169-174.

17. Jiang, C. Q.; Gao, M. X.; He, J. X. Study of the interaction between terazosin and serum albumin Synchronous fluorescence determination of terazosin. *Anal. Chim. Acta* **2002,** *452*, 185-189.

18. Hushcha, T. O.; Luik, A. I.; Naboka, Yu. N. Conformation changes of albumin in its interaction with physiologically active compounds as studied by quasi-elastic light scattering spectroscopy and ultrasonic method. *Talanta* **2000,** *53*, 29-34.

19. Hu, Y. J.; Liu, Y.; Wang, J. B.; Xiao, X. H.; Qu, S. S. Study of the interaction between monoammonium glycyrrhizinate and bovine serum albumin. *J. Pharm. Biomed. Anal.* **2004,** *36*, 915-919.

20. Yu, Y.; Li, Q. Studies on the interaction of paclitaxel with tubulin by an electrochemical method. *Anal. Chim. Acta* **2001,** *436*, 147-152.

21. Liang, A.; Chao, Y.; Liu, X.; Du, Y.; Wang, K.; Qian, S.; Lin, B. Separation, identification, and interaction of heparin oligosaccharides with granulocyte-colony stimulating factor using capillary electrophoresis and mass spectrometry. *Electrophoresis* **2005,** *26*, 3460-3467.

22. Casselt, J. M.; Steinhardt, J. Limitations Inherent in the ΔpH Method of Determining Binding Isotherms of Bovine Serum Albumin. *Biochemistry* **1969,** *8* (6), 2603-2609.

23. Bujalowski, W.; Jezewska, M. J. Quantitative determination of equilibrium binding isotherms for multiple ligand-macromolecule interactions using spectroscopic methods. In *Spectrophotometry & Spectrofluorimetry*, Gore, M. G., Ed.; Oxford Univeristy Press: 2000; pp 141-165.

24. Jezewska, M. J.; Bujalowski, W. Quantitative analysis of ligand-macromolecule interactions using differential dynamic quenching of the ligand fluorescence to monitor the binding. *Biophys. Chem.* **1997,** *64*, 253-269.

25. Norris, A. W.; Cheng, L.; Giguère, V.; Rosenberger, M.; Li, E. Measurement of subnanomolar retinoic acid binding affinities for cellular retinoic acid binding proteins by fluorometric titration. *Biochim. Biophys. Acta* **1994,** *1209*, 10-18.

26. Johnson, M. L.; Frasier, S. G. Nonlinear least-squares analysis. *Methods Enzymol.* **1985,** *117*, 301-342.

27. Deepa, S.; Mishra, A. K. Fluorescence spectroscopic study of serum albumin–bromadiolone interaction: fluorimetric determination of bromadiolone. *J. Pharm. Biomed. Anal.* **2005,** *38*, 556-563.

28. Scatchard, G. The attractions of proteins for small molecules and ions. *Ann. N. Y. Acad. Sci.* **1949,** *51*, 660-672.

29. Roy, S. Fluorescence Quenching Methods to Study Protein–Nucleic Acid Interactions. *Methods Enzymol.* **2004,** *379*, 175-187.

30. Lehrer, S. S. Solute Perturbation of Protein Fluorescence. The Quenching of the Tryptophyl Fluorescence of Model Compounds and of Lysozyme by Iodide Ion. *Biochemistry* **1971,** *10* (17), 3254-3263.

31. Maruyama, T.; Lin, C. C.; Yamasaki, K.; Miyoshi, T.; Imai, T.; Yamasaki, M.; Otagiri, M. Binding of Suprofen to Human Serum-Albumin - Role of the Suprofen Carboxyl Group. *Biochem. Pharm.* **1993,** *45* (5), 1017-1026.

32. Förster, Th. *Modern Quantum Chemistry;* Academic Press: New York, 1965; Vol. 3.

33. Earl, J. K.; Sperry, W. M. *Biochemist's handbook;* Kluwer Academic: London, 1961.

34. Seedher, N.; Singh, B.; Singh, P. Mode of interaction of metronidazole with bovine serum albumin. *Indian J Pharm Sci* **1999,** *61* (3), 143-148.

35. Valeur, B.; Brochon, J. C. *New trends in fluorescence spectroscopy;* 6th ed.; Springer Press: Berlin, 1999.

36. Liu, J.; Tian, J.; Zhang, J.; Hu, Z. Interaction of magnolol with bovine serum albumin: a fluorescence-quenching study. *Anal Bioanal Chem* **2003,** *376*, 864-867.

37. Levison, S. A. *Fluorescence polarization kinetic studies of macromolecular reactions. In Biochemical Fluorescence: Concepts;* Marcel Dekker: New York, 1975; Vol. 1.

38. Dandliker, W. B.; Dandliker, S. A.; Levison, S. A.; Kelly, R. J.; Hicks, A. N.; White, J. U. Fluorescence methods for measuring reaction equilibria and kinetics. *Methods Enzymol.* **1978,** *48*, 380-415.

39. Dandliker, W. B.; Hsu, N.; Levin, J.; Rao, B. R. Equilibrium and Kinetic Inhibition Assays Based upon Fluorescence Polarization. *Methods Enzymol.* **1981,** *74*, 3-28.

40. Bagshaw, C. R.; Eccleston, J. F.; Eckstein, F.; Goody, R. S.; Gutfreund, H.; Trentham, D. R. The Magnesium Ion-Dependent Adenosine Triphosphatase of Myosin. *Biochem. J.* **1974,** *141*, 351-364.

41. Binns, D. D.; Helms, M. K.; Barylko, B.; Davis, C. T.; Jameson, D. M.; Albanesi, J. P.; Eccleston, J. F. The Mechanism of GTP Hydrolysis by Dynamin II: A Transient Kinetic Study. *Biochemistry* **2000,** *39*, 7188-7196.

42. Otto, M. R.; Lillo, M. P.; Beechem, J. M. Resolution of Multiphasic Reactions by the Combination of Fluorescence Total-intensity and Anisotropy Stopped-Flow Kinetic Experiments. *Biophys. J.* **1994,** *67*, 2511-2521.

43. Eftink, M. R. The Use of Fluorescence Methods to Monitor Unfolding Transitions in Proteins. *Biophys. J.* **1994,** *66*, 482-501.

44. Sil, S.; Chakraborti, A. S. Binding of porphyrin to horseradish peroxidase: Effects on structure and function. *Int. J. Biol. Macromol.* **2005,** *36*, 16-22.

Chapter 4 - GST – GST (B14) Interaction

4.1 Introduction

Glutathione *S*-transferases (GSTs)[1] constitute a family of detoxification enzymes that are involved in the metabolism of endogenous and xenobiotic compounds[2,3,4,5]. All of these enzymes catalyze the conjugation of glutathione to the electrophilic center of a variety of substrates, resulting in a more water soluble product that can be further degraded or transported out of the cell. GSTs have been implicated in the development of anticancer drug resistance and have been found in elevated levels in tumors[6].

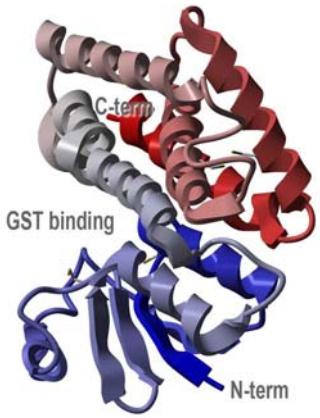

Figure 4.1 - Glutathione S-Transferase structure[7]

The Glutathione S-transferase (GST) Gene Fusion System is a versatile system for the expression, purification and detection of fusion proteins produced in *Escherichia coli*. The system is based on inducible, high-level expression of genes or gene fragments as fusions with *Schistosoma japonicum* GST[8]. Expression in *E. coli* yields fusion proteins with the GST moiety at the amino terminus and the protein of interest at the carboxyl terminus. The protein accumulates within the cell's cytoplasm.

The GST Gene Fusion System has been used successfully in many applications including molecular immunology[9], the production of vaccines[10,11] and studies involving protein-protein[12] and protein-DNA[13] interactions.

The interaction between GST and GST (B14) antibody was studied after the GST bioconjugation with fluorescein-5-maleimide.

Interactions between antigen and antibody involve non-covalent binding of an antigenic determinant to the variable region of both the heavy and light immunoglobulin chains. These interactions are analogous to those observed in enzyme-substrate interactions

and they can be defined similarly. To describe the strength of the antigen-antibody interaction, one can define the affinity constant (K) as shown:

$$AffinityK = \frac{[Ab - Ag]}{[Ab] \times [Ag]} = 10^4 to 10^{12} L / mol$$

Therefore, the greater the K, the stronger the affinity between antigen and antibody. These interactions are the result of complementarity in shapes, hydrophobic interactions, hydrogen bonds and Van der Waals forces.

- *Materials*

GST molecule was produced in *Escherichia coli* BL21 cells using pGEX vector systems. Bacteria were sonicated in buffer A1 (50mM TrisHCl pH 7.5, 1% TritonX100, 150 mM NaCl, 5mM MgCl2, 1 mM DTT) containing protease inhibitors. Lysates were incubated with glutathione-coupled Sepharose 4B beads (GE Healthcare Life Sciences) for 1 h at 4°C. After washing, the bounded beads were incubated with 2ml of buffer B1 (50mM TrisHCl pH 8.0, 100 mM NaCl, 2 mM DTT, 20 mM glutathione) overnight to perform affinity-chromatography separation. The eluates were dialyzed against PBS using Slide-A-Lyzer 3.5K (PIERCE). Recombinant protein concentrations were determined by Comassie-stained gels.

GST (B-14) is a mouse monoclonal antibody raised against the 26 kDa GST specific domain of a fusion protein encoded by a pGEX.3X recombinant vector. It is recommended for detection of glutathione-S-transferase (GST) of *Schistosoma japonicum* origin and GST fusion proteins. It was purchased from Santa Cruz Biotechnology Inc. and used as received.

4.2 Bioconjugation

GST protein has been bioconjugated with fluorescein-5-maleimide following the protocol reported in Chapter 2. GST presents only one cysteine residue at the N-terminal. The bioconjugation was repeated several times and the resulting D/P values are reported in Table 4.1.

The D/P value is higher than we could expect for a single cysteine protein. The bioconjugation was repeated several times and the fluorescein excess was also reduced (test e) but the D/P variation was not appreciable. The fact that the D/P is not equal to unity is probably due to fluorescein arrangement in GST hydrophobic pockets.

[GST] mg/ml	D/P	Test
1	2.70	a
1	3.30	b
1	2.78	c
1	3.3	d
0.35	2.71	e

Table 4.1 – Summary of bioconjugation tests

4.3 Interaction

4.3.1 Experimental

The interaction between GST and GST (B-14) was studied by fluorescence anisotropy. The concentration of the fluorescent-labeled ligand (GST conjugated with fluorescein-5-maleimide) is kept constant, and anisotropy is measured by changing the concentrations of the receptor (GST B14) solution. The anisotropy value at each concentration is measured and used to generate a binding isotherm. During observation of anisotropy, it is important to keep the temperature constant because the temperature greatly affects the molecular motion of the conjugate in the solution. Fluorescence anisotropy for each titration point was measured 5 times after a 3 minutes incubation at 20°C. The final concentration includes a dilution factor to correct for the volume of added protein solution.

The interactions were carried out by using three different methodologies, keeping in each experiment the GST concentration $1.00 \cdot 10^{-8}$ M. Different GST (B14) solutions at different concentrations were prepared by diluting a $2.50 \cdot 10^{-6}$ M mother solution.

The experimental conditions are the following:

- **interaction 1**

  [GST] = $1.00 \cdot 10^{-8}$ M

  [GST (B14)] = $2.50 \cdot 10^{-6}$ M

  Initial volume = 200 μL

  - 5 GST (B14) solutions at different concentration were prepared ($1.33 \cdot 10^{-9}$ M, $8.00 \cdot 10^{-9}$ M, $4.00 \cdot 10^{-8}$ M, $2.00 \cdot 10^{-7}$ M, $8.00 \cdot 10^{-7}$ M);
  - 3 additions of each antibody solution (total additions: 15);
  - Final volume = 350 μL.

- **interaction 2**

  [GST] = $1.00 \cdot 10^{-8}$ M

  [GST (B14)] = $2.50 \cdot 10^{-6}$ M

  Initial volume = 200 μL

  - 8 GST (B14) solutions at different concentration were prepared ranging from $7.00 \cdot 10^{-9}$ M to $2.00 \cdot 10^{-6}$ M;
  - 5 additions (5 μL each) of each antibody solution (total additions: 40);
  - Final volume = 400 μL

- **interaction 3**

  [GST] = $1.00 \cdot 10^{-8}$ M

  [GST (B14)] = $2.50 \cdot 10^{-6}$ M

  Initial volume = 200 μL

  - 4 GST (B14) solutions at different concentration were prepared: $7.00 \cdot 10^{-9}$ M, $7.00 \cdot 10^{-8}$ M, $7.00 \cdot 10^{-7}$ M, $2.50 \cdot 10^{-6}$ M;
  - 8 additions (5 μL each) of the first three antibody solution and 16 additions of the last one (total additions: 40);
  - Final volume = 400 μL

4.3.2 Data Analysis and Results

Results of a typical experiment are presented in Figure 4.1. Data are plotted as the anisotropy of the complex as a function of added GST (B14). Binding isotherms were fitted to Equation 4.1 by nonlinear regression (using the programs SigmaPlot, GraphPad and TableCurve).

$$A = A_f + \left(A_b - A_f\right)\left[\frac{K_a[L]}{1 + K_a[L]}\right] \qquad [4.1]$$

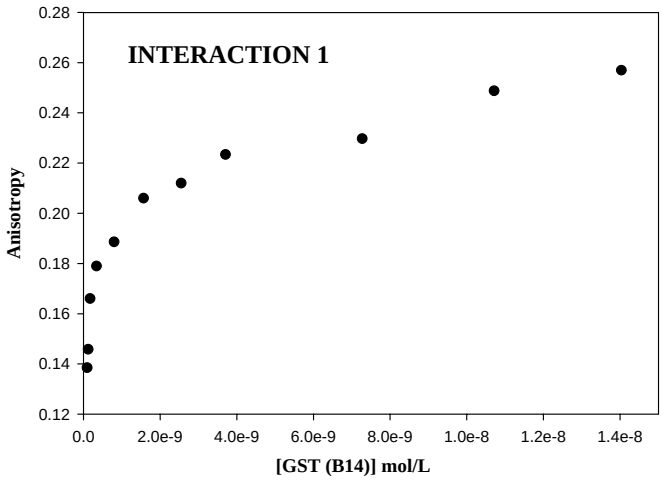

Figure 4.1 - GST, labelled with fluorescein-5-maleimide, interaction with B-14: Experiment 1

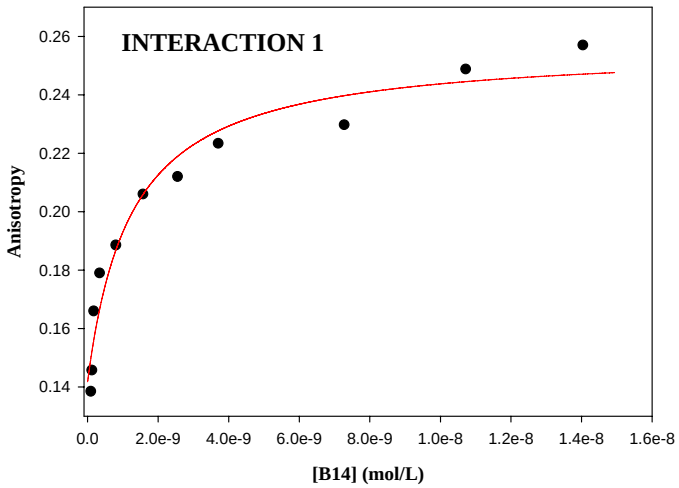

Fig. 4.2 - Fitting curve referring to GST – B-14 interaction: Experiment 1

By fitting the curve the following results were obtained:

r^2	0.95	
a	0.142	A_f
b	0.256	A_b
c	$8.08 \cdot 10^8$	K_a

Table 4.2 – Results from interaction 1

The obtained data a, b and c correspond to A_f, A_b e K_a respectively.

A_f is the anisotropy of free fluorescent molecules;

A_b is the anisotropy of bound fluorescent molecules;

K_a is the association binding constant.

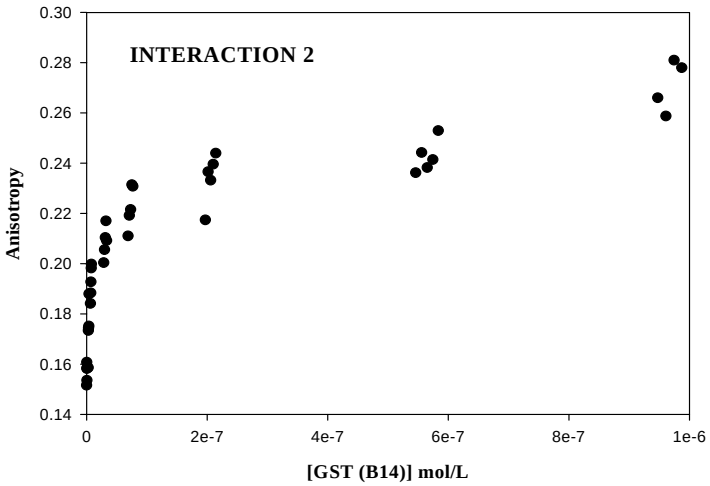

Figure 4.3 - GST, labelled with fluorescein-5-maleimide, interaction with B-14: Experiment 2

By fitting the curve the following results were obtained:

r^2	0.85	
a	0.140	A_f
b	0.248	A_b
c	$1.23 \cdot 10^8$	K_a

Table 4.3 - Results from interaction 2

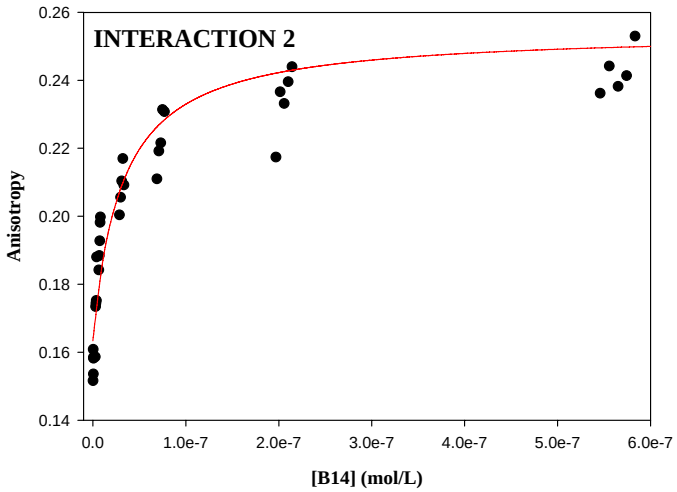

Figure 4.4 – GST, labelled with fluorescein-5-maleimide, interaction with B-14: Experiment 2

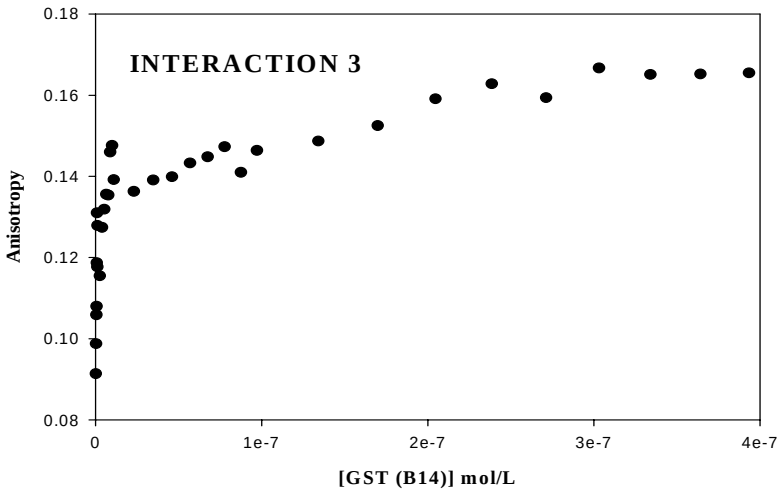

Figure 4.5 - GST , labelled with fluorescein-5-maleimide, interaction with B-14: Experiment 3

By fitting the curve the following results were obtained:

r^2	0.94	
a	0.09	A_f
b	0.140	A_b
c	$8.46 \cdot 10^8$	K_a

Table 4.4 - Results from Interaction 3

4.4 Conclusions

As it is evident from the reported graphs, an interaction between the GST protein and its antibody B14 does occur. Actually, a variation of the anisotropy signal (an increase in particularly in this case) by increasing the antibody concentration is visible.

In the following table the obtained binding constants are summarized:

Experiment	K_a	r^2
1	$8.08 \cdot 10^8$ M^{-1}	0.96
2	$1.23 \cdot 10^8$ M^{-1}	0.95
3	$8.46 \cdot 10^8$ M^{-1}	0.94

Table 4.5 – Summary of the obtained K_a

The binding constants obtained are in agreement with the few data available in literature and referring to protein–antibody interaction[14]. The molecular basis of the specificity of antigen-antibody interactions is still poorly understood. This is due partly to the difficulty of analyzing in detail the nature of the molecular contacts. In his study, Altschuh *et al.*[14] worked on the determination of kinetic constants for the interaction between a

monoclonal antibody and some peptides. They described a functional analysis of the interaction between a monoclonal antibody raised against tobacco mosaic virus (TMV) protein and a peptide corresponding to residues 134-146 of this protein. Differences in binding affinity resulting from single substitutions in the peptide were measured using the biosensor technology. They provided evidence of association constants in the order of 2.6–$3.7 \cdot 10^7$ M^{-1} depending from the different peptide involved. Another paper[15] reported the kinetic analysis of monoclonal antibody-antigen interactions providing a K_a which varies around $3.7 \cdot 10^7$ M^{-1} and $1.5 \cdot 10^8$ M^{-1}. Li *et al.*[16] utilized affinity capillary electrophoresis (ACE), a form of capillary zone electrophoresis (CZE) to determine the binding constant (K_a) of specific Abs against bovine serum albumin (BSA) and the healthy prion protein (PrPc), in buffer solutions at fixed pHs, approximating in vivo conditions. They derived K_a values as being $1.8 \cdot 10^7$ M^{-1} for the Rubenstein Ab and $1.9 \cdot 10^7$ M^{-1} for the VMRD Ab.

By comparing the results obtained for GST-B14 interaction with the one found in literature, we can then assert that a good binding specificity is present between GST and the antibody B14 and that the use of spectroscopic techniques, the fluorescence anisotropy in particular, is a useful and favourable tool to study biochemical problems.

Reference List

1. Vargo, M. A.; Nguyen, L.; Colman, R. F. Subunit Interface Residues of Glutathione S-Transferase A1-1 that Are Important in the Monomer-Dimer Equilibrium. *Biochemistry* **2004,** *43*, 3327-3335.

2. Armstrong, R. N. Structure, Catalytic Mechanism, and Evolution of the Glutathione Transferases. *Chem. Res. Toxicol.* **1997,** *10*, 2-18.

3. Mannervik, B.; Danielson, U. H. Glutathione transferases: structure and catalytic activity. *CRC Crit. ReV. Biochem. Mol. Biol.* **1988,** *23*, 283-337.

4. Wilce, M. C. J.; Parker, M. W. Structure and function of glutathione S-transferases. *Biochim. Biophys. Acta* **1994,** *1205*, 1-18.

5. Pickett, C. B.; Lu, A. L. H. Glutathione S-transferases: Gene structure, regulation, and biological function. *Annu. Rev. Biochem.* **1989,** *58*, 743-764.

6. Hayes, J. D.; Pulford, D. J. The glutathione Stransferases supergene family: Regulation of GST and the contribution of the isoenzymes to cancer chemoprotection and drug resistance. *CRC Crit. ReV. Biochem. Mol. Biol.* **1995,** *30*, 445-600.

7. Udomsinprasert, R.; Pongjaroenkit, S.; Wongsantichon, J.; Oakley, A. J.; Prapanthadara, L.; Wilce, M. C. J.; Ketterman, A. J. Identification, characterization and structure of a new Delta class glutathione transferase isoenzyme. *Biochem. J.* **2005,** *388*, 763-771.

8. Smith, D. B.; Johnson, K. S. Single-step purification of polypeptides expressed in Escherichia coli as fusion with glutathione S-transferase. *Gene* **1988,** *67*, 31-40.

9. Toye, B.; Zhong, G.; Peeling, R.; Brunham, R. C. Immunologic Characterization of a Cloned Fragment Containing the Species-Specific Epitope from the Major Outer Membrane Protein of Chlamydia trachomatis. *Infect. Immun.* **1990,** *58* (12), 3909-3913.

10. Fikrig, E.; Barthold, S. W.; Kantor, F. S.; Flavell, R. A. Protection of mice against the Lyme disease agent by immunizing with recombinant OspA. *Science* **1990,** *250*, 553-556.

11. Johnson, K. S.; Harrison, G. B. L.; Lightowlers, M. W.; O'Hoy, K. L.; Cougle, W. G.; Dempster, R. P.; Lawrence, S. B.; Vinton, J. G.; Heath, D. D.; Rickard, M. D. Vaccination against ovine cysticercosis using a defined recombinant antigen585. *Nature* **1989,** *338*, 585-587.

12. Kaelin, W. G.; Pallas, D. C.; DeCaprio, J. A.; Kaye, F. J.; Livingston, D. M. Identification of cellular proteins that can interact specifically with the T/ElA-binding region of the retinoblastoma gene product. *Cell* **1991,** *64*, 521-532.

13. Chittenden, T.; Livingston, D. M.; Kaelin, W. G. The T/E1A-binding domain of the retinoblastoma product can interact selectively with a sequence-specific DNA-binding protein. *Cell* **1991,** *65*, 1073-1082.

14. Altschuh, D.; Dubs, M. C.; Weiss, E.; Zeder-Lutz, G.; Van Regenmortel, M. H. V. Determination of Kinetic Constants for the Interaction between a Monoclonal Antibody and Peptides Using Surface Plasmon Resonance. *Biochemistry* **1992,** *31*, 6298-6304.

15. Karlsson, R.; Michaelsson, A.; Mattson, L. Kinetic-analysis of monoclonal antibody-antigen interactions with a new biosensor based analytical system. *J. Immunol. Methods* **1991,** *145* (1-2), 229-240.

16. Li, G.; Zhou, X.; Wang, J.; El-Shafey, A.; Chiu, N. H. L.; Krull, I. S. Capillary isoelectric focusing and affinity capillary electrophoresis approaches for the determination of binding constants for antibodies to the prion protein. *J. Chromatogr. A* **2004,** *1053*, 253-262.

Chapter 5 – GST-Tat86 – Peptide Interaction

Introduction

Tat (Trans Activator of Transcription) is a protein of HIV-1 with the main function of enhancing the transcription of viral RNAs[1], thus allowing the production of new viral particles and the consequent spreading of the virus. This function is mediated by a strongly basic region, corresponding to aa 48-58, which is responsible both of the nuclear import and of the binding to phosphates on the ribonucleic acid[2,3,4]. Due to its peculiar amino acidic sequence, and accordingly to the principle of viral economy, Tat has been demonstrated to modulate several other processes. As a nuclear factor, Tat can also activate the transcription of host genes, among which the cellular receptors and co-receptors for HIV-1 itself, CD4 and the chemokine receptors CCR5 and CXCR4 respectively[5]. Tat is also released by infected cells both in vitro and in vivo[6,7,8], and can enter surrounding cells, interfering with their gene expression[9,10]. When in the extracellular compartment, Tat acts also as a growth factor, inducing various cellular pathways by binding to trans-membrane receptors. For example, Tat stimulates angiogenesis by binding to VEGF Receptor-2, Flk-1[11,12]. These biochemical effects have been related to clinical outcomes. Large number of results suggest that Tat could contribute to the onset of disorders associated with HIV-1 infection, i.e. Kaposi's sarcoma[6,11], dementia[13], lymphoma[14], and kidney injury[15]. Interestingly, a direct, non-transcriptional function of Tat in the setting of a spreading viral infection has also been suggested[16]. This observation is confirmed by the ability of anti-Tat antibodies to reduce the viral load both in vitro and in vivo[17,18,19](reviewed in[20,21]). Despite the huge, and often controversial scientific production about the multifaceted roles of extracellular Tat, an insight into the molecular mechanism(s) responsible for a Tat-driven spreading of infection remained thus far elusive. Recent studies suggest that extracellular Tat is partially sequestered by heparin sulphate proteoglycans 27,28. As a consequence, Tat is concentrated at the cell surface, and protected from proteolytic degradation, thus remaining in a biologically active form[22].

HIV-1 Tat, a trans activator of viral gene expression, has the unusual property of being released by infected cells. Recently, it has been demonstrated that extracellular Tat is partially concentrated at the surface of both HIV-1-infected and surrounding uninfected cells[23]. There are evidences for a specific, high affinity interaction between Tat and the HIV-1 gp120 envelope protein, which leads to an enhanced ability of the virus to enter cells. The interacting sites of both Tat and gp120 have been mapped, and it has been shown that synthetic peptides mimicking these sites markedly inhibit HIV-1 infection. It has been demonstrated that membrane-associated Tat is an additional mediator of virus entry and that the Tat/gp120

interaction represents a critical step in HIV-1 spreading that may be a target for the design of a novel class of anti-AIDS drugs.

5.1 GST-Tat86 – CT319 Interaction: Steady-State Fluorescence

Introduction

The interaction between GST-Tat86 and CT319 was studied by steady-state fluorescence intensity by exploiting the intrinsic protein fluorescence of the aromatic amino acids.

5.1.1 Experimental

- *Reagents*

Recombinant wild-type **HIV-1 Tat** of 86 amino acids (Mitola et al., 2000) was expressed in *Escherichia coli* BL21 cells as glutathione S-transferase (GST) fusion protein, GST-Tat86. Bacteria were sonicated in buffer A2 (50mM TrisHCl pH 7.5, 1% TritonX100, 50 mM NaCl, 5mM MgCl2, 1 mM DTT) containing protease inhibitors. Lysates were incubated with glutathione-coupled Sepharose 4B beads (GE Healthcare Life Sciences) for 1 h at 4°C. After washing, the bounded beads were incubated with 2ml of buffer B2 (50mM TrisHCl pH 8.0, 50 mM NaCl, 2 mM DTT, 20 mM glutathione) overnight to perform affinity-chromatography separation. The eluates were concentrated to 0.3-0.5 mg/ml using Centrifugal Filter Device YM-10 MWCO 10.000 (CENTRICON), and then dialyzed against PBS with the employment of Slide-A-Lyzer 3.5K (PIERCE). Recombinant fusion protein gave a unique band after sodium dodecyl sulphate-polyacrylamide gel electrophoresis (SDS-PAGE) and Blue Comassie or silver stain. Recombinant protein concentrations were determined by Comassie-stained gels.

The CSFNITTEIRDKVKK (**CT319**) peptide was from New England Peptide (Fitchburg, MA).

- *Apparatus*

Fluorescence measurements were recorded using a LS55 Perkin Elmer spectrofluorimeter equipped with a xenon lamp source, a 5 mm path length quartz cell and a thermostat bath.

- *Experimental procedures*

The concentration of the GST-Tat86 is kept constant ($7 \cdot 10^{-8}$ M), and fluorescence intensity is measured by adding CT319 and by increasing its concentration. The fluorescence intensity spectrum at each concentration is collected and used to generate a binding isotherm. As already stated in chapter 3 and 4, during observation of fluorescence intensity, it is important to keep the temperature constant because the temperature greatly affects the molecular motion of the conjugate in the solution. Fluorescence intensity for each titration point was measured after a 3 minutes incubation at 20°C. The final concentration includes a dilution factor to correct for the volume of added peptide solution.

Samples were excited at 275 nm and spectra were collected from 300 to 500 nm. Slits widths were 2.5/20 nm. After pre-equilibration, the appropriate amount of protein stock was added (200 μl) and the fluorescence signal monitored until stable. The sample was then titrated with aliquots (from 5 to 30 μl) of peptide solution. Different peptide solutions at different concentrations were prepared by diluting a $5.0 \cdot 10^{-4}$ M mother solution. The interaction was studied with protein/peptide concentration ratio from 100:1 up to 1:100.

Titrations carried out by an addition of ligand causes dilution of the protein and hence reduction of the fluorescence intensity. For this reason, the volume dilution was kept minimum (total added volume was 142 μl) and a simple correction factor based on the added volume was used for obtaining a correct measure of fluorescence intensity.

The experimental conditions are the following:

[GST-Tat86] = $7.00 \cdot 10^{-8}$ M

[CT319] = $5.0 \cdot 10^{-4}$ M

Initial volume = 200 μL

- 6 different CT319 solutions at different concentration were prepared ($9.33 \cdot 10^{-9}$ M, $5.60 \cdot 10^{-8}$ M, $2.80 \cdot 10^{-7}$ M, $1.40 \cdot 10^{-6}$ M, $5.60 \cdot 10^{-6}$ M, $4.20 \cdot 10^{-5}$ M);
- 2 or 3 additions of each CT319 solution were added in order to study all the protein/peptide concentration ratio needed (100:1, 75:1, 50:1, 25:1, 10:1, 5:1, 3:1, 2:1, 1:1, 1:1.5, 1:2 and so on up to 1:100)
- final volume = 342 μL.

5.1.2 Results

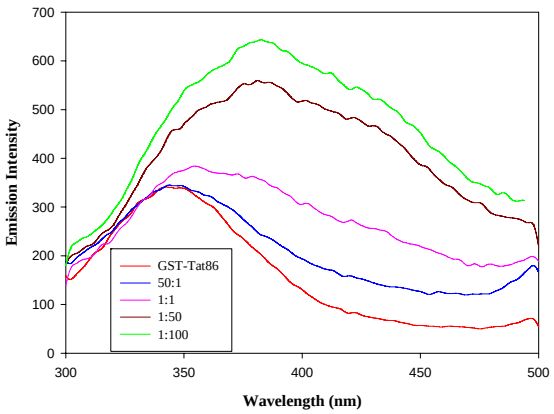

Figure 5.1 – Fluorescence spectra of the interaction between GST-Tat86 and CT319: experiment b

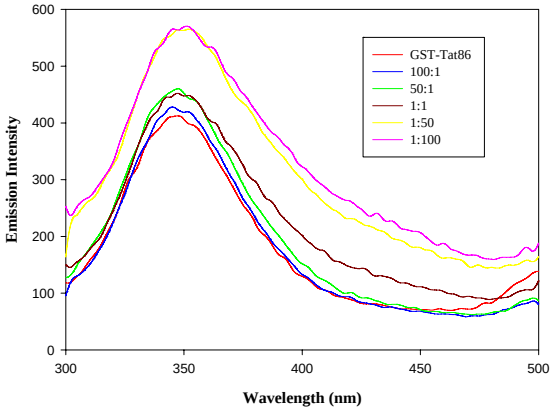

Figure 5.2 – Fluorescence spectra of the interaction between GST-Tat86 and CT319: experiment c

Fluorescence intensity spectra were collected over a range of 300 and 500 nm as reported in figure 5.1. The obtained maximum fluorescence intensity was plotted against the CT319 concentration and fitted to the one site specific binding equation already reported in chapter 3 (Equation 3.2) and the association and dissociation binding constants were calculated.

Some example of the obtained binding curves are reported in the following figures.

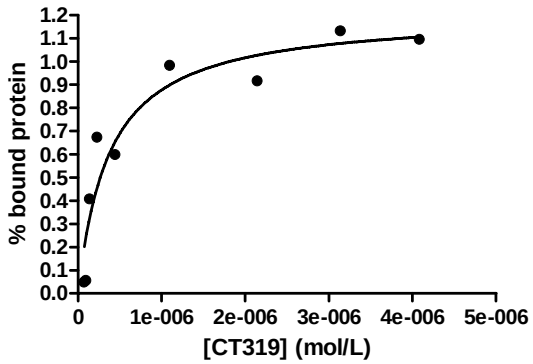

Figure 5.3 – Binding curve obtained from experiment b

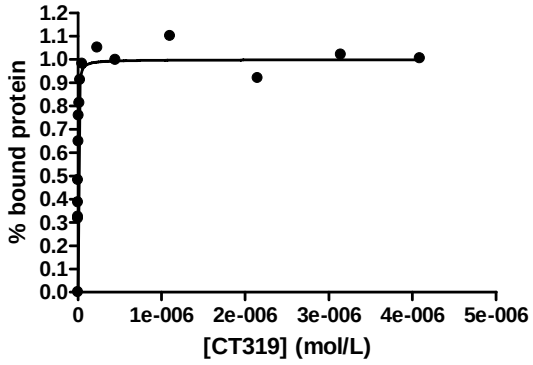

Figure 5.4 – Binding curve obtained from experiment e

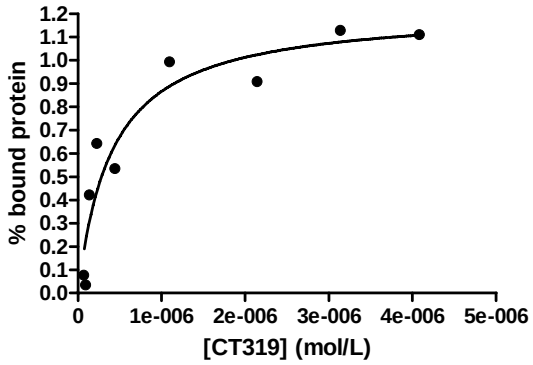

Figure 5.5 – Binding curve obtained from experiment d

A results summary is reported in the following table:

Interaction	K_a (M^{-1})	K_d (M)	B_{max}
a	$9.71 \cdot 10^{+8}$	$1.03 \cdot 10^{-9}$	-
b	$2.67 \cdot 10^{+6}$	$3.75 \cdot 10^{-7}$	1.21
c	$2.20 \cdot 10^{+8}$	$4.55 \cdot 10^{-9}$	1.05
d	$2.46 \cdot 10^{+6}$	$4.06 \cdot 10^{-7}$	1.22
e	$4.29 \cdot 10^{+8}$	$2.33 \cdot 10^{-9}$	1.00
f	$5.00 \cdot 10^{+5}$	$2.00 \cdot 10^{-6}$	1.29

Table 5.1 – Results summary of GST-Tat86/CT319 interaction

5.1.3 Conclusions

An increase of the fluorescence intensity signal by increasing the peptide concentration is visible (see figure 5.2) and is ascribed to the fact that an interaction between GST-Tat86 protein and CT319 does occur. In some cases, as reported in figure 5.1, an increase of the peptide concentration causes a shift of the emission maximum to longer wavelength (red shift) along with an increase of the intensity emission signal.

The results show that the obtained binding constants differ in the same set of interactions. The fact that the experimental conditions are the same in all the seven tests does not explain the reasons of these variances. The K_a and K_d obtained are of the same order of magnitude with the data available in literature referring to protein-protein interaction. In particular, one set of results with K_d in the nanomolar range is in very good agreement with the result obtained by Marchiò et al.[23] and referring to a very similar interaction. They provide evidence for a specific interaction between Tat and the HIV-1 glycoprotein 120 (gp120) envelope protein by Surface Plasmon Resonance (SPR).

The variation of the obtained binding constants can be due to the presence of many tryptophan residues (GST has 7 Trp while Tat has one Trp at the NH_2-terminal). Each tryptophan residue has a unique environment with respect to associated amino acids and solvent interactions. Since tryptophan residues are so sensitive, this means that the spectral properties of each residues will be different providing different ways of interaction.

Also, tryptophan fluorescence is easily quenched because the indole nucleus tends to donate electrons while it is in the excited state. This makes the interpretation of fluorescent spectra that are based on intrinsic fluorescence very difficult and it has led to an application which rely on covalently attached fluorescent labels. It is better to label one of the two species involved and study the interaction by following the fluorophore signal.

5.2 GST-Tat86 – V2 Interaction: Steady-State Fluorescence

Introduction

The aim of this work was to study the interaction between GST-Tat86 and V2 (a small peptide with almost the same aa sequence of CT319) by steady-state fluorescence anisotropy. Some attempts of labelling GST-Tat86 and V2 with fluorescein-5-maleimide have been made.

The GEIKNCSFNITTSIRDKVQK (**V2**) peptide was from New England Peptide (Fitchburg, MA).

5.2.1 GST-Tat86 Bioconjugation

GST-Tat86 fusion protein has been bioconjugated with fluorescein-5-maleimide following the protocol reported in Chapter 2 and 3. GST-Tat86 presents eleven cysteine residues of which one is to be ascribed to GST. The bioconjugation was repeated two times and the resulting D/P values are reported in Table 5.1:

[GST-Tat86] mg/ml	D/P	Test
0.5	1.0	a
0.5	2.5	b

Table 5.1 – Summary of bioconjugation tests

The D/P value is lower than we could expect for a multi cysteine protein. The bioconjugation was repeated but the D/P variation was not appreciable. Anyway, such a low value is a good result because it means that there is one or two fluoresceins for each GST-Tat86 which will be involved and detected in the interaction. This selective bioconjugation can help in having more reliable data since what it will be followed in fluorescence will be ascribed to the interacting fluorescein per molecule of protein.

5.2.2 V2 Bioconjugation

Some attempts of V2 bioconjugation were made but several problems were faced. First of all, the peptide concentration was very low and the bioconjugation protocol was difficult to perform. A huge problem of purification of the excess of fluorescein-5-maleimide raised. Actually, after the bioconjugation protocol, the excess of fluorophore (usually 25 fold) have to be removed in order to get the labelled protein alone and ready for the interaction studies. The purification by using Sephadex® G25 resulted impossible since the difference between the molecular weights of the two species involved were too small. The fact is that the labelled protein has a molecular weight of 2709 g/mol while the fluorophore is only 427 g/mol. The purification was made by using different Sephadex® resins with different exclusions size (G10 and G15) but the result was not a good separation. A separation attempt by HPLC was also made. The Bioconjugation solution has been adsorbed on a Grace Vydac C18 monomeric column, 250*4.6 mm, 5 μm particle size, 300 Å size pore. Then, the three distinct fractions have been eluted with the following three different mobile fases:

- 0% CH_3OH/100% H_2O with 0.1% trifluoroacetic acid (TFA) for removing the solvent and buffer, DMF and PBS;
- 50% CH_3OH/50% H_2O for removing the excess of fluorescein;
- 95% CH_3OH/5% H_2O to get the labelled V2.

The obtained labelled V2 was characterized by UV-Vis spectroscopy and the D/P was calculated. The value 0.002 was a proof of the failure of bioconjugation. The Bioconjugation and the HPLC purification process were repeated but the same D/P value was obtained.

A V2 characterization was performed in order to check and find the reason of the failed bioconjugation. A mass analysis was made and the results show the presence of V2 dimers in the solution to be bioconjugated. This is the reason for the low D/P value found. A bioconjugation on the cysteine residues resulted impossible since all the Cys present had reacted to form disulfide bonds.

Figure 5.6 shows the chromatogram of the peptide and it can be seen the presence of both the monomer and the dimer. Moreover, figure 5.7 confirms the presence of the dimer from the mass spectra made on the V2.

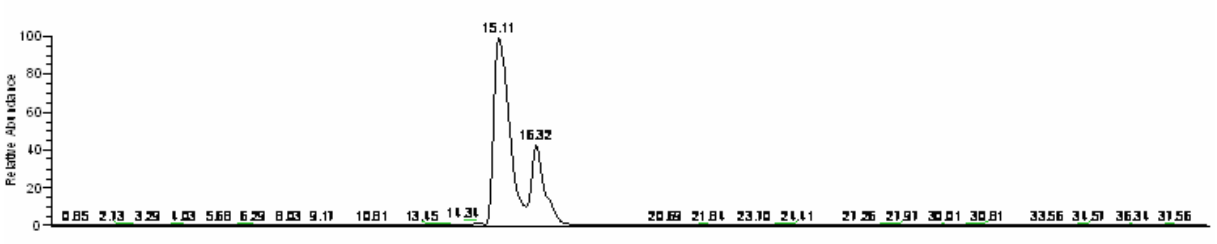

Figure 5.6 – Chromatogram performed on V2

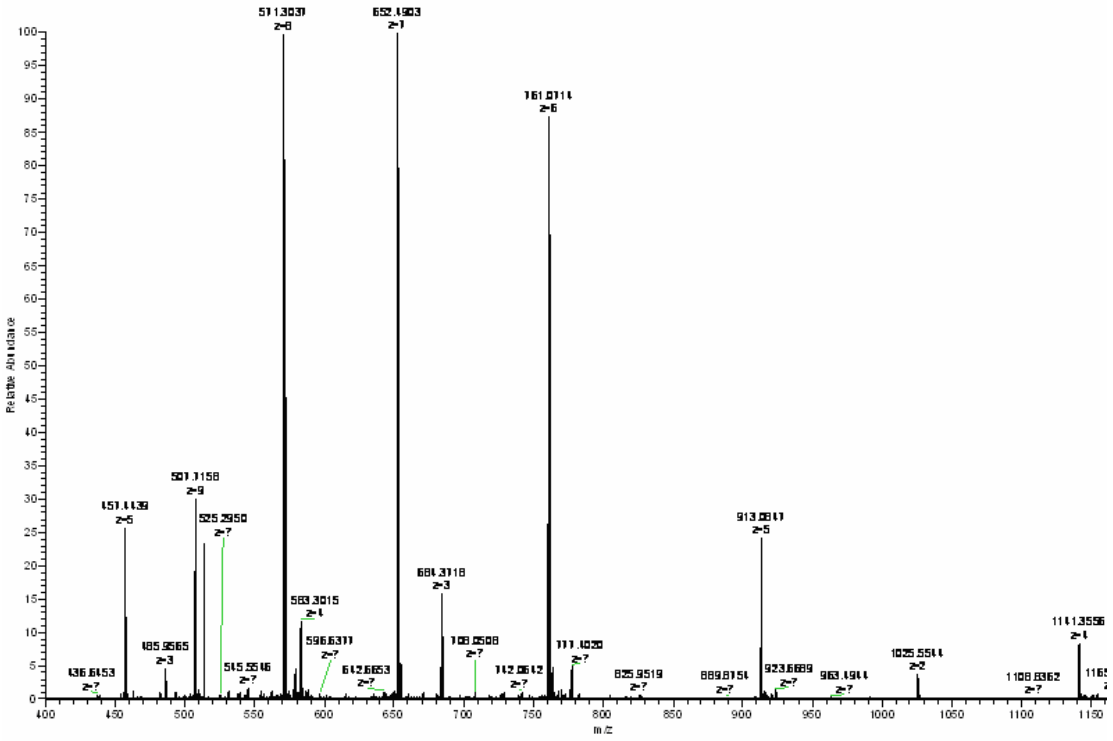

Figure 5.7 – Mass spectrum performed on V2

5.2.3 Conclusions

Some attempts of interaction studies with labelled GST-Tat86 and V2 have been made but the results were not as good as expected. The most important problem was that by bioconjugating the bigger protein involved in the interaction, the signal followed in anisotropy is not the best one. It is usually advisable to label the smaller species since it is

easier to modify the ligand if it is a small molecule because it will generally be easier to produce a well characterized product and the fluorophore will be close to the binding site in the complex and therefore more likely to give fluorescence intensity changes.

Thus, since the V2 bioconjugation resulted impossible, the mainly idea was to synthesise the peptide already biolabelled.

5.3 GST-Tat86 – labelled-V2 Interaction: Steady-State and Stopped-flow Fluorescence

Introduction

The interaction between GST-Tat86 and V2 labelled at the N-terminal with 5-carboxyfluorescein was studied by both steady-state and stopped-flow fluorescence.

5-carboxyfluorescein-V2 (5-carboxyfluorescein-GEIKNCSFNITTSIRDKVQK-OH) was purchased from New England Peptide (Fitchburg, MA).

5.3.1 Steady-State Fluorescence Intensity

5.3.1.1 Experimental

As already stated in chapter 3 and 4, experiments were performed in a time drive mode in order to check whether the solution had reached the stability. Samples were excited at 295 nm and monitored at 350 nm in order to selectively excite the GST-Tat86 Trp residues. A study performed by exciting the carboxyfluorescein labelled to V2 was not possible due to the very low amount of protein. Slits widths were 2.5/15.0 nm. After pre-equilibration, 400 μl of protein stock solution were added and the fluorescence signal monitored until stable. The sample was then titrated with aliquots (10 or 20 μl) of V2 solution. The concentration of the GST-Tat86 is kept constant ($1 \cdot 10^{-7}$ M), and fluorescence intensity is measured by adding V2 and by increasing its concentration. Titrations carried out by an addition of ligand causes dilution of the protein and hence reduction of the fluorescence intensity. For this reason, the volume dilution was kept minimum and a simple correction factor based on the added volume was used for obtaining a correct measure of fluorescence intensity.

Moreover, the fluorescence intensity spectrum at each concentration was also collected and used to generate a binding isotherm.

The experimental conditions are the following:

[GST-Tat86] = $1.00 \cdot 10^{-7}$ M

[V2] = $2.5 \cdot 10^{-6}$ M

Initial volume = 400 µL

Final volume = 720 µL

5.3.1.2 Results

One example of GST-Tat 86/V2 titration is reported in figures 5.8. Fluorescence intensity spectra were collected over a range of 300 and 500 nm.

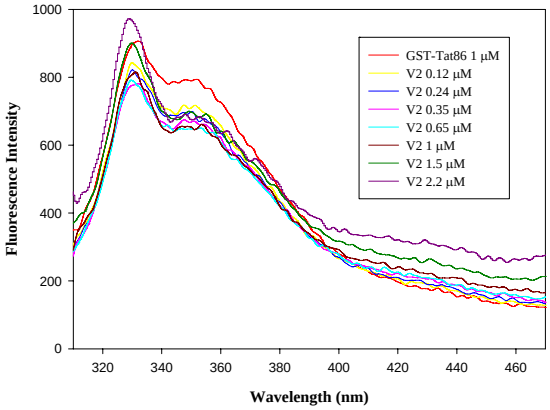

Figure 5.8 – Fluorescence spectra of the interaction between GST-Tat86 and V2

It is evident that, even by working with almost the same experimental conditions reported in the first part of the chapter, the fluorescence emission spectra are very different. It is true that the interaction studied in Chapter 5.1 was between GST-Tat86 and another small peptide but, since CT319 and V2 have almost the same aa sequence and the same biological activity, they should behave in a similar way. As it can be seen in figure 5.8, the fluorescence intensity of the titrated protein does not decrease linearly by increasing the V2 concentration as happened from the BSA-fluorescein sodium salt interaction. A plot of the fluorescence intensity maximum against V2 concentration is reported in Figure 5.9 as a further demonstration. Moreover, the shape of the spectrum is also quite strange. The presence of two peaks in the protein emission spectrum both in presence and absence of V2 does not agree with the old GST-Tat86 spectrum. Maybe some further compounds is present or some protein modification occurred.

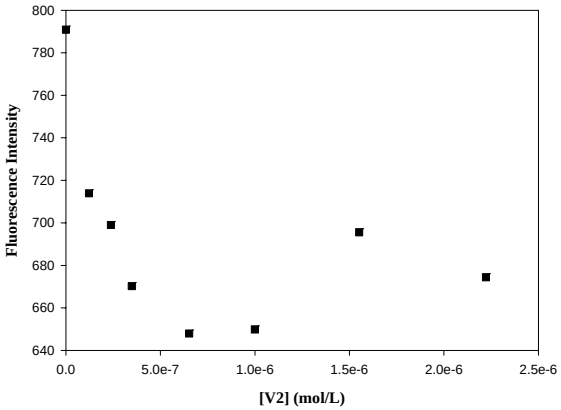

Figure 5.9 – Fluorescence emission intensity versus V2 concentration

A further study on this interaction has been made by exciting the fluorophore and two spectra were collected in presence and absence of protein. As it can be seen in figure 5.10, the shape of the spectrum does not change with the GST-Tat86 addition, nor a peak wavelength shift is observed.

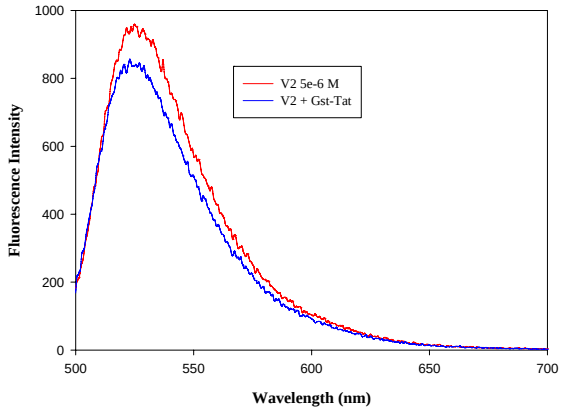

Figure 5.10 – Fluorescence spectra of the interaction between GST-Tat86 and V2

A binding study by following the quenching of the protein by the addition of the ligand have been performed unfortunately leading to very poor results. The experiment has been repeated as much as possible (due to the very low amount of reagents) but in every case, the V2 quenching on the GST-Tat86 was too low to let build a good binding isotherm. The collected data were indeed very difficult to fit and a data treatment by the methods reported in Chapter 3 was not possible.

5.3.2 Steady-State Fluorescence Anisotropy

5.3.2.1 Experimental

After pre-equilibration, 400 μl of V2 labelled with 5-carboxyfluorescein stock solution were added in the cuvette and the fluorescence anisotropy signal monitored. The sample was then titrated with aliquots (10 or 20 μl) of GST-Tat86 solution.

The experimental conditions are the following:

[V2] = $5.00 \cdot 10^{-7}$ M

[GST-Tat86] = $2.5 \cdot 10^{-06}$ M

Initial volume = 400 μL

Final volume = 720 μL

The anisotropy value at each concentration is measured and used to generate a binding isotherm. During observation of anisotropy, it is important to keep the temperature constant because the temperature greatly affects the molecular motion of the conjugate in the solution. Fluorescence anisotropy for each titration point was measured 10 times after a 6 minutes incubation at 25°C. The final concentration includes a dilution factor to correct for the volume of added protein solution.

The excitation wavelength was 492 nm while the emission wavelength was 517 nm, slit width were 2.5/5.0 nm, integration time 5 seconds. The calculated G factor was 1.15.

5.3.2.2 Results

As it can be seen from Figure 5.11, there is nearly no variation in the anisotropy value (it varies from 0.036 up to 0.045) by increasing GST-Tat86 concentration. It seems like the interaction between V2 and the protein does not occur. By calculating the total intensity value from the anisotropy data (using equation 1.1) and plotting it in a graph versus the protein concentration, an increase of the fluorescence intensity is detectable providing that an interaction does occur (as already evident from the steady-state intensity measurements) but there is no way of fitting these data in order to get any binding constants.

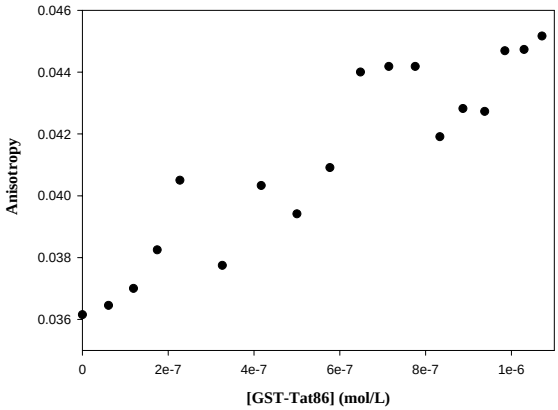

Figure 5.11 – Fluorescence anisotropy of GST-Tat86-V2 interaction

5.3.3 Stopped-flow Fluorescence Intensity and Anisotropy

5.3.3.1 Experimental

Fluorescence measurements were recorded using a SX20 stopped-flow spectrometer fitted with a 515 nm cut-off filter between the cell and fluorescence detector and equipped with a thermostatic bath. Data acquisition, visualisation and analysis is provided by Pro-Data software running under Windows™ XP.

The excitation wavelength was 485 nm. Slits widths of the excitation monochromator were 0.2 mm. 5-carboxyfluorescein V2 concentration (0.2 nM) was kept constant and several shots of different GST-Tat86 concentration were performed:

[5-carboxyfluorescein V2] = 20 nM in HEPES buffer;

[GST-Tat86] = 200, 400, 600 and 800 nM in HEPES buffer.

All the concentrations are syringe concentrations and will be halved into the cell. For each condition at least ten scans of about 500 data points each were acquired and averaged. The buffer used is 0.05 M HEPES buffer, pH 7.5 with 1mM DTT to avoid the V2 dimerization.

5.3.3.2 Results

The interaction was followed by both intensity and anisotropy but poor results were collected by both method. The concentrations used were too low for the interaction to be detectable. By pushing together the fluorescent ligand and the protein in the observation cell, no change in the intensity signal was detected. Moreover, by switching to the anisotropy mode, the first step of GF calculation was impossible since the concentrations were too low and the calculated GF was 0.07 while this value should be around 1. Therefore, the measurements were not carried out.

5.3.4 Conclusions

The interaction between V2 labelled with 5-carboxyfluorescein with GST-Tat86 was studied by fluorescence spectroscopy. The interaction was first followed by detecting the fluorescence intensity variation by keeping GST-Tat86 concentration constant and by adding the ligand. The intensity spectra underwent a variation which was not linear with the ligand concentration. Therefore, a study exploiting the fluorescence anisotropy was chosen. The fluorescent labelled V2 was titrated by GST-Tat86 but there was no change in the anisotropy signal. It should have increased by the formation of the complex protein-ligand since the mobility of the fluorophore should have decreased.

The kinetics of the interaction was also followed both in intensity and anisotropy mode. But in both cases, the concentrations and the amount of the samples in study were not enough for a complete study. Actually, the concentrations used were too low to be detectable.

Reference List

1. Marciniak, R. A.; Calnan, B. J.; Franke, A. D.; Sharp, P. A. HIV-1 Tat protein trans-activates transcription in vitro. *Cell* **1990,** *63*, 791-802.

2. Chang, H. K.; Gallo, R. C.; Ensoli, B. Regulation of Cellular Gene Expression and Function by the Human Immunodeficiency Virus Type 1 Tat Protein. *J. Biomed. Sci.* **1995,** *2*, 189-202.

3. Cullen, B. R. Does HIV-1 Tat induce a change in viral initiation rights? *Cell* **1993,** *73*, 417-420.

4. Jeang, K. T.; Xiao, H.; Rich, E. A. Multifaceted Activities of the HIV-1 Transactivator of Transcription, Tat. *J. Biol. Chem.* **1999,** *274*, 28837-28840.

5. Huang, L.; Bosch, I.; Hofmann, W.; Sodroski, J.; Pardee, A. Tat Protein Induces Human Immunodeficiency Virus Type 1 (HIV-1) Coreceptors and Promotes Infection with both Macrophage-Tropic and T-Lymphotropic HIV-1 Strains. *J. Virol.* **1998,** *72*, 8952-8960.

6. Ensoli, B.; Barillari, G.; Salahuddin, S. Z.; Gallo, R. C.; Wong-Staal, F. Tat protein of HIV-1 stimulates growth of cells derived from Kaposi's sarcoma lesions of AIDS patients. *Nature* **1990,** *345*, 84-86.

7. Ensoli, B.; Buonaguro, L.; Barillari, G.; Fiorelli, V.; Gendelman, R.; Morgan, R. A.; Wingfield, P.; Gallo, R. C. Release, Uptake, and Effects of Extracellular Human Immunodeficiency Virus Type 1 Tat Protein on Cell Growth and Viral Transactivation. *J. Virol.* **1993,** *67*, 277-287.

8. Westendorp, M. O.; Frank, R.; Ochsenbauer, C.; Stricker, K.; Dhein, J.; Walczac, H.; Debatin, K. M.; Krammer, P. H. Sensitization of T cells to CD95-mediated apoptosis by HIV-1 Tat and gp120. *Nature* **1995,** *375*, 497-500.

9. Helland, D. E.; Welles, J. L.; Caputo, A.; Haseltine, W. A. Transcellular Transactivation by the Human Immunodeficiency Virus Type 1 tat Protein. *J. Virol.* **1991,** *65*, 4547-4549.

10. Thomas, C. A.; Dobkin, J.; Weinberger, O. K. TAT-Mediated Transcellular Activation of HIV-1 long Terminal Repeat Directed Gene Expression by HIV-1-Infected Peripheral Blood Mononuclear Cells. *J. Immunol.* **1994,** *153*, 3831-3839.

11. Albini, A.; Barillari, G.; Benelli, R.; Gallo, R. C.; Ensoli, B. Angiogenic properties of human immunodeficiency virus type 1 Tat protein. *Proc. Natl. Acad. Sci. USA* **1995,** *92*, 4838-4842.

12. Albini, A.; Soldi, R.; Giunciuglio, D.; Giraudo, E.; Benelli, R.; Primo, L.; Noonan, D.; Salio, M.; Camussi, G.; Rockl, W.; Bussolino, F. The angiogenesis induced by HIV-1 Tat protein is mediated by the Flk-1/KDR receptor on vascular endothelial cells. *Nat. Med.* **1996,** *2*, 1371-1375.

13. Liu, Y.; Jones, M.; Hingtgen, C. M.; Bu, G.; Laribee, N.; Tanzi, R. E.; Moir, R. D.; Nath, A.; He, J. J. Uptake of HIV-1 Tat protein mediated by low-density lipoprotein receptor-related protein disrupts the neuronal metabolic balance of the receptor ligands. *Nat. Med.* **2000,** *6*, 1380-1387.

14. Chirivi, R. G.; Taraboletti, G.; Bani, M. R.; Barra, L.; Piccinini, G.; Giacca, M.; Bussolino, F.; Giavazzi, R. Human Immunodeficiency Virus-1 (HIV-1)-Tat Protein Promotes Migration of Acquired Immunodeficiency Syndrome–Related Lymphoma Cells and Enhances Their Adhesion to Endothelial Cells. *Blood* **1999,** *94*, 1747-1754.

15. Conaldi, P. G.; Bottelli, A.; Baj, A.; Serra, C.; Fiore, L.; Federico, G.; Bussolati, B.; Camussi, G. Human Immunodeficiency Virus-1 Tat Induces Hyperproliferation and Dysregulation of Renal Glomerular Epithelial Cells. *Am. J. Pathol.* **2002,** *161*, 53-61.

16. Huang, L. M.; Joshi, A.; Willey, R.; Orenstein, J.; Jeang, K. T. Human immunodeficiency viruses regulated by alternative trans-activators: genetic evidence for a novel non-transcriptional function of Tat in virion infectivity. *EMBO J.* **1994,** *13*, 2886-2896.

17. Cafaro, A.; Caputo, A.; Fracasso, C.; Maggiorella, M. T.; Goletti, D.; Baroncelli, S.; Pace, M.; Sernicola, L.; Koanga-Mogtomo, M. L.; Betti, M.; Borsetti, A.; Belli, R.; Åkerblom, L.; Corriasi, F.; Buttò, S.; Heeney, J.; Verani, P.; Titti, F.; Ensoli, B. Control of SHIV-89.6P-infection of cynomolgus monkeys by HIV-1 Tat protein vaccine. *Nat. Med.* **1999,** *5*, 643-650.

18. Re, M. C.; Vignoli, M.; Furlini, G.; Gibellini, D.; Colangeli, V.; Vitone, F.; La Placa, M. Antibodies against full-length Tat protein and some low-molecular-weight Tat-peptides correlate with low or undetectable viral load in HIV-1 seropositive patients. *J. Clin. Virol.* **2001,** *21*, 81-89.

19. Agwale, S. M.; Shata, M. T.; Reitz, M. S.; Kalyanaraman, V. S.; Gallo, R. C.; Popovic, M.; Hone, D. M. A Tat subunit vaccine confers protective immunity against the immune-modulating activity of the human immunodeficiency virus type-1 Tat protein in mice. *Proc. Natl. Acad. Sci. USA* **2002,** *99*, 10037-10041.

20. Goldstein, G. HIV-1 Tat protein as a potential AIDS vaccine. *Nat. Med.* **1996,** *2*, 960-964.

21. Gallo, R. C. Tat as one key to HIV-induced immune pathogenesis and Pat toxoid as an important component of a vaccine. *Proc. Natl. Acad. Sci. USA* **2007,** *96*, 8324-8326.

22. Chang, H. C.; Samaniego, F.; Nair, B. C.; Buonaguro, L.; Ensoli, B. HIV-1 Tat protein exits from cells via a leaderless secretory pathway and binds to extracellular matrix-associated heparan sulfate proteoglycans through its basic region. *Aids* **1997,** *11*, 1421-1431.

23. Marchiò, S.; Alfano, M.; Primo, L.; Gramaglia, D.; Butini, L.; Gennero, L.; De Vivo, E.; Arap, W.; Giacca, M.; Pasqualini, R.; Bussolino, F. Cell surface–associated Tat modulates HIV-1 infection and spreading through a specific interaction with gp120 viral envelope protein. *Blood* **2005,** *105* (7), 2802-2811.

Chapter 6 – MEK-ERK Interaction

6.1 Introduction

The ERK signalling cascade[1] is a central MAPK pathway component, composed of protein kinases that sequentially phosphorylate and activate each other. The ERK cascade is stimulated by a large variety of extracellular signals, and, as a consequence, regulates many distinct and even opposing cellular processes, including proliferation, differentiation, survival and even apoptosis[2,3,4,5]. The ability of the ERK cascade to initiate and regulate all these effects raises the question as to how its specificity is determined. In order to execute all its functions, the ERK cascade is heavily regulated at several levels, mainly by different phosphatases, but also by other interacting proteins. Studying all these regulatory mechanisms can, therefore, lead to a better understanding of oncogenic transformation and may induce to a better design of drugs that can be used in the combat of cancer.

The signaling via this cascade (Figure 6.1) is usually initiated by activation of small G proteins (e.g. Ras), which transmit the signal further by recruiting the MAP3K tier Raf kinases to the plasma membrane, where they are activated[6]. Other MAP3K components that participate in the activation of ERKs under specific conditions are (i) c-Mos that acts specifically in the reproductive system[7]; (ii) the protooncogene TPL2[8]; and (iii) MEKK1[9] that acts mainly under stress conditions. An additional protein kinase in this tier might be the kinase suppressor of Ras (KSR), but the role of its catalytic activity is still controversial[10], as it seems to act mainly as a scaffold protein for the ERK cascade[11]. All these MAP3Ks transmit the signals further by phosphorylating and activating the MAPKK tier proteins, MAPK/ERK kinases (MEKs[12,13]), which funnel upstream signals into the characteristic linear cascade, as observed in lower organisms[14]. MEKs are activated by phosphorylation of two Ser residues in their activation loop (Ser218 and Ser222 in MEK1) located within a Ser–Xaa–Ala–Xaa–Ser/Thr motif[15], typical to all MAPKKs. This phosphorylation may be regulated in part by a direct interaction of the domain for versatile docking (DVD) region in MEKs with their upstream activators[16]. The activity of MEKs is regulated by additional phosphorylation/dephosphorylation processes as well. Amongst these are the phosphorylation of Ser386 of MEK1 by ERKs[17], which can either inhibit ERKs activity[18], or under other conditions, facilitate the activation by enhancing the binding of MEK1 to the scaffold Grb10[19]. Phosphorylation of Ser298 of MEK1 by p21-activating protein (PAK1) plays an accessory role in MEKs' activation[20,21], a process that can be inhibited by a feedback phosphorylation on Thr292 of MEK1 by ERKs[22]. Several other phosphorylation sites on

MEK1, which might regulate its activity are detailed elsewhere[23]. Finally, the downregulation of MEKs involves a rapid dephosphorylation of pSer218 and pSer222, mainly by the protein Ser/Thr phosphatase PP2A[24], but possibly also other phosphatases.

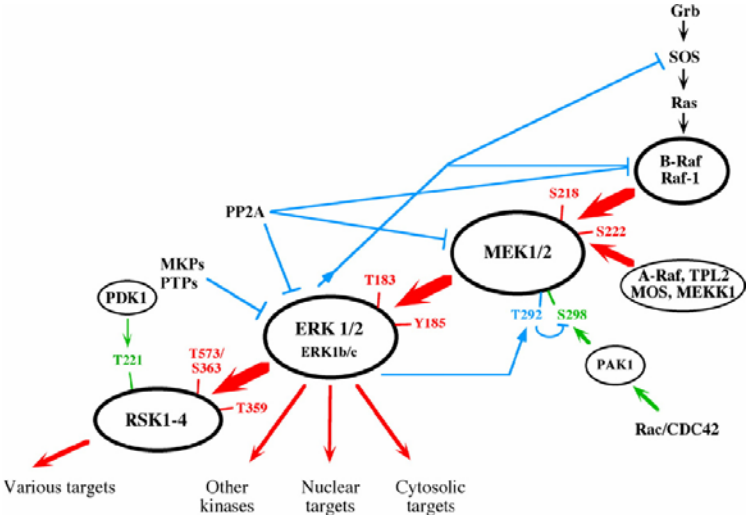

Figure 6.1 - Schematic representation of the ERK signaling cascade. Activation and inactivation processes are indicated. Dashed lines indicate indirect activations, and bold arrows stand for the main pathway upon growth factor activation. Red: activatory phosphorylation. Green: accessory phosphorylation. Blue: inhibitory phosphorylation and dephosphorylation

As already mentioned, this work is part of a wider research project whose aim is the modeling of known converging signal pathways elicited by tyrosine receptor kinases involved in angiogenesis. This approach could provide a useful tool to understand what are the mechanisms of each signaling and to find some sensible nodes of the protein network that would allow to finely tune cell functions. A complete signaling cascade was reconstructed by mathematical description of the INTEGRIN/VEGFR-induced pathways and the attention was focused on a useful group of proteins to work on reported in Figure 6.2. MEK-ERK interaction belongs to this pathway.

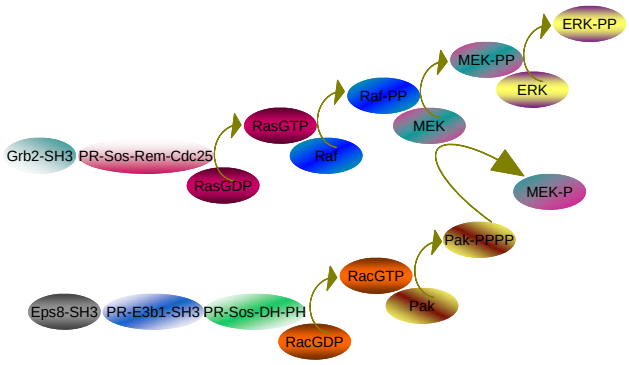

Figure 6.2 - Schematic representation of the chosen proteins

- *Materials*

MAP Kinase 1/**ERK1**, unactive was purchased from Upstate®.

N-terminal GST-tagged, recombinant, full-length, human MAP Kinase 1/ERK1, expressed in *E. coli*. Purified using glutathione-agarose. Purity 97% by SDS-PAGE and Coomassie blue staining. MW = 70kDa.

MEK1, active was purchased from Upstate®.

N-terminal GST and *C*terminal 6His-tagged, recombinant full-length human MEK1 expressed in *E. coli*. Purified using glutathione agarose followed by Ni^{2+}/NTA agarose, activated using c-Raf and the re-purified using Ni^{2+}/NTA agarose. Purity 98% by SDS-PAGE and Coomassie blue staining. MW = 71kDa

6.2 Bioconjugation

ERK unactive protein has been bioconjugated with fluorescein-5-maleimide following the protocol reported in Chapter 2. ERK presents ten cysteine residues. The bioconjugation was performed only once due to the very small quantity of the reagent and the resulting D/P value was 4.13. ERK concentration was 0.4 mg/ml and the excess of fluorescein-5-maleimide used was 50 times. This excess was removed by Sephadex® G25 desalting column.

6.3 Interaction

The interaction between MEK and biolabelled ERK was studied by stopped-flow fluorescence intensity.

The concentration of the fluorescent-labeled protein (ERK conjugated with fluorescein-5-maleimide) is kept constant, and some shots at different MEK concentration are performed and the signal is followed by measuring fluorescence intensity.

- *Apparatus*

Fluorescence measurements were recorded using a SX20 stopped-flow spectrometer fitted with a 515 nm cut-off filter between the cell and fluorescence detector and equipped with a thermostat bath (25°C). Data acquisition, visualisation and analysis is provided by Pro-Data software running under Windows™ XP.

- *Experimental procedures*

The excitation wavelength was 285 nm. Slits widths of the excitation monochromator were 0.2 mm. Biolabelled ERK concentration ($1.00 \cdot 10^{-8}$ M) was kept constant and several shots of different MEK concentration were performed:

[biolabelled ERK] = 10 nM in PBS buffer,

[MEK] = 100 nM, 120 nM, 140 nM and 160 nM in PBS buffer.

The reported concentrations are syringe concentrations, this means that the real concentrations in the cuvette are halved. For each condition at least five scans were acquired and averaged.

Raw data were analyzed and plotted to a double exponential function by using Pro-Data Viewer 4.0.17 from Applied Photophysics Ltd and from this data treatment the observed rate constants were obtained as explained in chapter 1.2 and 3.3.

- *Intensity Results*

The binding of MEK to ERK was investigated under pseudo-first-order conditions. Figure 6.3 shows that on mixing 10 nM ERK with 120 nM MEK there is a decrease in fluorescence intensity which can be well fitted to a double exponential with a rate constant of 12.49 s^{-1}.

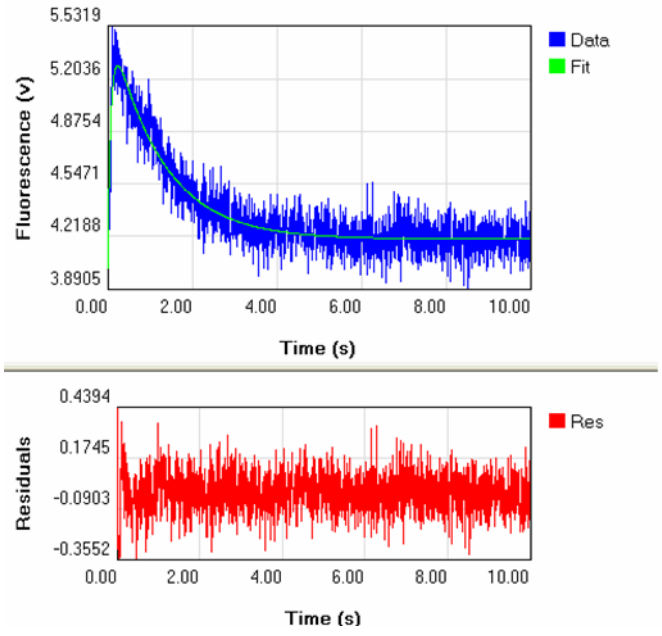

Figure 6.3 - Stopped-flow fluorescence intensity record of the binding of MEK to ERK. One syringe contained 10 nM ERK and the other syringe contained 120 nM MEK. The solid green line is the best fit to the data to a double exponential giving rate constants of 12.49 s^{-1}. The data are the averages of five reactions. Residuals are also reported (red trace in the bottom)

The dependence of the observed rate constant of binding of MEK to ERK was investigated over the range of 100-160 nM MEK. Measurements could not be made above

this concentration because of the very small amount of protein available. The dependence of the observed rate constant of binding of ERK to MEK concentration is shown in Figure 6.4.

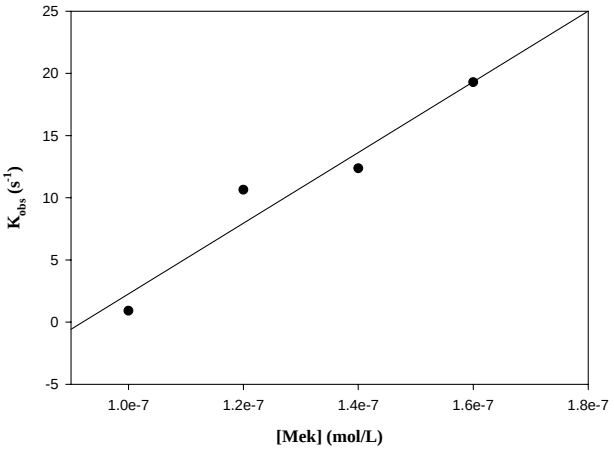

Figure 6.4 – Dependence of the observed rate constant determined by fluorescence intensity of the binding of ERK to MEK concentration

As already reported in the previous chapters, the slope of the straight line is the k_{on} (second-order rate constant; units, M^{-1} sec^{-1}) and the intercept on the ordinate is k_{off} (first-order rate constant; units, sec^{-1}). The second-order rate constant k_{on} is $2.84 \cdot 10^{8}$ M^{-1} sec^{-1}. As it can be seen, the intercept on the ordinate has a small negative value. This show that the interaction is nearly completely shifted toward the formation of the complex. A vary high value of the K_a and a low value of the K_d is then expected. The association constant K_a can be evaluated as $2.84 \cdot 10^{8}$ M^{-1} while the dissociation constant K_d is $3.52 \cdot 10^{-9}$ M.

6.4 Conclusions

This work provided an approach for studying the binding of MEK with ERK. The interaction has been studied by stopped-flow measurements. The association and dissociation rate constants (k_{on} and k_{off}) were determined from the kinetic studies while the dissociation and association binding constants (K_d and K_a) were determined from the k_{on}/k_{off} ratio.

The binding constant obtained is in agreement with the few data available in literature referring to MEK-ERK interaction. They are comparable with the constants found by Fujioka et al.[25] and are in good agreement with the values reported in the same paper as a comparison[26,27].

In their work, Fujioka *et al.* have developed several kinetic simulation models in order to comprehend the Ras/ERK MAPK cascade, which comprises Ras, Raf, MEK, and ERK. To monitor both the activation and nuclear translocation of ERK, they developed probes based on the principle of fluorescence resonance energy transfer. The dissociation constants of Ras-

Raf, Raf-MEK, and MEK-ERK complexes were estimated using a fluorescent tag that can be highlighted very rapidly. Finally, the same fluorescent tag was used to measure the nucleocytoplasmic shuttling rates of ERK and MEK. Using these parameters, they developed a kinetic simulation model consisting of the minimum essential members of the Ras/ERK MAPK cascade. They calculated the half-life of the MEK-ERK complex ($\tau_{1/2}$ = 7.8 s). From these half-lives, they estimated the dissociation rates (Table 6.1), assuming that the diffusion of the probe could be neglected and that the initial dissociation was well described by a single exponential function.

Reaction	**Fujioka et al.[25]**			**Sasagawa er al.[26]**			**Bhalla et al.[27]**		
	k_f	k_b	K_d	k_f	k_b	K_d	k_f	k_b	K_d
	(s/μM)	(s)	(μM)	(s/μM)	(s)	(μM)	(s/μM)	(s)	(μM)
(p)MEK + ERK ↔ (p)MEK·ERK	0.88	0.088	0.1	16	0.6	0.035	16.3	0.6	0.037

Table 6.1 – Results summary taken from Fujioka et al.[25] (p means phospho-)

In particular, Sasagawa *et al.*[26] and Bhalla *et al.*[27] have reported almost the same values for the binding constants obtained by different methods (simulation/prediction analysis).

Reference List

1. Shaul, Y. D.; Seger, R. The MEK/ERK cascade: From signaling specificity to diverse functions. *Biochim. Biophys. Acta* **2007,** *1773*, 1213-1226.
2. Seger, R.; Krebs, E. G. The MAPK signaling cascade. *FASEB J.* **1995,** *9*, 726-735.
3. Torii, S.; Nakayama, K.; Yamamoto, T.; Nishida, E. Regulatory Mechanisms and Function of ERK MAP Kinases. *J. Biochem.* **2004,** *136*, 557-561.
4. Vial, E.; Pouyssegur, J. Regulation of tumor cell motility by ERK mitogen-activated protein kinases. *Ann. N. Y. Acad. Sci.* **2004,** *1030*, 208-218.
5. Yoon, S.; Seger, R. The extracellular signal-regulated kinase: Multiple substrates regulate diverse cellular functions. *Growth Factors* **2006,** *24*, 21-44.
6. Wellbrock, C.; Karasarides, M.; Marais, R. The RAF Proteins take Centre Stage. *Mol. Cell. Biol.* **2004,** *5*, 875-885.
7. Gotoh, Y.; Nishida, E. Activation mechanism and function of the MAP kinase cascade. *Mol. Reprod. Dev.* **1995,** *42*, 486-492.
8. Salmeron, A.; Ahmad, T. B.; Carlile, G. W.; Pappin, D.; Narsimhan, R. P.; Ley, S. C. Activation of MEK-1 and SEK-1 by Tpl-2 protooncoprotein, a novel MAP kinase kinase kinase. *EMBO J.* **1996,** *15*, 817-826.
9. Lange-Carter, C. A.; Pleiman, C. M.; Gardner, A. M.; Blumer, K. J.; Johnson, G. L. A Divergence in the MAP Kinase Regulatory Network Defined by MEK Kinase and Raf. *Science* **1993,** *260*, 315-317.

10. Kolesnick, R.; Xing, H. R. Inflammatory bowel disease reveals the kinase activity of KSR1. *J. Clin. Invest.* **2004,** *114*, 1233-1237.

11. Morrison, D. K.; Davis, R. J. REGULATION OF MAP KINASE SIGNALING MODULES BY SCAFFOLD PROTEINS INMAMMALS. *Annu. Rev. Cell Dev. Biol.* **2003,** *19*, 91-118.

12. Ahn, N. G.; Seger, R.; Bratlien, R. L.; Diltz, C. D.; Tonks, N. K.; Krebs, E. G. Multiple Components in an Epidermal Growth Factor-stimulated Protein Kinase Cascade. *J. Biol. Chem.* **1991,** *266*, 4220-4227.

13. Gomez, N.; Cohen, P. Dissection of the protein kinase cascade by which nerve growth factor activates MAP kinases. *Nature* **1991,** *353*, 170-173.

14. Herskowitz, I. MAP Kinase Pathways in Yeast: For Mating and More. *Cell* **1995,** *80*, 187-197.

15. Alessi, D. R.; Saito, Y.; Campbell, D. G.; Cohen, P.; Sithanandam, G.; Rapp, U.; Ashworth, A.; Marshall, C. J.; Cowley, S. Identification of the sites in MAP kinase kinase-1 phosphorylated by $p74^{raf1}$. *EMBO J.* **1994,** *13*, 1610-1619.

16. Takekawa, M.; Tatebayashi, K.; Saito, H. Conserved Docking Site Is Essential for Activation of Mammalian MAP Kinase Kinases by Specific MAP Kinase Kinase Kinases. *Mol. Cell* **2005,** *18*, 295-306.

17. Matsuda, S.; Gotoh, Y.; Nishida, E. Phosphorylation of Xenopus Mitogen-activated Protein (MAP) Kinase Kinase by MAP Kinase Kinase Kinase andM AP Kinase. *J. Biol. Chem.* **1993,** *268*, 3277-3281.

18. Brunet, A.; Pages, G.; Pouyssegur, J. Growth factor-stimulated MAP kinase induces rapid retrophosphorylation and inhibition of MAP kinase kinase (MEK1). *FEBS Lett.* **1994,** *346*, 299-303.

19. Nantel, A.; Mohammad-Ali, K.; Sherk, J.; Posner, B. I.; Thomas, D. Y. Interaction of the Grb10 Adapter Protein with the Raf1 and MEK1 Kinases. *J. Biol. Chem.* **1998,** *273*, 10475-10484.

20. Frost, J. A.; Steen, H.; Shapiro, P.; Lewis, T.; Ahn, N.; Shaw, P. E.; Cobb, M. H. Cross-cascade activation of ERKs and ternary complex factors by Rho family proteins. *EMBO J.* **1997,** *16*, 6426-6438.

21. Slack-Davis, J. K.; Eblen, S. T.; Zecevic, M.; Boerner, S. A.; Tarcsafalvi, A.; Diaz, H. B.; Marshall, M. S.; Weber, M. J.; Parsons, J. T.; Catling, A. D. PAK1 phosphorylation of MEK1 regulates fibronectin-stimulated MAPK activation. *J. Cell. Biol.* **2003,** *162*, 281-291.

22. Eblen, S. T.; Slack-Davis, J. K.; Tarcsafalvi, A.; Parsons, J. T.; Weber, M. J. Mitogen-Activated Protein Kinase Feedback Phosphorylation Regulates MEK1 Complex Formation and Activation during Cellular Adhesion. *Mol. Cell. Biol.* **2004,** *24*, 2308-2317.

23. Resing, K. A.; Mansour, S. J.; Hermann, A. S.; Johnson, R. S.; Candia, J. M.; Fukasawa, K.; Vande, W. G.; Ahn, N. G. Determination of v-Mos-Catalyzed Phosphorylation Sites and Autophosphorylation Sites on MAP Kinase Kinase by ESI/MS. *Biochemistry* **1995,** *34*, 2610-2620.

24. Sontag, E.; Fedorov, S.; Kamibayashi, C.; Robbins, D.; Cobb, M.; Mumby, M. THE INTERACTION OF SV40 SMALL TUMOR-ANTIGEN WITH PROTEIN PHOSPHATASE-2A STIMULATES THE MAP KINASE PATHWAY AND INDUCES CELL-PROLIFERATION. *Cell* **1993,** *75*, 887-897.

25. Fujioka, A.; Terai, K.; Itoh, R. E.; Aoki, K.; Nakamura, T.; Kuroda, S.; Nishida, E.; Matsuda, M. Dynamics of the Ras/ERK MAPK Cascade as Monitored by Fluorescent Probes. *J. Biol. Chem.* **2006,** *281* (13), 8917-8926.

26. Sasagawa, S.; Ozaki, Y.; Fujita, K.; Kuroda, S. Prediction and validation of the distinct dynamics of transient and sustained ERK activation. *Nat. Cell Biol.* **2005,** *7* (4), 365-373.

27. Bhalla, U. S. Signaling in Small Subcellular Volumes. II. Stochastic and Diffusion Effects on Synaptic Network Properties. *Biophys. J.* **2004,** *87*, 745-753.

General Conclusions

Four different interactions were chosen and studied in order to explore four different kinds of interactions: protein-ligand, protein-antibody, protein-peptide and protein-protein interactions.

- **Protein-ligand**

The binding of fluorescein sodium salt with different bovine serum albumins (BSA) was investigated by steady-state and stopped-flow fluorescence. This interaction was chosen for a preliminary study for protein-ligand interactions because of BSA low cost and availability. The dissociation and association rate constants (k_{on} and k_{off}) were determined from the kinetic studies while the dissociation and association binding constants (K_d and K_a) were determined both by the quenching of the fluorescence of BSA in the presence of fluorescein and from stopped-flow measurements from the k_{on}/k_{off} ratio. This work also reported the average distance between tryptophan and bound fluorescein based on Förster's energy transfer theory and a thermodynamic study of the mode of interaction which is important for confirming binding modes.

The best results were obtained by fitting raw data by non-linear regression and Lineweaver-Burk equations. The Modified Stern-Volmer and Scatchard's plots gave less reliable data since the fitting was much more difficult. The agreement of the constants is good for two sets of measurements of two BSA (A and B). The K_d and K_a obtained for the third BSA (C, A7030) differ in the same set of experiments.

The fact that there is no agreement between the two sets of data coming from intensity and anisotropy measurements can be explained from the fact that fluorescence intensity and fluorescence anisotropy sense different aspects of the interaction. The true binding constants could be evaluated by using a global analysis which unfortunately was not available to us.

- **Protein-antibody**

The interaction between GST with his antibody α-GST (B14) was studied by fluorescence anisotropy, after GST bioconjugation with fluorescein-5-maleimide, leading to the K_d and K_a determination. By comparing the results obtained for GST-B14 interaction with the one found in literature and referring to protein-antibody interactions, we can then assert that a good binding specificity is present between GST and the antibody B-14 and that the use of spectroscopic techniques, the fluorescence anisotropy in particular, is a useful and favourable tool to study biochemical problems.

- **Protein-peptide**

GST-Tat86 interaction with two small peptides (CT319 and V2) having similar aa sequence and the same biological activity was studied by steady-state fluorescence exploiting the intrinsic Trp residues fluorescence. The results show that the obtained binding constants differ in the same set of interactions. One set of results is in agreement with the K_d obtained from BIAcore studies and reported by Marchiò *et al.* (*Blood* **2005,** *105*, 2802-2811) for a very similar interaction (K_d=8.1 nM). The variation of the obtained binding constants can be due to the presence of many tryptophan residues (8) each with a different environment.

The reaction was then followed by steady-state and stopped-flow fluorescence after the peptide Bioconjugation leading to very poor results due to the difficulties of the peptide bioconjugation.

Finally, the interaction between V2 labelled with 5-carboxyfluorescein with GST-Tat86 was studied by fluorescence spectroscopy. The interaction was first followed by detecting the fluorescence intensity variation by keeping GST-Tat86 concentration constant and by adding the ligand. The intensity spectra changes were not linear with the ligand concentration. Therefore, the interaction was also followed by exploiting fluorescence anisotropy. The fluorescent labelled V2 was titrated by GST-Tat86 but there was no change in the anisotropy signal. The kinetics of the interaction was also followed both in intensity and anisotropy mode. But in both cases, the concentrations and the amount of the samples in study were not enough for a complete study. Actually, the concentrations used were too low to be detectable.

- **Protein-protein**

The interaction between two proteins belonging to the already mentioned pathway was studied. The interaction between MEK-ERK was followed by stopped-flow fluorescence after ERK bioconjugation with fluorescein-5-maleimide. The second-order rate constant k_{on} is $2.84 \cdot 10^8$ M^{-1} sec^{-1} while the k_{off} has a small negative value. This shows that the interaction is nearly completely shifted toward the formation of the complex. The binding constant obtained is in agreement with the few data available in literature referring to this interaction obtained either from simulation/prediction analysis or different techniques.

All these interaction studies have provided evidences of the possibility of studying protein-ligand interactions by spectroscopic methods exploiting different techniques (steady-state fluorescence intensity, anisotropy, quenching, and fluorescence stopped-flow intensity and anisotropy) but has also outlined all the difficulties and the limits of the reported

techniques. In particular it should be stressed the need of high quantity of high purity proteins or, more generally, biomolecules.